Atomic Force Microscopy of dynamic protein DNA interactions

John van Noort

Atomic Force Microscopy of dynamic protein DNA interactions

ATOMIC FORCE MICROSCOPY

OF DYNAMIC

PROTEIN DNA INTERACTIONS

PROEFSCHRIFT

ter verkrijging van
de graad doctor aan de Universiteit Twente,
op gezag van de rector magnificus,
Prof. dr. F. A. van Vught,
volgens besluit van het College voor Promoties
in het openbaar te verdedigen
op vrijdag 25 juni te 16.45 uur.

door
Simon Johannes Theodorus van Noort
geboren op 15 augustus 1971
te Lisse.

Dit proefschrift is goedgekeurd door:

Promotor: Prof. Dr. J. Greve
Assistent-promotor: Dr. B. G. de Grooth

Contents

Chapter 1

Introduction

1.1 Visualization of biomolecules

Developments in microscopy

Throughout history advances in medicine and biology have evolved together with the development of microscopical techniques. With the invention of the microscope by Van Leeuwenhoek in the 17th century, a new era of life science began. Since that time the optical microscope has developed into an invaluable tool for fundamental research by revealing structure-function relations. The fundamental knowledge of biological systems that is available now, has changed our view on life and has proven essential for understanding and prevention of a great diversity of diseases. With the expanding knowledge on the chemical and physical basis of processes essential for life, a growing need for techniques to study these processes in even greater detail developed. A wide variety of biochemical techniques is now available to study the molecular origin of these processes functionally. However, for the study of the structure of these biomolecules, that have a typical size of 1 to 100 nm, only a limited number of tools are available.

Although many technical advances in optical microscopy, in combination with sophisticated preparation and labelling procedures, have extended the capabilities of traditional optical microscopy, the spatial resolution is fundamentally limited by the diffraction limit. Following the

Figure 1.1 The well-known (but highly idealised) structure of B-DNA [1]. The helix structure has a diameter of 2.0 nm, and the distance between bases is 0.33 nm.

Rayleigh criterion, features can only be resolved spatially if their distance exceeds $0.61\lambda / \sin(\theta)$, where λ denotes the wavelength of light and θ the opening angle of the lens. Due to the diffraction limit optical methods usually yield a resolution of several hundreds of nanometers, which is insufficient to visualize the structure of (complexes of) individual molecules.

Although not suitable for high-resolution imaging, X-ray scattering has contributed a lot to the structure determination of biomolecules. Already in 1954 Crick and Watson revealed the now well-known helix structure of B-DNA, by analysis of the crystal diffraction pattern [1], shown in figure 1.1. Nowadays a great number of biomolecules have been structurally resolved with atomic resolution using X-ray crystallography and NMR, which yields similar data. It is however the interaction between individual molecules that relates their structure to their function. Though a number of protein–nucleic acid complexes have been crystallized and resolved, this number increases at a much slower rate, because of the difficulty of crystallizing such structures and the complexity of the interpretation of such large assemblies of molecules. Furthermore these techniques usually resolve only an average crystal structure, neglecting the dynamics of molecular processes.

Electron microscopy (EM) has proven to be successful for imaging large aggregates of biomolecules with a resolution of several tens of nanometers, filling in the gap between low-resolution light microscopy and high-resolution structure determination. However because biological matter is transparent for this short wavelength, high-energy, electromagnetic radiation, samples need to be shadowed with a metal coating to obtain contrast. The metal coating in combination with the incompatibility of EM with physiological conditions, like imaging in buffer, prevents imaging of active processes involving biomolecules.

Scanning Probe Microscopy

With the invention of the Scanning Tunneling Microscope (STM) Binnig et al. [2] introduced a new family of microscopes. Based on a very local probe or tip, a strongly distance-dependent interaction and close proximity of the probe and the object, a Scanning Probe Microscope (SPM) is capable to visualize structures down to the atomic scale. The localization of the interaction, that is the origin of the high resolution, is of the order $\sqrt{R + D / \kappa}$, where D is the effective interaction distance, R the effective probe size, $1/\kappa$ the decay length of the interaction [3]. Topography maps can be constructed by measuring the height at which the tip rasterscans over a surface.

In STM the tunneling current between a metal tip and a conducting surface is used to measure the tip-sample distance. Though very useful for a vari-

ety of surface sciences the necessity of conducting samples prevented the use of STM for biological applications. It was only when Binnig et al. [4] realized that atomic forces, that caused STM artifacts, can be used to measure tip sample distances very accurately, that the Atomic Force Microscope (AFM) was invented. By mounting a sharp tip on a very flexible cantilever a local and sensitive force sensor is created that can be operated in a similar way as the STM. Using forces rather than tunneling current the AFM is not limited to conducting samples and even in aqueous solutions high-resolution topography images can be obtained.

In the past 10 years a large number of biological applications of AFM has been presented, for reviews see [5,6]. Biological applications of AFM range from visualization of cells, membranes and arrays of membrane proteins to individual proteins and DNA. Besides for imaging, the AFM can also be used to measure mechanical properties of the sample like elasticity and stiffness and for manipulation of individual molecules.

A relatively new development in SPM is the use of a Near-field Scanning Optical Microscope (NSOM) for biological applications [7]. In the NSOM a sharp, aluminium coated fiber, with a ~100 nm aperture, is operated in a similar way as the AFM. Through the small aperture light can be coupled into the sample, and in this way optical contrast can be obtained with a spatial resolution which is determined by the size of the aperture itself. In this way optical properties can be visualized with a spatial resolution beyond the diffraction limit. However, only a very limited number of biological applications have been reported, mainly because of the high demands that are put on the force feedback, due to the high stiffness of the fiber probe, and the difficulties encountered in making good probes.

1.2 Atomic Force Microscopy

Atomic Force Microscope setup

For imaging biomolecular processes with an AFM we will use, and further develop, an AFM setup based on the design described by Van der Werf et al. [8], shown in figure 1.2. Microfabricated Si_3N_4 cantilevers with a sharp pyramidal tip form the basis of the AFM. For scanning the cantilever is mounted under a piezo tube that is used to move the tip over the sample. In the piezo a laserdiode is located and the laserbeam is focused on the cantilever. The reflection of the laser light is projected via a mirror onto a quadrant photodiode. The difference in the intensity between the left and the right half of the detector is proportional to the cantilever deflection and is thus a meas-
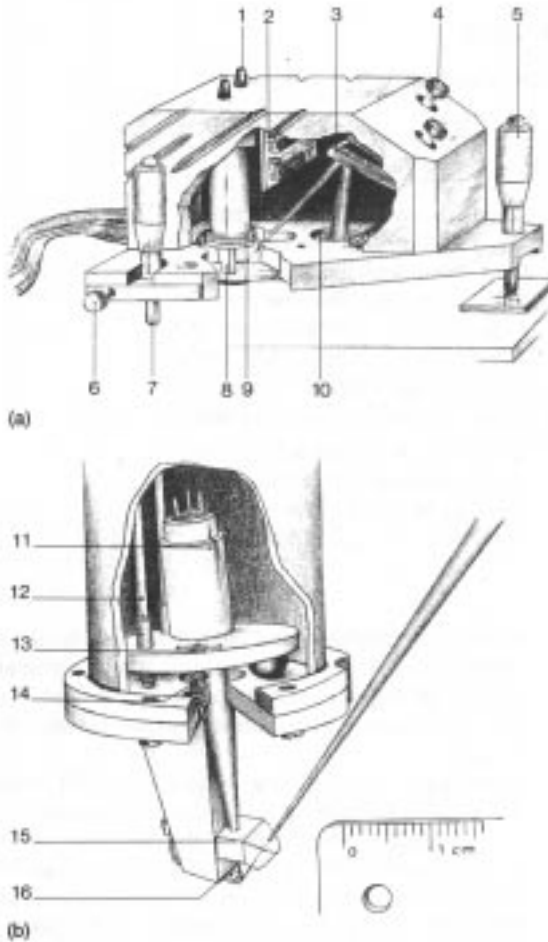
Figure 1.2 Schematic drawing of the AFM design used in this thesis. a) the overall layout b) a close-up of the laserdiode and the cantilever holder. 1) adjustment knobs for manipulation of the laser beam, 2) preamplifier electronics, 3) beam-steering mirror, 4) adjustment knobs for the mirror, 5) fine approach, 6) adjustment knobs for the lateral position of the cantilever, 7) coarse approach, 8) cantilever holder, 9) piezo tube, 10) quadrant detector, 11) laser diode and focusing lens, 12) flexible rods, 13) adjustable plate, 14) springs, 15) optical window for laser beam, 16) cantilever with tip.

ure for the tip position. For imaging, the tip is rasterscanned over the sample, and at each position the cantilever deflection is measured, with which a topography map can be constructed.

Modes of operation

Three different modes of operation are commonly used for AFM imaging. In *constant height mode*, the deflection of the cantilever is used as a measure

for the height of the tip. To reduce normal forces applied to the sample the deflection signal can be kept constant in a feedback loop. In this *constant force mode* the voltage applied to the piezo is used as a measure for the height. Though force feedback may reduce the normal force to less than 1 nN, frictional forces can build up to several hundreds of nN because the tip is constantly in contact with the sample while it is scanned over the surface. In constant force mode these lateral forces are most harmful for soft, fragile biological matter.

A reduction of lateral forces can be achieved using *tapping mode* [9]. In this mode the cantilever is oscillated at its resonance frequency. The tip is lowered until it approaches the surface, and due to the interaction with the surface the oscillation amplitude decreases. This reduction of the amplitude is kept constant in a feedback loop, and the feedback signal is used for imaging. In this way the tip sample contact time is limited to a very short period during impact, and as a result frictional forces are negligible compared to the normal forces. For biological applications, especially in aqueous environment, tapping mode operation is preferable because of the reduction of tip induced damage.

1.3 AFM of protein DNA complexes

Results reported in literature

A very competitive field of application of the AFM is the visualization of DNA and DNA-protein complexes, see figure 1.3. A growing number of papers report observation of DNA and proteins at molecular resolution. A complete overview of all these studies is beyond the scope of this chapter, for a review see [10], but in this paragraph the properties that can be measured with an AFM are summarized.

The most obvious, but not straight forward, parameter that can be measured is the size, or the volume, of the protein. A broad range of protein sizes has been studied, varying from small transcription regulatory proteins like Cro dimers (M = 14.7 kD) to large multi-subunit molecules such as RNA polymerase (M ~ 450 kD). Though the height resolution of AFM is very good, Wyman et al. have shown that the size of a protein is generally underestimated using tapping mode AFM [11]. Using relative dimensions, the ratio and distance between various proteins within one image may be determined. For Cro protein three dimers located only 0.3 nm from each other could be resolved [12]. Complexes of DNA and RecA protein which coats

DNA before genetic recombination, have been visualized showing a 10 nm periodic structure that corresponds to the size of the protein.

Though the dimensions of molecular structures cannot be measured accurately, the shape of the structure can be resolved with good precision. Using the apparent persistence length of DNA molecules, Rivetti et al. [13] studied the dynamics of DNA immobilization on various substrates. Protein induced conformational changes of DNA show up in AFM images as a local bend in the shape of a DNA. Determination of the bending angle of complexes of several DNA binding proteins by AFM confirms measurements done with other methods.

Although potentially an AFM can be equally well operated in liquid as in air, up till now surprisingly little papers have been reported of DNA visualization in buffer solution. Even less papers report processes of individual biomolecules observed with AFM [14]. In 1994 Guthold et al. [15] reported observation of RNA polymerase-DNA complexes in buffer, using constant force mode AFM, though the image quality was rather poor. Only in 1997 by joint effort of two groups, actual transcription activity was visualized using AFM [16,17]. Very little has been published using AFM for visualization of protein-DNA interactions until today, despite of the great potential. It is this kind of application that is the subject of this thesis.

DNA repair by photolyase

To demonstrate and further develop the capabilities of AFM we choose as a system to work upon the process of DNA repair by the protein photolyase. Photolyase is a relatively small protein (M ~ 55 kD), that was discovered in 1949 when enhanced survival of UV-irradiated bacteria was found, after illumination with visible light [18]. The substrate of photolyase is UV-irradiated DNA. UV irradiation induces the formation of cyclobutane pyrimidine dimers from two neighbouring bases. The photoreactivation follows a simple reaction scheme. In the dark the enzyme first binds to UV-damaged
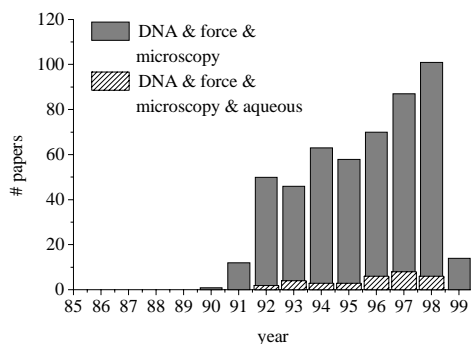
Figure 1.3 Results of a literature search in 'Science Citation Index Expanded' for keywords 'DNA', 'force' and 'microscopy' from 1988 to 1999. When the search is limited with the key word 'aqueous' only a fraction of the papers is selected. Global inspection of the results show that this search covers most of the papers known by the author, and can be assumed representative for published literature.

DNA to form an enzyme-substrate complex. Then, in a light dependent step, the dimer is split and photolyase dissociates from the repaired DNA.

Despite of the low content of photolyase in bacteria a 10^4 to 10^5-fold increase in cell survival has been reported [18]. Target finding and substrate recognition, that must be crucial steps in the reaction mechanism of photolyase and most other DNA-interacting proteins, should be very efficient to achieve such a high effectiveness. AFM may help to get a better understanding of these processes.

Photolyase is particularly suitable for this study for a number of reasons. First, the protein does not need any other resources, except for visible light, to complete the reaction, making it a quite simple system. By simply switching on the light, it is even possible to trigger the photoreactivation reaction. Secondly, the reaction has been studied extensively and even the crystal structures of two species are known [19,20]. However, the structure of the cocrystal has not been resolved yet, and in combination with other studies, visualization of the complex may help to get a better understanding of the substrate recognition. Its relatively small size is on the edge of resolution for EM, making AFM a unique tool to image these complexes. Furthermore, the protein, the substrate and the protein-DNA complex are quite stable, simplifying sample preparation. And finally it has a high substrate specificity and high quantum yield, simplifying interpretation of the results obtained from single molecules.

1.4 AFM imaging parameters

Requirements

AFM imaging of fragile samples like individual molecules puts high demands on the measurement. The first complication of AFM imaging of individual molecules is tip-induced damage. For reproducible imaging of molecules the interaction forces need to be controlled carefully to prevent damage. The maximal force that can be allowed to act on a DNA molecule has been de subject of several papers, but the values found vary. Guthold et al. [21] reported that dissection of DNA requires a force of 400 pN. However, very recently, the strength of an individual covalent bond was measured to be a few nN, depending on the force-loading rate [23]. A related, still unanswered, question is the effect of the scanning tip on the activity of the molecules. When pulling on a DNA strand conformational changes can already occur at a force of 65 pN [24]. Unless such small forces can be prevented, tip-induced distortions are likely to occur in the study of molecular activity

with an AFM and may affect the reaction, but to what extent is unknown up till now.

A second complicating factor is the necessity to immobilize molecules on a very flat substrate, to be able to recognize the molecules. Successful imaging of DNA both in air and in liquid, has been reported using Mg^{2+} treated mica as a substrate [23]. Steric hindrance by the surface will affect the protein-DNA reaction but again the extent of it remains unclear. Weaker immobilization of the molecules may reduce the hindrance of the surface, but the resulting higher mobility of the molecules will complicate AFM imaging.

A third challenge that is related to the mobility of the molecules over the surface is the time resolution of the AFM. For an undistorted topography image movement of the molecules should be slow compared to the frame acquisition time. Movement can be either caused by diffusion of the molecule or by conformational changes that can be related to reactions between molecules. Conformational changes of various proteins have been measured and time constants in the order of milliseconds have been reported [25]. Thus imaging of such processes would require a frame rate of at least 1 kHz, while measuring an AFM image generally takes about 1 min.

Forces

Under aqueous conditions the forces between the tip and the sample, that are responsible for the cantilever deflection can be split into Born repulsion, hydration forces, Van der Waals forces and electrostatic forces. When imaging in air an extra, attractive, capillary force is present that builds up when the tip touches the hydration layer which covers the sample. In ambient conditions the latter can be over 100 nN, and is dominant over other attractive forces.

The force sensitivity of the cantilever is inversely proportional to its spring constant; the lower the spring constant the more sensitive the AFM. The weakest cantilevers that are commercially available are made of Si_3N_4 and have a spring constant of approximately 0.01 N/m. For tapping mode however, the oscillation energy of the cantilever should exceed the energy dissipation during impact of the tip, and for this reason very weak cantilevers cannot be used.

Resolution

The resolution perpendicular to the surface mainly depends on the sensitivity of the cantilever and the piezo and is of the order 0.1 nm. The lateral resolution is more difficult to determine. As already mentioned in this chapter,

the resolution that can be achieved using a local probe technique depends on the interaction distance, the decay length of the interaction and on the probe size. As the interaction force is the sum of a number of forces with different distance dependencies, the decay length of the interaction depends on the tip-sample distance. At a long distance, i.e. in the range of several nanometers, electrostatic interactions dominate the tip-sample interaction. Oxidation of the Si_3N_4 tip results in a net negative charge of the tip in buffer [26] which can result in electrostatic forces up to 1 nN in the case of a charged surface. The decay length of the electrostatic interaction, known as the Debye-length, scales with the salt concentration c as $1/\kappa$ = 0.304 nm / $\sqrt{c}$. Thus at physiological conditions the decay length can range from 0.1 to 100 nm. At a closer distance, smaller than 0.5 nm from the surface, Van der Waals force and Born repulsion become dominant, which have a very short range distance dependence. If these short-range forces are dominant, the tip sample interaction is very local and will not limit the resolution. However, because of the steep force gradient, the interaction force can in this case build up to very high values, if the AFM is not operated carefully. When imaging very soft samples, like cells, indentation of the elastic surface can result in a very small force gradient, effectively decreasing the localization of the interaction and thus the resolution.

When the force gradient exceeds the spring constant of the cantilever, the tip 'snaps' into contact. The resolution of an AFM image is then determined by the geometrical convolution of the tip and the sample. The resolution is approximately $\sqrt{rR}$, where r is the effective radius of the sample and R the effective radius of the tip. The size of microfabricated Si_3N_4 tips is not well defined, and varies between batches. It usually has an end radius of approximately 20-50 nm. DNA molecules with a diameter of 2 nm will then have an apparent width of ~10 nm. Corrugations on the tip can yield an effective radius an order of magnitude smaller, and using these corrugations on a very flat sample much better resolution can be obtained. By the combination of careful control of the forces, optimization of the salt concentration and a well defined flat crystal array of proteins Müller et al. routinely report sub-nanometer resolution [27]. In conclusion, to achieve optimal lateral resolution the tip radius, the tip sample distance and the interaction decay should be optimised, if possible.

Temporal resolution

Optimization of the temporal resolution of the AFM-setup is one of the main objectives in this thesis. The maximal scan velocity depends on the hardware and should be evaluated with respect to the forces that are ap-

plied to the sample. When imaging in aqueous solution, the dominant noise source is thermal noise that is caused by Brownian forces acting on the force sensor. These thermal fluctuations are a direct result of the presence of buffer solution around the sample. It is impossible to distinguish them from sample-induced force fluctuations without extensive, relatively slow, time averaging. Thus a trade-off between speed and sensitivity has to be made, and the forces that are allowed to act on the sample ultimately limit the scan velocity.

1.5 Outline of this thesis

By combining high spatial resolution with high temporal resolution the major advantage of AFM is exploited, namely its capability to visualize functional biomolecules in their natural environment. In this thesis various topics will be dealt with that are related to repeatedly imaging individual molecules with an AFM. From these molecular movies reliable data should be obtained linking their appearance in an AFM image to dynamical properties of functioning molecules.

In chapter 2 however, first a detailed study of the tip-sample interaction is described when the AFM is operated in tapping mode under ambient conditions. It nicely demonstrates the complications that may occur in interpreting an AFM image. In spite of the high normal resolution, the accuracy of the height measurement can be severely affected by differences in the tip-sample interaction.

Using tapping mode AFM in air photolyase-DNA complexes are visualized in chapter 3. It is shown that at specific complexes a bend of the DNA can be seen, while in non-specific complexes DNA does not bend. The consequences for the conformation and the flexibility of the complex will be discussed.

The search for damaged sites by photolyase is studied in chapter 4. To visualize this process it is necessary to operate the AFM in physiological buffer. All parameters that are required for successful imaging of loosely bound molecules are discussed in detail. Then the mobility of DNA strands is analysed and finally individual photolyase molecules are followed in time. The experiments shown in this chapter also nicely demonstrate the problems with AFM imaging of molecular processes: the effect of the surface, tip-induced motion of molecules, and the relatively poor temporal resolution.

The factors limiting the temporal resolution are discussed in chapter 5. Because ultimately the scan velocity of the tip is limited by the resonance

frequency of the cantilever, the only way to improve the temporal resolution using commercially available cantilevers is by zooming in. In chapter 5 a drift correction scheme is proposed and tested, which allows fast imaging of small areas without suffering from lateral drift. The procedure is applied to measure the surface diffusion of very loosely bound DNA plasmids.

Finally, in chapter 6 a model of the tip-sample interaction force is presented. Experimentally obtained parameters are used and the resulting cantilever deflection traces are compared with measurements. The effect of electrostatic forces on the interaction force is analysed using the developed model, and an experimental scheme based on higher harmonics mapping is proposed to measure electrostatic forces during tapping mode.

1.6 References

1   Calladine, C. R., H. R. Drew. 1997. Understanding DNA, the molecule and how it works. Acedemic Press Limited, San Diego, USA.

2   Binnig, G., H. Rohrer, Ch. Gerber, and E. Weibel. 1982. Surface studies by scanning tunneling microscopy. *Phys Rev. Lett.* 49: 57-61.

3   Rohrer, H. 1994. Scanning tunneling microscopy: a surface tool and beyond. *Surface science* 299: 956-964.

4   Binnig, G., C. F. Quate, and Ch. Gerber. 1986. Atomic force microscope. *Phys. Rev. Lett.* 56: 930-933.

5   Bustamante, C., D. Keller. 1995. Scanning force microscopy in biology. *Physics Today* 1995: 32-38.

6   Lal, R., and S.A. John. 1994. Biological applications of atomic force microscopy. *Am J. Physiol.* 266 (Cell Physiol. 35): C1-C21.

7   Garcia-Parajo, M. F., J.-A. Veerman, S. J. T. van Noort, B. G. de Grooth, J. Greve, N. F. van Hulst. 1998. Near-field optical microscopy for DNA studies at the single molecular level. *Bioimaging* 6: 43-53.

8   Van der Werf, K.O., C.A. Putman, B. G. de Grooth, F.B. Segerink, E.H. Schipper, N. F. van Hulst, and J. Greve. 1993. Compact stand-alone atomic force microscope. *Rev. Sci. Instr.* 64: 2892-2897.

9   Zhong, Q., D. Innis, K. Kjoller, and V. Ellings. 1993. Fractured polymer/silica fiber structure studied by tapping mode atomic force microscopy. *Surf. Sci. Lett.* 290: L688.

10 Bustamante, C., C. Rivetti. 1996. Visualizing protein-nucleic acid interactions on a large scale with the scanning force microscope. *Annu. Rev. Biophys. Biomol. Struct.* 25: 395-429.

11 Wyman, C., I. Rombel, A. K. North, C. Bustamante, and S. Kustu. 1997. Unusual oligomerisation required for activity of NtrC, a bacterial enhancer-binding protein. *Science* 275: 1658-1661.

12 Erie, D.A., G. Yang, H.C. Schultz, and C. Bustamante. 1994. DNA bending by Cro protein in specific and nonspecific complexes: implications for protein site recognition and specifty. *Science* 266: 1562-1566.

13 Rivetti, C., C. Walker, and C. Bustamante 1998. Polymer Chain Statistics and Conformational Analysis of DNA Molecules with Bends or Sections of Different Flexibility. *J. Mol. Biol.* 280: 41-60.

14 Keller, D. 1998. Making movies of molecular motions. *Biophys. J.* 74: 2743-2744.

15 Guthold, M., M. Bezanilla, D. A. Erie, B. Jenkins, H.G. Hansma, and C. Bustamante. 1994. Following the assembly of RNA polymerase-DNA complexes in aqueous solutions with the scanning force microscope. *Proc. Natl. Acad. Sci USA* 91: 12927-12931.

16 Kasas, S., N. H. Thomson, B. L. Smith, H. G. Hansma, X. Zhu, M. Guthold, C. Bustamante, E.T. Kool, M. Kashev, and P. K. Hansma. 1997. Escherichia coli RNA Polymerase activity observed using atomic force microscopy. *Biochemistry* 36: 461-468.

17 Guthold, M., X. Zhu, C. Rivetti, G. Yang, N.H. Thomson, S. Kasas, H.G. Hansma, B. Smith, P.K. Hansma, and C. Bustamante. 1997. One-dimensional diffusion and transcription by E. coli RNA polymerase observed with the scanning force microscope. *J. Biol. Chem.* "submitted for publication".

18 Yasui, A., and A. P. M. Eker. 1996. DNA photolyases. In: DNA damage and repair, Vol 2. editors J. A. Nickoloff, and M. F. Hoekstra, Humana Press Inc. NY, USA.

19 Park, H.-W., S.-T Kim, A. Sancar, and J. Deisenhofer. 1995. Crystal structure of DNA photolyase from Escherichia coli. *Science* 268: 1866-1872.

20 Tamada, T., K. Kitadoro, Y. Higuchi, K. Inaka, A. Yasui, P.E. de Ruiter, A.P.M. Eker, and K. Miki. 1997. Crystal structure of DNA photolyase from Anacystus nidulans. *Nature Stuct. Biol.* 4: 887-891.

21 Guthold, M., G. Matthews, R. Taylor, D. Erie, F. Brooks, and R. Superfine. 1999. Quantitative manipulation of DNA in liquid with the nanomanipulator scanning forcemicroscope. *Biophys J.* 76: A351.

22 Smith, S. B., Y. Cui, and C. Bustamante. 1997. Overstrechting DNA beyond its B-form length. *Science* 271: 795-798.

23 Wagner, P. 1998. Imobilization strategies for biological scanning probe microscopy. *FEBS Lett.* 430: 112-115.

24 Grandbois, M., M. Beyer, M. Rief, H. Clausen-Schauman, and H. Gaub. 1999. How strong is a covalent bond? *Science* 283: 1727-1730.

25 Thomson, N. H., M. Fritz, M. Radmacher, J. P. Cleveland, C. F. Schmidt, and P. K. Hansma. Protein tracking an detection of protein motion using Atomic Force Microscopy. *Biophys. J.* 70: 2421-2431.

26 Butt, H.-J. 1991. Electrostatic interaction in atomic force microscopy. *Biophys. J.* 60: 777-785.

27 Müller, D. J., D. Fotiadis, S. Scheuring, S. A. Müller, and A. Engel. 1999. Electrostatically balanced imaging of biological specimens by atomic force microscopy. *Biophys. J.* 76: 1101-1111.

Chapter 2

Height anomalies in tapping mode in air

caused by adhesion

Abstract

Height anomalies in tapping mode Atomic Force Microscopy (AFM) in air are shown to be caused by adhesion. Depending on the damping of the oscillation the apparent height of a sticking surface is reduced compared to less sticking surfaces. These height artefacts result from a modulation of oscillatory movement of the cantilever. Damping and excitation of the cantilever by the driver continuously compete and as a consequence, a severe modulation of the cantilever oscillation occurs, depending on the phase mismatch between the driver and the cantilever. Phase images of tapping mode AFM show contrast that correlates with adhesion. Examples of a partially removed gold layer on mica, a Langmuir-Blodgett film and DNA show height artefacts ranging up to 10 nm.

13

2.1 Introduction

In recent years the use of the tapping mode in Atomic Force Microscopy (AFM) has gained increasing popularity [1]. In tapping mode the cantilever, on which the tip is mounted, is oscillated at resonance. As the tip approaches the surface the oscillation is damped and the reduced amplitude is kept constant in a feedback loop. Because the tip only touches the sample during the impacts, the lateral forces on the sample, which are liable for the destructive nature of the constant force mode, are significantly reduced. Furthermore, the penetration of the tip into the surface will be less because of the viscoelastic properties of the sample. Thus both damaging and indentation of the sample by the tip are minimised.

Because of this gentleness, tapping mode AFM has become favourable in most biological AFM studies. The resulting height measurements, however, have been the subject of discussion in a number of papers [2,3,4]. In order to explain the discrepancies in the height measurements a detailed analysis of the dynamics of the oscillating tip is necessary. In this paper a study of one aspect of the contrast mechanism of tapping mode in air is presented: the way in which adhesion between the tip and the sample affects the height information in the acquired tapping mode image. In the samples we have studied large adhesion differences are caused by differences in the thickness of the adsorbed water layer, which is a function of the hydrophobicity. In order to rule out indentation of the sample and thus affecting the height measurement, we use only hard samples.

2.2 Analysis

In order to estimate the interactions between tip and sample, calculations on a driven, damped harmonic oscillator as a model system have shown quite useful [5]. The movement of the cantilever, z can be described by equation 2.1, using an effective mass m, a spring constant k and a quality factor Q:

$$m \frac{\partial^2 z}{\partial t} + m \frac{\omega}{Q} \frac{\partial z}{\partial t} + kz(t) = kA\sin(\omega t) + F\big(z(t)\big) \tag{2.1}$$

When the driver oscillates at the resonance frequency ω_0 of the cantilever with an amplitude A and the tip does not impact on the sample, the height dependent force F is negligible. This results in a free oscillation z of the cantilever:

$$z(t) = QA\,\sin(\omega t + \phi) \tag{2.2}$$

and a phase shift ϕ between the driver and the cantilever, being equal to 90° at resonance.

The impact of the tip on the sample causes a non-linearity in the movement of the cantilever which can be modelled as a height dependent force F. This force depends on the (visco-)elastic properties of the sample when the tip is in contact, but equals zero if not. At low frequencies this force-distance curve is experimentally accessible and has shown useful in a number of applications. The influence of the elasticity of the sample on the tip penetration for example, can be accounted for, both in theory using numerical methods and in experiment [6,7].

When, for delicate samples, the repulsive forces are minimised, i.e. a small damping of the oscillation is used, attractive adhesion forces, which can range up to 100 nN, become dominant. The force F(z(t)) is not only discontinuous, the hysteresis of the adhesion force should also be included, making it non-trivial to solve equation 2.1 numerically. Only a few papers deal with these attractive forces between the tip and the sample in the tapping mode [8,9].

In ambient conditions the adhesion between the tip and the sample can be attributed mainly to the water contamination layer on the sample. In force distance curves one can observe the tip snapping in the water layer a few nanometers above the surface. The tip will be decelerated by the viscous damping of this water layer. When the tip retracts the water layer has to be disrupted. Using an environmental Scanning Electron Microscope, Amrein [10] has visualised nicely the water layer covering tip and sample. Both for the disruption of the water layer and for the viscous damping in the water layer, energy will be dissipated at the expense of energy of the oscillating cantilever. So after the impact the cantilever will not reach the same amplitude as before the impact, and the tip may not hit the sample surface during the next swing. Next to this effect, the sticking of the tip will increase the interaction time, which results in an extra phase lag. Because of this additional phase lag with the driver, the excitation is less efficient, also affecting the cantilever amplitude.

After the impact the cantilever, which has less energy than before, will gain amplitude again. The response of the oscillating system can be expressed with the time constant τ [11]:

$$t = 2\ Q/\omega_0 \tag{2.3}$$

Thus when the driver starts oscillating, the amplitude of the cantilever grows exponentially with a rise time τ.

Depending on the quality factor Q and the amount of damping, it may take longer than one oscillation period before the amplitude is sufficient to impact on the sample again. Thus a periodic modulation of the oscillation will occur, resulting in a decrease of the average amplitude as detected by the AFM setup. The smaller average amplitude will enter the feedback mechanism which is used to keep the oscillation amplitude constant. The AFM system will then respond to it like it responds to a decrease of amplitude caused by an increase in height of the sample: it will retract. In this way surfaces with a large adhesion force are expected to appear higher in topography than surfaces with a small adhesion force. Though under ambient conditions the main constituent in the adhesion force is capillary force of the contamination layer, other interaction forces are expected to result in similar effects.

The phase of the oscillating cantilever is very sensitive for the damping of the cantilever oscillation. Recently the phase was introduced [12] as a new contrast parameter in tapping mode AFM, claiming it to be sensitive for both the viscoelasticity and the elasticity of the surface [9]. Magonov et al. [13] have shown how viscous damping of the cantilever tapping on polymer blends can be monitored using phase imaging. Next to (visco-)elasticity, tip sample adhesion is suspected to cause phase contrast. In the present paper adhesion induced phase contrast in tapping mode AFM is also studied. In order to separate elasticity effects from effects caused by adhesion, only rigid samples are used. This excludes many biological samples. The conclusions, however, are general and can be applied to all samples.

2.3 Experimental setup

For the measurements a home built stand-alone AFM was used, offering a great flexibility in parameter settings and tip choice [14]. In tapping mode the AFM measures, while keeping the oscillation amplitude constant, both topography and phase of the oscillation. In this chapter the set-point of the amplitude will be referred to as the damping and will be expressed in percentage of the free oscillation amplitude. The phase of the deflection is measured relative to the driver. Because the mechanical construction between the driver and the cantilever introduces an extra phase shift, only relative values of the phase are measured.

When the phase of the oscillating signal varies, a proper amplitude detection scheme is necessary in order to measure the correct amplitude, which consists of a real and an imaginary part. If a lock-in amplifier is used for amplitude detection only the real part of the oscillating signal is measured.

A change of phase will reduce the apparent amplitude to Acos(Df), which would affect the height measurement even further. In order to separate phase and amplitude information we used a true Root Mean Square (RMS) amplitude detector, bandwidth 5 kHz, to measure the modulus of the amplitude.

Next to the constant force and tapping mode, our AFM system can also acquire real time adhesion force images in the *adhesion mode*. In this mode a force-distance curve is generated for each pixel, out of which both topography and adhesion force are extracted on-line. A detailed description of this mode is presented elsewhere [15].

For the experiments reported in this study a 100 ㎜ triangular Si_3N_4 cantilever (Park Scientific, Sunnyvale, Ca) was used. According to the manufacturers specifications this cantilever has a spring constant of 0.58 N/m, a resonance frequency of about 95 kHz, a tip radius of 20 nm and a quality factor of about 80. The design of the AFM-head allows large oscillation amplitudes, up to 300 nm, which are necessary to overcome the adhesion forces exerted on this relatively weak cantilever. The properties of this cantilever enable one to acquire tapping mode, constant force mode and adhesion mode images without changing the cantilever. Thus the adhesion force, which depends on both the tip and the sample, is equal in experiments using different modes.

In order to follow the cantilever deflection more closely, deflection traces were recorded using a digital oscilloscope (LeCroy 9360, 600MHz). The scope was triggered by the driver in order to be able to compare the phase of the different traces.

2.4 Results

Gold and mica

For the first set of experiments an evaporated gold layer on a mica substrate was used. The gold layer was partially removed by cleavage, resulting in patches of freshly cleaved mica. In air the capillary force of the thin contamination layer that covers the sample is the main constituent of the tip-sample adhesion [16]. Thus differences in adhesion in this sample are correlated with the hydrophobicity. The latter can be quantified by measurement of the contact angle of a water drop on the surface. The contact angle measurement yielded ± 55° for the gold layer and ± 15° for the freshly cleaved mica.
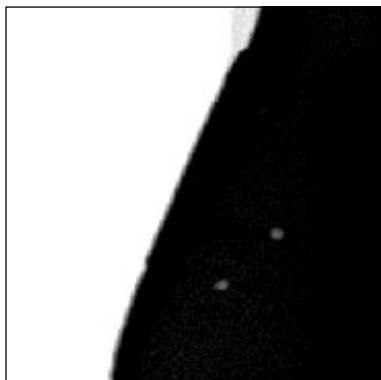
Figure 2.1 Constant force mode AFM image of a partially removed, evaporated gold (left) layer on mica (right). Scan area 5 * 5 mm², height range 200 nm. Acquisition rate: 200 ms / line.

Figure 2.1 shows the topography of the partially removed, evaporated gold layer on mica, as measured by constant force AFM. The adhesion force was measured using the adhesion mode and yielded an average of 60 nN at the hydrophilic mica surface and 21 nN at the gold surface.

Figure 2.2a shows a histogram of the height distribution of the image shown in figure 2.1. In the same plot the height distribution is compared with a tapping mode image of the same scan area. The latter was acquired with an oscillation amplitude of 200 nm. The height step at a mica gold fracture as measured by tapping mode AFM appears 9 nm less than measured with constant force mode. The stiffness of both surfaces ensures that elasticity does not affect the measurement. In order to make sure that the anomalous height measurement is indeed solely caused by adhesion the experiment was repeated with a similar, but silanized, AFM tip. The silanization took place by incubating the tip for 5 minutes in a solution of DiChlorodiMethylSilan (DCMS), which results in a covalent bond between Si_3N_4 and DCMS. This procedure reduced the adhesion forces down to 10 nN at the mica surface and 7 nN at the gold surface, while all other properties of the tip were not noticeably affected. The resulting height distributions, which were measured at another area of the sample, correspond quite well, as is shown in figure 2.2b. The difference in the average measured height step is reduced to less than 1 nm. This result proves that the height artefact is indeed exclusively caused by adhesion between the tip and the sample.

To gain more insight in the dynamics of the oscillating cantilever a few oscillations of the deflection of the cantilever have been plotted in figure 2.3. The deflection was measured with a fresh untreated tip, at the gold and the mica surface while the system was in the feedback loop. This ensured the average amplitude to be 208 nm during both experiments, corresponding to a damping of the free oscillation amplitude of 31%. In figure
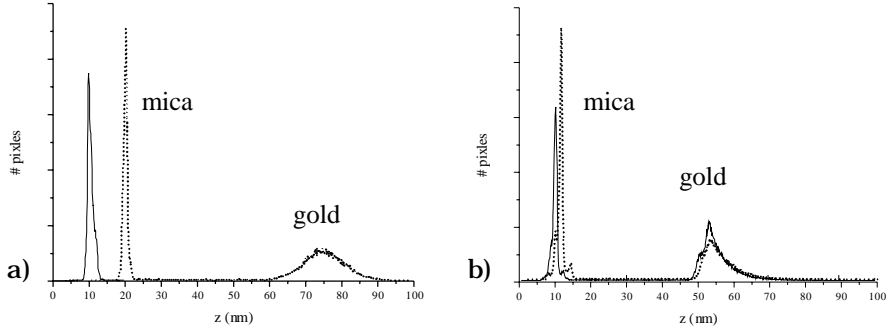
Figure 2.2 Height distributions of tapping mode image (dotted line) compared with constant force mode image (solid line) of the sample shown in figure 2.1. The histograms were shifted to a coincidence of the peak corresponding to the gold surface. The tapping amplitude was 200 nm. a) fresh Si_3N_4 tip, b) a hydrophobic tip, which reduced the adhesion force, at a different part of the sample.

2.3a the deflection of the cantilever tapping on the mica surface, which has the largest adhesion force, shows a phase shift of about 34° compared to the curve that was acquired while tapping on the gold surface. Furthermore, detailed examination of this curve reveals a small deviation of its sinusoidal shape.

The deflection at the gold surface still looks nicely sinusoidal when the damping of the free oscillation amplitude is increased to 65% in figure 2.3b. The oscillation of the cantilever tapping on the mica surface however, is severely modulated. The tip only touches the surface at the very bottom of the deflection curve. It is clear that in the case of large adhesion forces and severe damping the tip does not impact on the surface every time it moves downward. In stead, after each impact on the surface the oscillation is severely damped. Due to the high quality factor and the large damping it takes a few oscillations before the amplitude is recovered and the tip impacts on the surface again. This sequence is repeated continuously, and in order to keep a constant average amplitude, the tip has to be retracted from the sample, which accounts for the anomalous height measurement.

Next to the modulation of the sinusoidal movement of the cantilever, the phase of the oscillation is shifted backward by an average of 91° compared to tapping on the gold surface. When the damping of the free oscillation amplitude is increased from 31 to 65% the phase is hardly affected when tapping at the gold surface. In the inset of figure 2.3b it is shown that the tip touches the gold surface every oscillation period. On the mica only during one of the four shown oscillations the tip impacts on the surface. Dur-
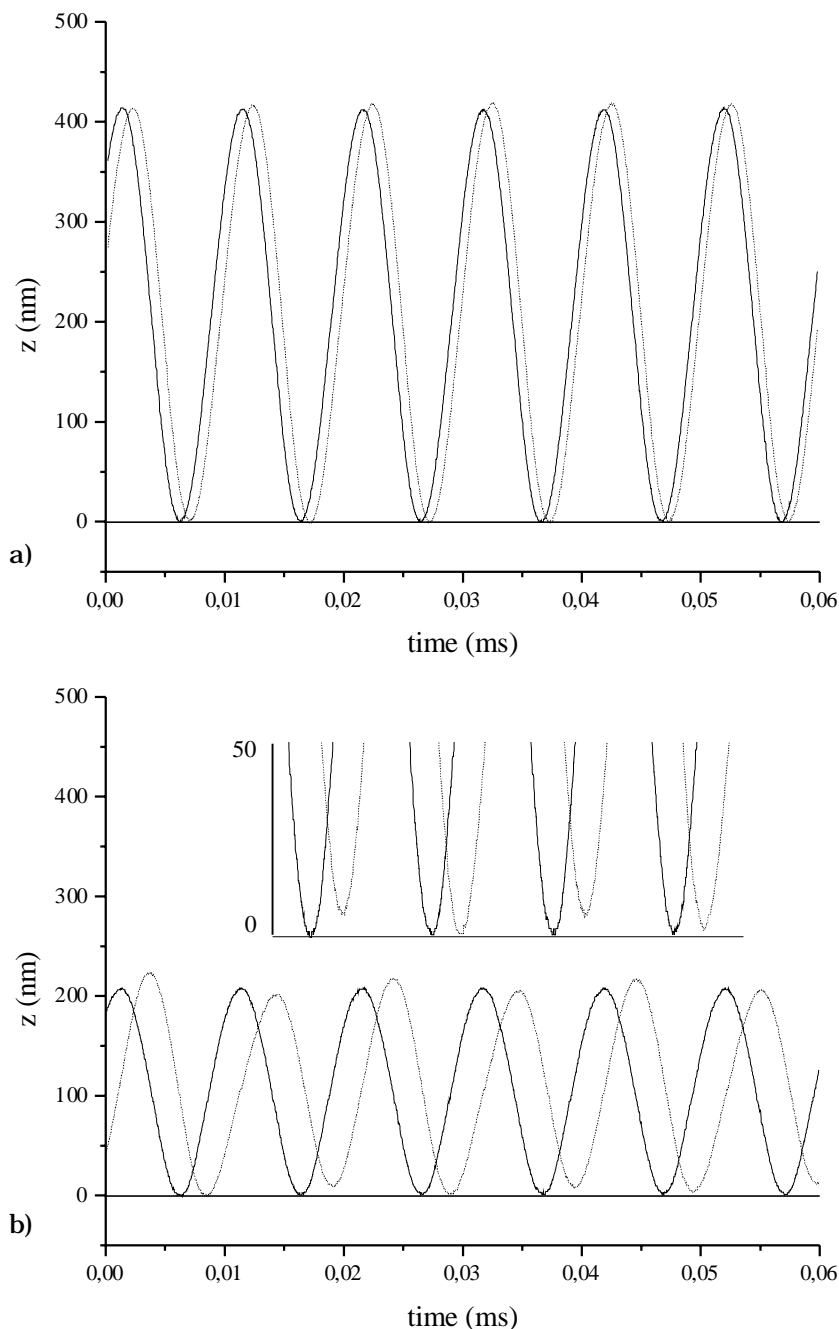
Figure 2.3 Deflection of the cantilever tapping on a hydrophobic gold surface (solid line) and a hydrophilic mica surface (dotted line). Amplitude damping a) 31%, b) 65% of the free oscillation amplitude. Data acquisition was triggered by the driver oscillation in order to match the phase of the curves. When tapping on mica with a high damping the tip does not reach the surface every oscillation period (see inset figure 2.3b), and has a severe phase lag compared to tapping on gold.

ing the intermediate periods the tip approaches the surface, but it retracts at a distance of 3 to 10 nm from it. Furthermore, on mica, a subtle variation of the phase shift of the cantilever occurs, decreasing as amplitude is gained. In the intermediate regime of damping the number of oscillation periods between impacts grows and the phase shift decreases as the damping increases (data not shown). Remarkably, when sufficient damping is applied, damping of the oscillation can also occur when the tip does not impact on the sample as can be seen in the last period of the cantilever tapping on mica. Because of the large phase shift the cantilever is driven out of phase.

Depending on the exact phase of the cantilever compared to the driver, damping and excitation continuously compete, resulting in a large modulation of the oscillatory movement.

Langmuir-Blodgett film

To study the adhesion related distortions on tapping mode AFM further, a Langmuir-Blodgett (LB) film of lignoceric acid deposited on a silicon substrate was used. Lignoceric acid is a 24 carbon saturated fatty acid naturally occurring in animal tissue. The layer was deposited at such a surface pressure that only half the surface was covered.

Figure 2.4a shows a topographic image of the LB film, measured with adhesion mode AFM. The layer thickness of the LB film yields 1.6 nm which equals the height as measured in constant force mode. The hydrophilic silicon substrate has a larger adhesion than the hydrophobic LB film which can be seen as a high intensity in figure 2.4b. The average adhesion force at the silicon substrate was 47 nN while at the LB film the adhesion force yielded 32 nN. The adhesion mode images were recorded at the end of the experiment, because using this mode the loading force was highest (100 nN). In figure 2.4 it can be seen that during a few lines the LB film was ruptured by the tip.

Figure 2.5 shows the implications the extra damping due to adhesion can have on tapping mode topography and phase images. The images represent the same area as shown in figure 2.4 and were acquired with increased damping of the oscillation. As the damping increases from 8% in figure 2.5a to 73% in figure 2.5e, the apparent height difference between the surfaces decreases and indeed in figure 2.5e the topography contrast is inverted. Cross sections of the images shown in figure 2.4 and 2.5 are plotted in figure 2.6. The average layer thickness measured in the sequential tapping mode images was 1.2, 0.8 and -0.3 nm, whereas the adhesion mode topography image show layer thickness of 1.6 nm. When the damping of
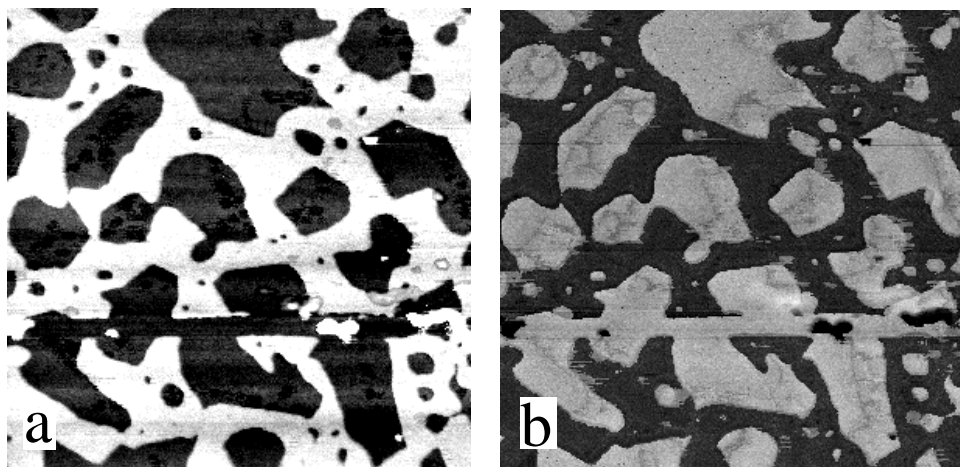
Figure 2.4 Adhesion mode AFM image of a lignoceric acid Langmuir-Blodgett film. Scan area 2 * 2 mm². a) topography, height range 2 nm, b) adhesion force, range 30 - 60 nN. Acquisition rate: 1400 ms / line. The dark areas in the topography image represent the holes in the LB film and have the highest adhesion force.

the oscillation was smallest, as shown in figure 2.5a, the most reliable height is measured. The height measured with the adhesion mode, where a loading force of 100 nN was used, matched the height measured with the constant force mode, using a loading force of 10 nN. Hence indentation is not likely to play an important role in the height anomalies.

Like the gold on mica sample the phase images of the LB film (figure 2.5b, 2.5d and 2.5f) show increasing contrast as the oscillation is damped. As the holes in the LB film have a higher adhesion, the tip sticks longer to the surface, which results in a phase shift of the cantilever oscillation. Indeed the phase correlates with differences in adhesion force when sufficient damping is used.

DNA

Finally to show the relevance of the height artefact for biological samples a plasmid DNA (pSK31) sample is shown. The DNA solved in a $MgCl_2$ buffer was precipitated on a mica surface as described previously [17]. The height of DNA appears usually a factor of two smaller than would be expected based on the crystal structure of double stranded DNA, that is shown in chapter 1. This effect is commonly attributed to indentation of the DNA [3,18]. Using non-contact AFM it was possible to measure the correct height of about 2 nm [19]. Figure 2.7 shows an image of DNA in which the damping of the oscillation is increased from top to bottom. As a result of this the
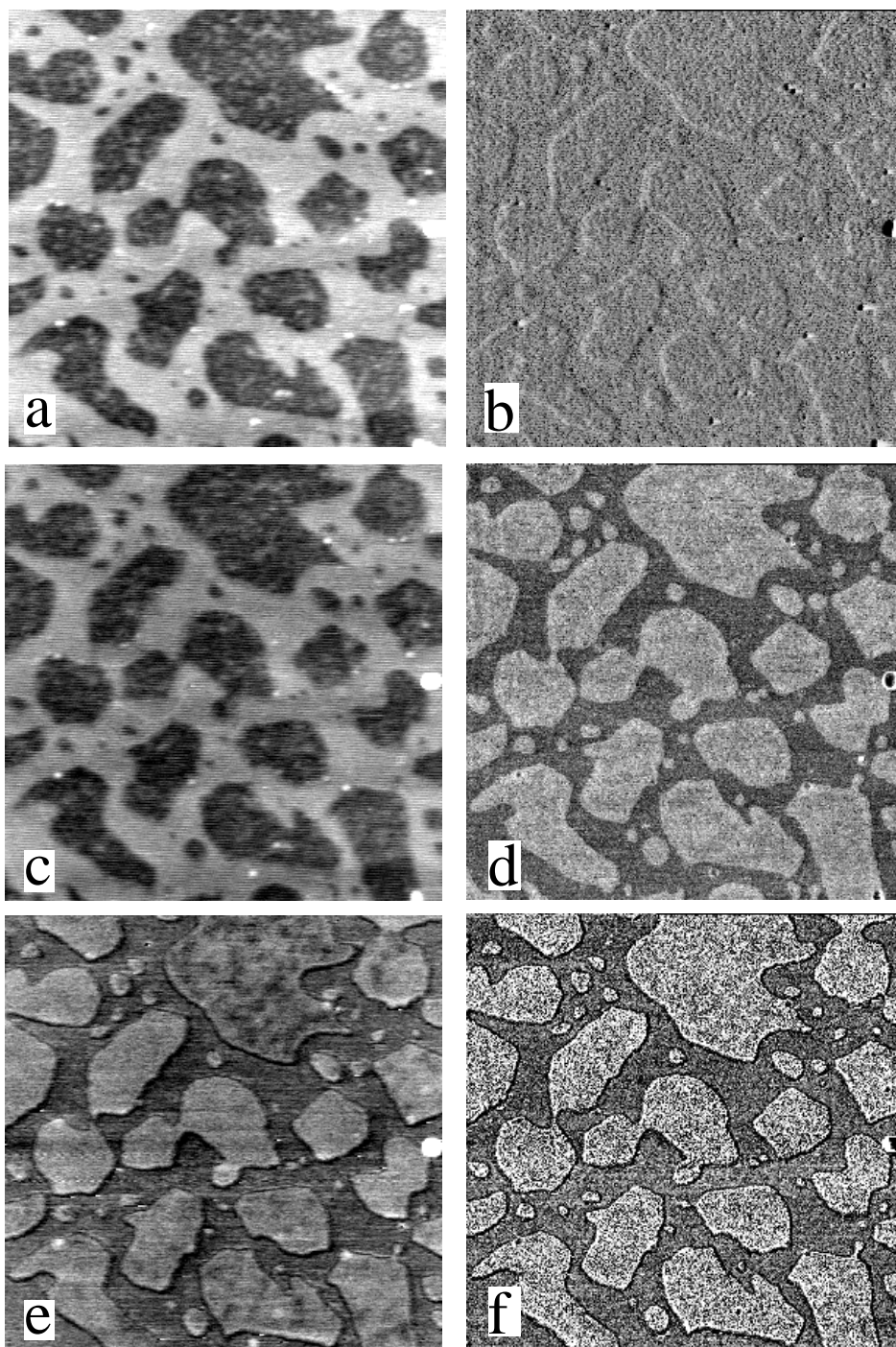
Figure 2.5 Tapping mode AFM image of a lignoceric acid Langmuir-Blodgett film. Scan area 2 * 2 ㎛². a), c) and e) topography, height range 2 nm; b), d) and f) corresponding phase, range 5°. The damping of the free oscillation (amplitude 135 nm) was increased from a) 8%, c) 31% to e) 73%. Acquisition rate: 200 ms ∕ line.
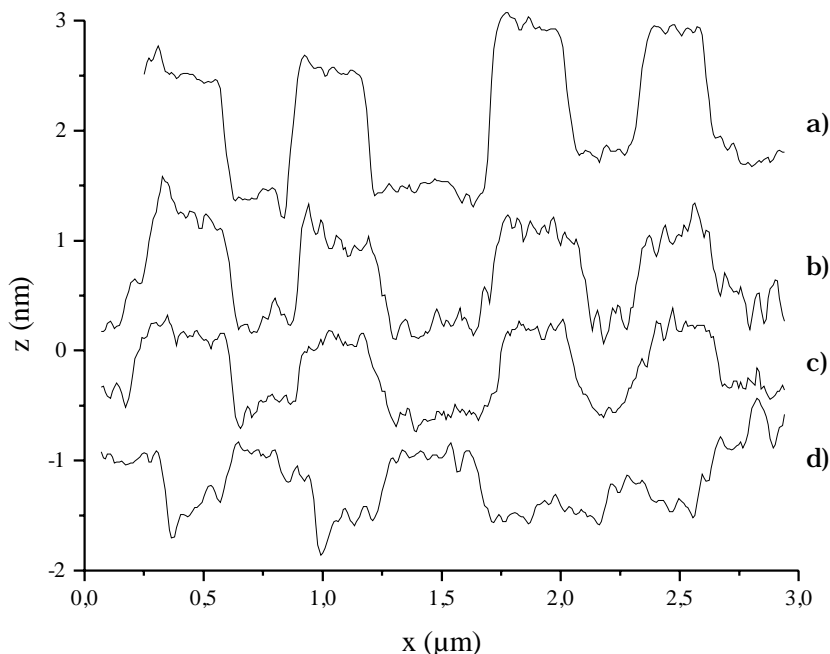
Figure 2.6. Cross sections of the lignoceric acid LB-film topography images, taken from a) figure 2.4a, b) figure 2.5a, c) figure 2.5c, and d) figure 2.5e.

height of the DNA strands decreases from +1.5 to -0.5 nm. The negative height proves that indentation of the DNA cannot exclusively account for the discrepancy in these height measurements using tapping mode.

2.5 Detailed analysis of the cantilever oscillation

In the previous section it was shown that height measurements performed with tapping mode AFM can have errors of up to 10 nm if the differences in adhesion force are sufficiently large. This is caused by a severely affected cantilever oscillation due to tip-sample adhesion. When the tip sticks to the surface after an impact, extra damping of the oscillation occurs. Because of the high Q it takes time to gain amplitude again, and the AFM system responds to the reduced amplitude by retracting the tip. Increased damping results in a larger deviation from a sinusoidal movement and thus to a larger artefact in the topography images.

This behaviour can be explained by close analysis of the dynamics of the cantilever. When the oscillation is temporarily slowed down by adhesion, due to the high Q the amplitude will be gained slower as the oscillation is
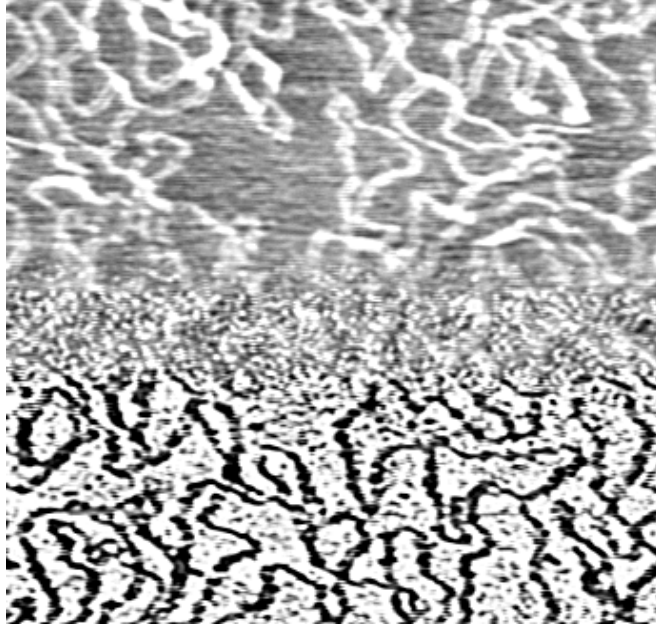
Figure 2.7 DNA plasmids on a mica surface. The damping of the oscillation was increased from top to bottom. Scan area 2 * 2 μm², height range 2 nm.

closer to free resonance. As a result of this the number of oscillations between each impact will increase as the damping is decreased, but what is more important for obtaining reliable topography data, the average deviation of amplitude is smaller. This is clearly demonstrated in figure 2.3, where little damping hardly causes a modulation of the oscillation while increased damping combined with adhesion causes a large modulation of the cantilever movement. As the deviation of the sinusoidal movement is less when little damping is applied, the error in the measured average amplitude is less, resulting in a more reliable height measurement.

The phase lag between the driving force and the oscillating cantilever can also affect the cantilever movement. In resonance the undamped cantilever is 90° out of phase compared to the driver. In the case of extreme damping and large adhesion it can occur that after an impact the cantilever is so far out of phase that the amplitude first decreases due to the out of phase excitation, and only later increases again. Phase mismatches of up to 181° are shown in figure 2.3b. Using a small damping the phase shift is less and the modulation of the oscillation will be less severe. It is expected that the use of a lock-in amplifier would only enlarge the anomaly in the apparent height, as out of phase signal does not contribute to the measured amplitude.

Distortions of the sinusoidal deflection may be expected when extra inter-action of the tip with the sample affects the cantilever movement. If the tip sticks longer to the sample and the surface is not indented, a flattening of the deflection is expected to occur. From the deflection curves in figure 2.3, however, one cannot reveal actual damping of the cantilever motion during contact. This is due to the limited bandwidth of our detection electronics, which can measure up to 500 kHz. Higher harmonics, which are necessary to describe such small distortions, are not detected by the electronics. Thus the deflection signal may not represent the fine details of the cantilever movement. In chapter 6 of this thesis a more rigorous treatment of higher harmonic distortions of the cantilever oscillation is given, then for a canti-lever tapping in liquid.

2.6 Discussion

The data presented in this study are typical for a series of deflection curves measured with different parameters like adhesion and damping. The modu-lation of the sinusoidal deflection curve is always present if the adhesion force is not negligible. The magnitude and period of the modulation how-ever decrease with increasing amplitude, indicating a reduced influence of the adhesion. However, because of the large number of parameters that influence both the adhesion force and the dynamic behaviour of the canti-lever, it was not feasible to obtain an exact relation between adhesion and height anomalies and phase of the oscillation in this experimental study. Theoretical studies of the dynamic behaviour of the cantilever in the case of grazing incidence may reveal more insight in this mechanism.

The results of a model developed by Nordmark [20] for the dynamics of grazing impact oscillators, which have been widely used both in theoretical and in experimental studies, show a variety of border collision bifurcations [20,21]. The number of oscillations per impact very sensitively depends on the characteristics of the system like driving frequency, amplitude etc. The periodic modulations of the sinusoidal movement can be stable, but truly chaotic behaviour can also occur. In macroscopic systems with a large spring constant the effect of adhesion forces between the oscillator and the border can usually be neglected. However, in AFM systems with very weak canti-levers the magnitude of the attractive adhesion force can not be neglected and the hysteresis of the interaction forces shows to be quite important in the case of grazing incidence. Though these theoretical studies do not take adhesion in account, the modulations of the sinusoidal motion that are observed are extremely sensitive for the frequency of the driver. Exact con-

trol of this parameter is not feasible in our experimental setup, but it may account for some variation in our experiments.

At a frequency far below the resonance frequency of the cantilever the mapping of adhesion force has proved very powerful to reveal information about the chemical properties of the sample [15]. Though it is hard to quantify the effect of adhesion on the phase, especially because the adhesion force may be very sensitive for the interaction time [18], qualitatively it is shown that phase contrast is related to adhesion. To reveal adhesion in the phase images of tapping mode not only reduces the acquisition time compared to mapping the adhesion at a low frequency, it also enables one to use this contrast parameter for very fragile samples which can only be scanned using this mode. On the other hand the contrast in the phase images can be minimised in order to obtain more reliable topography data in tapping mode AFM.

As a consequence of the complex dynamic behaviour of the cantilever the tip only exerts a force on the sample during the limited number of impacts on the sample. As the damping increases both the average number of impacts per oscillation and the force per impact increase as the amplitude grows faster. So small damping of the amplitude is not only preferable in order to obtain more reliable topography data , it also minimises the forces exerted on the sample and thus reduces sample damaging and indentation.

The mechanism described in this article not only applies to the relatively weak cantilevers shown in this study. Contrast inversion of DNA has also been measured using stiffer Silicon cantilevers, more commonly used for tapping mode AFM. The larger Q factor, and thus larger rise times of the oscillation amplitude make these cantilevers even more susceptible for adhesion induced height anomalies.

2.7 Conclusions

Differences in adhesion at the sample surface result in height anomalies in tapping mode AFM in air. When small features like for example LB films, DNA and proteins are the subject of research these differences can even result in negative heights. In order to explain the discrepancies careful analysis of the involved forces and the dynamics of the cantilever is necessary. Less damping of the free oscillation reduces the adhesion induced height anomalies, but some margin in the amplitude set-point is always necessary for a stable feedback loop. For more reliable topography data it

might be preferable to reduce the adhesion for example by modification of the tip.

Acknowledgements

2.8 References

1   Hansma, H. G. 1996. Atomic force microscopy of biomolecules *J. Vac. Sci. Technol. B* 14(2): 1390-1394.

2   Schabert, F. A and J. P. Rabe. 1996. Vertical dimension of hydrated biological samples in tapping mode scanning force microscopy. *Biophys. J.* 70: 1514-1520.

3   Wyman, C. E., E. Grotkopp, C. Bustamante, and H. C. M. Nelson. 1995. Determination of heat-shock transcription factor-2 stoichiometry at looped DNA complexes using scanning force microscopy. *EMBO J.* 14: 117-123.

4   Fritz, M., M. Radmacher, J. P. Cleveland, M. W. Allersma, R. J. Steward, R. Gieselmann, P. Janmey, C. F. Schmidt, and P. K. Hansma. 1995. Imaging globular and filamentous proteins in physiological buffer solutions with tapping mode atomic force microscopy. *Langmuir* 11: 3531-3535.

5   Chen, J., R. K. Workman, D. Sarid, and R. Höper. 1994. Numerical simulations of a scanning force microscope with a large-amplitude vibrating cantilever. *Nanotechnology* 5: 199-204.

6   Spatz, J. P., S. Sheiko, M. Möller, R. G. Winkler, P. Reineker, and O. Marti. 1995. Forces affecting the substrate in resonant tapping force microscopy. *Nanotechnology* 6: 40-44.

7   Radmacher, M., R. W. Tillmann, and H. E. Gaub. 1993. Imaging viscoelasticity by force modulation with the atomic force microscope. *Biophys. J.* 64: 735-742.

8   Burnham, N.A., A. J. Kulik, and G. Gremaud.1995. Nanosubharmonics: the dynamics of small nonlinear contacts. *Phys. Rev. Lett.* 74: 92-95.

9   Tamayo, J., and R. García. 1996. Deformation, contact time, and phase contrast in tapping mode scanning force microscopy. *Langmuir* 12: 4430-4435.

10 Amrein, M., Institut für Medizinische Physik und Biophysk, Universität Münster, personal communication.

11 Albrecht, T. R., P. Grutter, D. Horne, and D. Rugar. 1991. Frequency-modulation detection using high-Q cantilevers for enhanced force microscope sensitivity. *J. Appl. Phys* 69(2): 668-672.

12 Magonov, S. N. and M. Allen. Application note Digital Instruments, Inc.

13 Magonov, S. N. and V. Elings. 1997. AFM study of thermotropic structural transitions in poly(diethylsiloxane). *Polymer* 38(2): 297-307.

14 Van der Werf, K. O., C. A. J. Putman, B. G. de Grooth, F. B. Segerink, E. H. Schipper, N. F. van Hulst and J. Greve. 1993. Compact stand-alone atomic force microscope. *Rev. Sci Instrum.* 64: 2892-2897.

15 Van der Werf, K. O., C. A. J. Putman, B. G. de Grooth, and J. Greve. 1994. Adhesion force imaging in air and in liquid by adhesion mode atomic force microscopy. *Appl. Phys. Lett.* 65: 1195-1197.

16 Thundat, T., R. Warmack, D. Allison, L. Bottomley, A. Lourenco, and T. Ferrel. 1992. Atomic force microscopy of deoxyribonucleic-acid strands adsorbed on mica - the effect of humidity on apparent width and image contrast. *J. Vac, Sci. Technol. A.* 10: 630-635.

17 Vesenka, J. P., M. Guthold, C. Tang, D. Keller, E. Delaine and C. J. Bustamante. 1992. Substrate preparation for reliable imaging of DNA-molecules with the scanning force microscope. *Ultramicroscopy* 42-44: 1243-1249.

18 Yang, G., J. P. Vesenka, and C. J. Bustamante. 1995. Effects of tip-sample forces and humidity on the imaging of DNA with a scanning force microscope. *Scanning* 18: 344-350.

19 Anselmetti, D., M. Dreier, R. Lüthi, T. Richmond, E. Meyer, J. Frommer, and H.-J. Günterodt. 1994. Biological materials studied with dynamic force microscopy. *J. Vac. Sci. Technol. B* 12(3): 1500-1503.

20 Nordmark, A B. 1991. Nonperiodic motion caused by grazing incidence in an impact oscillator. *J. Sound Vib. B* 145: 279-297.

21 De Weger, J., D. Binks, J. Molenaar, and W. van de Water. 1996. Generic behaviour of grazing impact oscillators. *Phys. Rev. Lett.* 76(21): 3951-54.

Chapter 3

DNA bending by photolyase in specific and

non-specific complexes

Abstract

Specific and non-specific complexes of DNA and photolyase are visualised with Atomic Force Microscopy. As a substrate for photolyase a 1150 bp DNA restriction fragment was UV-irradiated to produce damaged sites at random positions. Using the contour length of DNA, comparison with an 800 bp undamaged DNA fragment made it possible to separate populations of specific and non-specific photolyase complexes on the 1150 bp fragment, relieving the need for highly specific substrates. Thus it was possible to compare DNA bending for specific and non-specific interactions. Non-specific complexes show no significant bending but increased rigidity compared to naked DNA, whereas specific complexes show DNA bending by 36° and higher flexibility.

3.1 Introduction

Many genome transactions require proteins to recognise and act at specific sequences or structures in DNA. Specific site recognition often requires or results in changes in DNA conformation. Analysis of DNA deformation within a specific protein-DNA complex can yield important information on the mechanism of site recognition. The flexibility of DNA complexed to protein has been suggested to play a role in site recognition and can also be expected to influence downstream biochemical reactions [1]. Within its resolution limits, Atomic Force Microscopy (AFM) studies of protein-DNA complexes yield valuable information on the global arrangement of proteins and DNA, as well as the variety and distribution of different structures in a population.

Protein induced DNA bending can easily be measured by AFM. Where comparison is possible, AFM determined bending angles agree well with those determined by X-ray crystallography and gel band shift methods [2]. However among these methods AFM uniquely reveals the flexibility of protein-DNA complexes through analysis of the distribution of the DNA bending angles.

Photolyase, a ~55 kD protein, uses near-UV or visible light (300 – 500 nm) to reverse UV-induced dimerisation of two adjacent pyrimidine bases in DNA. Photolyase binds to pyrimidine dimers with high specificity and affinity independent of the surrounding DNA sequence [3]. Based on the crystal structure of photolyase, Park et al. [4] speculated about structural features involved in binding to and repair of DNA. However, the three-dimensional structure of the photolyase-DNA complex has not yet been determined, leaving the detailed mechanism of substrate recognition and specific binding to UV-induced pyrimidine dimers in DNA largely unknown.

In this study data will be presented on the conformation of DNA when photolyase is bound at specific and non-specific sites. In our experiments UV-irradiated fragments that contain randomly located damaged sites can be distinguished from fragments that had not been irradiated, based on their contour length. Thus, populations of specific and non-specific interactions can be discriminated, relieving the need for a highly defined substrate necessary for other techniques. A direct comparison is made between the bending and flexibility of specific and non-specific complexes and naked DNA.

3.2 Theory

Sample preparation

Structural characterization of protein-DNA complexes with AFM is only reliable when the deposition process itself does not affect the conformation of the complexes [2]. Though in solution DNA obviously has a three-dimensional structure, for imaging with AFM it is necessary to deposit the complexes on a flat, two-dimensional substrate. Mica is most commonly used as a substrate for DNA deposition, using bivalent cations to bind the DNA on the surface [5]. In the case of a weak surface DNA interaction, DNA can equilibrate on the surface and is able to find its most favourable conformation. Because the electrostatic interaction responsible for DNA immobilisation is non-specific and does not depend on the bending angle, a good representation of the three-dimensional structure in the two-dimensional plane should then be expected. When the DNA surface interaction is much bigger then the protein-DNA interaction the deposition process can result in a structural change or even dissociation of the complex. In this case, local bending angles at the site of the protein-DNA complex will be dominated by the global conformation of the DNA that is formed during the deposition process and not by a local deformation caused by these proteins. Thus, for interpretation of the images weak binding conditions are necessary.

DNA surface binding forces depend on the deposition buffer that is used to deposit the DNA and pretreatment of the surface [6]. The mechanism of deposition can be characterised by evaluation of the persistence length of the DNA. For a polymer that can freely move in two dimensions the persistence length p can be obtained with:

$$p = \frac{\left\langle R^2 \right\rangle}{l} \tag{3.1}$$

where l is the contour length and R is the end-to-end distance. Both variables can easily be measured from AFM images. Strong DNA surface interactions will limit the mobility of the polymer, and the observed conformation of the DNA will resemble a projection of the three-dimensional conformation, resulting in a shorter end-to-end distance, and thus a shorter apparent persistence length.

For quantitative interpretation of the number of complexes, it is necessary that the protein-DNA complex is stable during deposition. In the case of DNA repair by photolyase (*E*) the reaction can be described as:

$$E + DNA(UV) \xrightarrow[\overset{k_2}{\longleftarrow}]{k_1} E \bullet DNA \xrightarrow{k_3, h\nu} E + DNA \qquad (3.2)$$
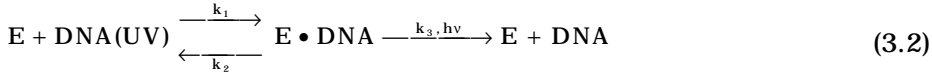
with k_n the rate constant for the corresponding reaction [3]. The stability of the complex itself may vary between incubation and deposition. For a representative measurement, incubation of the reaction should last at least $1/k_1$. Because optimal buffer conditions for this reaction do not correspond to optimum deposition conditions for DNA on mica, the reaction mixture is diluted in a low salt Mg_2Cl buffer, which may change the equilibrium. The dilution and deposition process should be done as fast as possible, shorter than $1/k_2$, to prevent dissociation. However, the lifetime of the complex in the deposition buffer may differ from the lifetime of the complex in the reaction buffer, which may decrease the number of complexes. To prevent photorepair, sample preparation can be performed in the dark until reaction products are immobilised.

DNA bending

In this report we follow Bustamante and Rivetti [2] and define a bending angle Θ as the deviation of DNA from linearity as shown in figure 3.1. DNA is a flexible polymer, and the energy necessary to bend DNA can be expressed in a Talylor series at its position of minimum energy:

$$E(\Theta) = E(\langle\Theta\rangle) + \tfrac{1}{2}\left(\frac{\partial^2 E(\Theta)}{\partial\Theta^2}\right)_{\Theta=\langle\Theta\rangle} \left(\Theta - \langle\Theta\rangle\right)^2 + ... \qquad (3.3)$$

Neglecting higher order terms, the energy to bend the DNA by an angle Θ can be expressed as:

$$\Delta E(\Theta) = \tfrac{1}{2}k\left(\Theta - \langle\Theta\rangle\right)^2$$
$$k \equiv \left.\frac{\partial^2 E(\Theta)}{\partial\Theta^2}\right|_{\Theta=\langle\Theta\rangle} \qquad (3.4)$$

using a spring constant k in analogy with a harmonic oscillator. From equation 3.4, and assuming a Boltzmann distribution, the normalised angle distribution function $P(\Theta)$ can be obtained:

$$P(\Theta) = \sqrt{\frac{k}{2\pi k_b T}}\ e^{-\frac{k\left(\Theta-\langle\Theta\rangle\right)^2}{2k_b T}} \qquad (3.5)$$
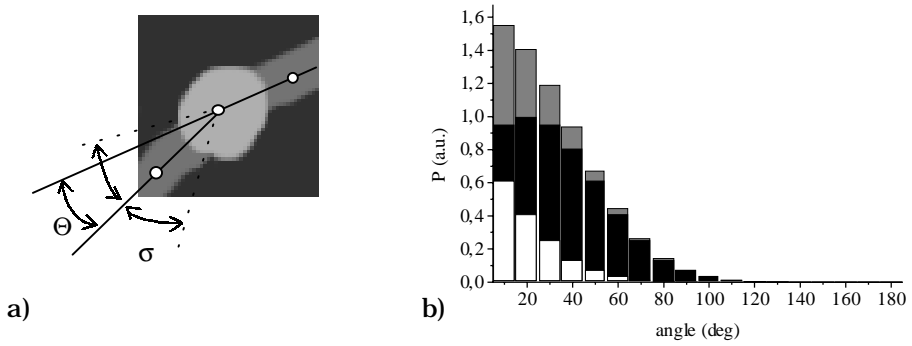
Figure 3.1 a) Schematic drawing of the bending angle determination. The bending angle Θ is measured as the deviation from linearity of three points along the trajectory of the DNA molecule, located at the centre of the protein and 15 nm up and down stream of the centre of the protein. The points are printed as white dots, and in this example $\Theta = 20°$. The flexibility of the complex is represented by the dotted lines that show the standard deviation $\sigma = 30°$. b) the corresponding angle distribution, plotted in black. Because only positive angles are measured, the angle distribution is reflected at $\Theta = 0$, white bars, and the measured distribution is the sum of the black and the white area. The summed distribution, plotted in grey bars, would result in an erroneous fit of a gaussian distribution of $\Theta = 5 \pm 35°$.

with temperature T and Boltzmann constant k_b. For an unperturbed DNA strand the distribution will be isotropic, resulting in an average angle $<\Theta> = 0$. The width of the angle distribution, σ is characteristic for the rigidity of the complex, following the relation

$$\sigma^2 = \frac{k_b T}{k} \tag{3.6}$$

Because of the limited resolution, the exact conformation of the Protein-DNA contact site can not be resolved and the measured angle will be a result of both the flexibility of the protein-DNA complex and the DNA arms themselves. Within the persistence length of DNA however, deviations from linearity of the molecule are dominated by protein induced deformations. For a naked DNA molecule with persistence length p, the angle distribution measured between three points on the chain, separated by a distance l can be approximated for small l by:

$$\sigma^2 = \frac{\frac{1}{2} l}{p} \tag{3.7}$$

From AFM topography images the bending angle is obtained by measurement of the deviation from linearity of the DNA at the position of the complex. Using this definition of the bending angle, only absolute values of Θ are obtained. Therefore the angle distribution will be truncated at $\Theta = 0$, see figure 3.1b, resulting in a broadened shape of the distribution that should not be confused with decreased rigidity of the complex. To describe the obtained angle distribution correctly the distribution should be fitted by:

$$P(\Theta) = Ae^{-\frac{(\Theta - \langle \Theta \rangle)^2}{2\sigma^2}} + Ae^{-\frac{(\Theta + \langle \Theta \rangle)^2}{2\sigma^2}} \tag{3.8}$$

where A denotes a normalization constant.

3.3 Materials and methods

Sample preparation

DNA photolyase from *Anacystis nidulans* was purified to apparent homogeneity as described previously [7]. As a substrate for photolyase 1150 bp DNA was irradiated with ~3800 J/m² UV (254 nm) introducing damage, mainly pyrimidine dimers, at random sites. In the reaction mixture consisting of 100 mM NaCl, 4 mM Hepes pH 6.5, 5 mM $MgCl_2$, 1 mM β-mercaptoethanol, 8.0 µg/ml of the damaged fragment was mixed with 4.8 µg/ml of an 800 bp restriction fragment and 0.45 µg/ml photolyase to a final volume of 10 µl. After 10 min the reaction mixture was diluted 10 times in deposition buffer, consisting of 20 mM Hepes pH 6.5, 5 mM $MgCl_2$, 1 mM β-mercaptoethanol. Within one minute a 5 µl drop was pipetted onto a freshly cleaved mica disk and after ~ 30 s rinsed with water and blown dry with nitrogen gas. To prevent photorepair before immobilisation, all sample manipulation was performed in the dark.

AFM setup

Triangular Si_3N_4 cantilevers purchased from Park Scientific instruments (Sunnyvale, Ca, USA), with a spring constant of 0.5 N/m and a resonance frequency of 110 kHz, were used in a home built AFM [8]. Images with a scan area of 2 x 2 µm², 512 x 512 pixels, were acquired in tapping mode, using a free peak-peak amplitude of 200 nm, an amplitude set-point of 180 nm and a pixel rate of 6 kHz.

Image processing and data analysis

AFM data were processed using Interactive Data Language (RSI, Co, USA) in a self-written software package. Standard image processing consisted of line subtraction by fitting of a 2nd-order polynomial to each line in the image. The contours of DNA molecules were hand-traced by selection of 2 to 8 points along a DNA strand, using an algorithm similar to the one described by Rivetti et al. [6]. Proteins were manually selected. Because tip-sample convolution limits the resolution of AFM images, the DNA strand can only be resolved about 10 nm from the centre of the protein. Bending angles were determined following the procedure schematically drawn in figure 3.1. The measured bending angle distributions were fitted with equation 3.8.

3.4 Results

A typical AFM image of photolyase-DNA complexes is shown in figure 3.2a. Photolyase appears as 3 nm high globular structures on DNA molecules. As previously described in chapter 2, the height of tapping mode AFM images is not very accurate, depending on tip surface interaction and feedback settings [9], which explains the discrepancy between theoretical and observed height of the DNA and the protein. On both 1150 bp and 800 bp restriction fragments photolyase molecules are observed. Figure 3.2b shows a zoom of an undamaged, 800 bp molecule, figure 3.2c shows an UV-irradiated 1150 bp DNA fragment. The latter fragment is longer, and contains more photolyase molecules.

The contour length of all DNA molecules was determined by hand tracing, and the resulting contour length distribution is plotted in figure 3.3. Two peaks at 252 and 366 nm, corresponding to 800 and 1150 bp, are clearly resolved. Thus UV-damaged DNA fragments can be clearly distinguished from undamaged DNA fragments based on their contour lengths. For the rest of this analysis fragments with measured contour lengths smaller than 300 nm were classified as non-damaged, fragments longer than 330 nm were classified as UV irradiated.

Table 3.1 Summary of the number of photolyase-DNA complexes found on undamaged and UV-damaged DNA fragments.

	UV	# phot.	#DNA	phot. / DNA	# phot. / kb
800 bp	-	396	220	1.8	2.3
1150 bp	+	1544	432	3.6	3.1
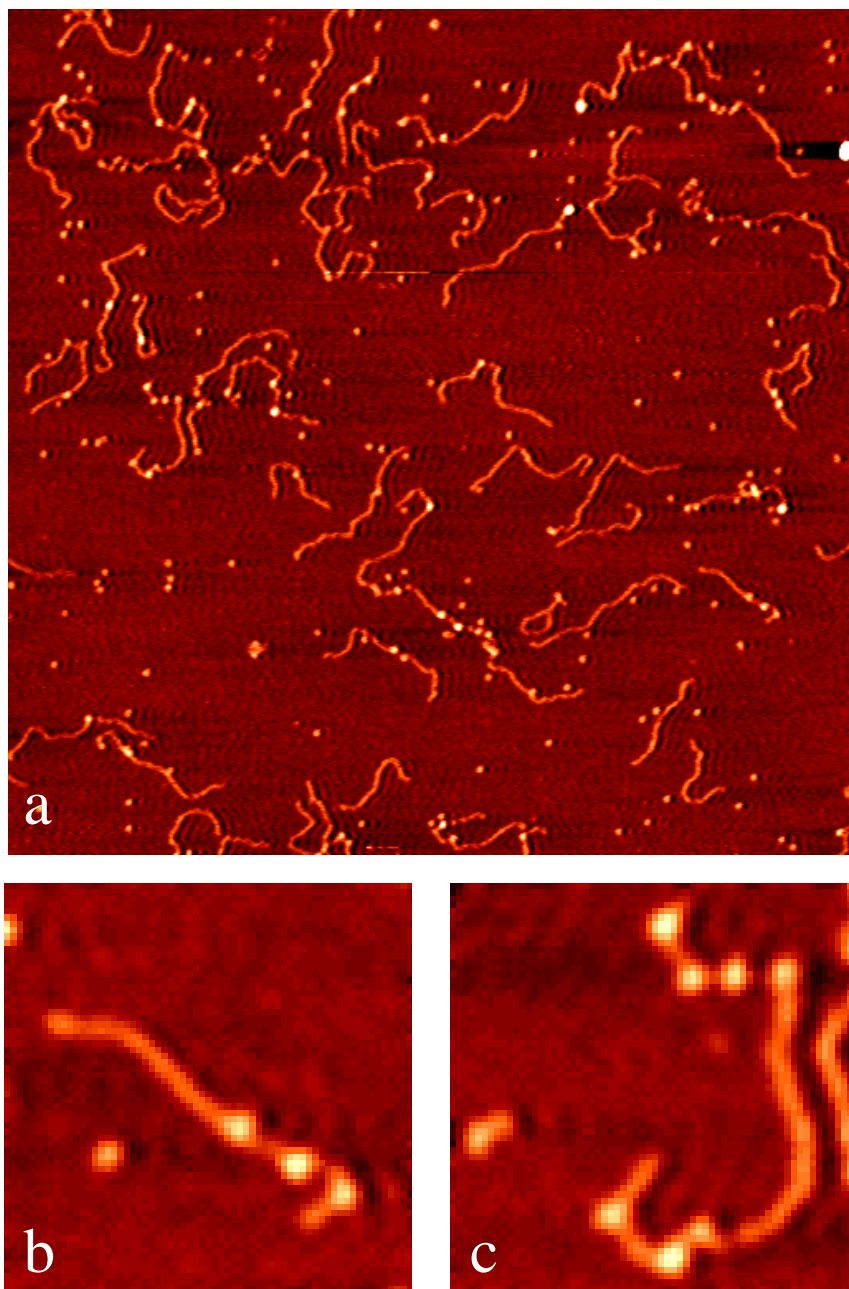
Figure 3.2 a) an AFM image of reaction mixture of photolyase, 800 bp and 1150 bp restriction fragments, scan area 2*2 μm², height range 4 nm. The 1150 bp restriction fragments were irradiated with UV before deposition. b) software zoom of an 800 bp DNA fragment with photolyase. c) software zoom of a 1150 bp DNA fragment with photolyase, scan area 250 * 250 nm². The latter fragment is clearly longer, and contains more photolyase molecules.

The number of photolyase-DNA complexes on both DNA fragments is listed in table 3.1. We expect the same number of non-specific complexes per kb on both damaged and non-damaged fragments. Thus 74 % of the photolyase molecules bound to UV-irradiated fragments are non-specific complexes, resulting in an average of 0.9 specific complexes per 1150 bp DNA fragment. Assuming a complex dissociation constant $K_d \sim 10^{-8}$ [3], half of the damaged sites are expected to be occupied by photolyase in the reaction buffer, and the number of damaged sites can be estimated to be ~2 per 1150 bp molecule. This number is approximately 10 times less than we expected based on the UV dose the DNA was exposed to. However, in the dilution step that is necessary for immobilisation of DNA on mica, specific complexes may have dissociated, causing an underestimation of the number of damaged sites (see discussion). Because the 800 bp fragment is used as an internal reference, our characterisation of specifically bound photolyase protein on damaged DNA will not be influenced by the likelihood that not all damaged DNA sites are bound.

The ability for DNA to diffuse over the surface was checked by measurement of the persistence length of undamaged DNA molecules that did not contain any photolyase molecules. DNA molecules that can diffuse over the surface are expected to have a persistence length of 53 nm, which is also found for DNA in solution [10]. For DNA molecules that can not diffuse over the surface a much smaller persistence length has been measured [6]. Using equation 3.2 we found a persistence length of 56 nm measured for 45 undamaged DNA fragments. This shows that under the conditions used, DNA is able to diffuse freely to find the energetically most favourable conformation. Thus, immobilisation of DNA photolyase complexes is not expected to have perturbed protein induced bending of DNA.

The bending angle of all the complexes located more than 15 nm from a DNA end was measured. Distributions of bending angles on both fragments
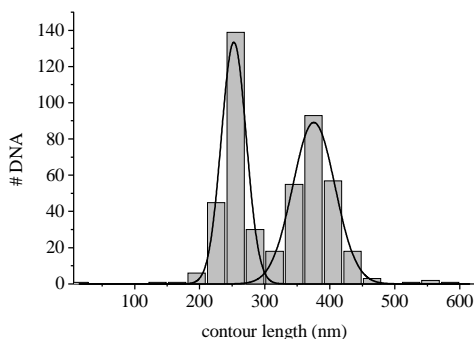
Figure 3.3 Measured contour length distribution of a mixture of 800 and 1150 bp restriction fragments. Solid lines show gaussian fit of two peaks, resulting in 252 ± 36 nm for the smaller fragment and 366 ± 64 nm for the longer fragment.

are shown in figure 3.4a and 3.4b. On 800 bp fragments all complexes are non-specific photolyase-DNA interactions. When fitted with equation 3.8 a bending angle of 0 ± 18° was measured for these non-specific complexes.

On 1150 bp fragments a much broader distribution of bending angles is measured, originating from both specific and non-specific interactions. The bending angle distribution of specific complexes can be obtained by subtraction of the contribution of non-specific complexes from the angle distribution on 1150 bp DNA fragments. In this experiment 74% of the complexes on 1150 bp DNA fragments are non-specific. Thus the fitted distribution of non-specific complexes was divided by the number of complexes that contributed to figure 3.4a. This distribution was multiplied by 0.74 times the number of complexes contributing to figure 3.4b and subtracted from it. The result represents the bending angle distribution of specific photolyase-DNA complexes and is plotted in figure 3.4c. The fit of this distribution reveals an average bending angle of 36 ± 30°.

For comparison, the bending angle of DNA at random positions at least 50 nm away from a complexed photolyase was also measured, shown in figure 3.4d, resulting in an angle of 0 ± 24°. As expected no bending of DNA is measured.

The standard deviation of the bending angle distribution does not represent the error in the measurement, but is proportional to the flexibility of the structure following equation 3.5. The flexibility of a DNA molecule is characterised by its persistence length and the standard deviation of the bending angle can be related to this persistence length using equation 3.7. The standard deviation of the angle distribution of unbound DNA amounted 24°, which is slightly more than 21° that can be expected based on a persistence length found by measurement of the end-to-end distance.

For protein-DNA complexes the standard deviation of the bending angle reflects the flexibility of the protein-DNA complex. However, because of resolution limitations, we could only measure the bending angle over 30 nm, a much bigger range than photolyase can cover. The flexibility of the DNA extending from the protein will add to the standard deviation, resulting in a broader angle distribution than that of the complex itself. The measured average angle however, is not affected. The standard deviation of the bending angle of protein-DNA complexes can be compared with that of unbound DNA. The results of the bending angle measurement are summarised in table 3.2. Both the decrease in standard deviation of the non-specific and the increase of the standard deviation of the specific complex relative to naked DNA are statistically relevant with a confidence level of more than 99.9%. Thus in non-specific complexes photolyase decreases the flexibility
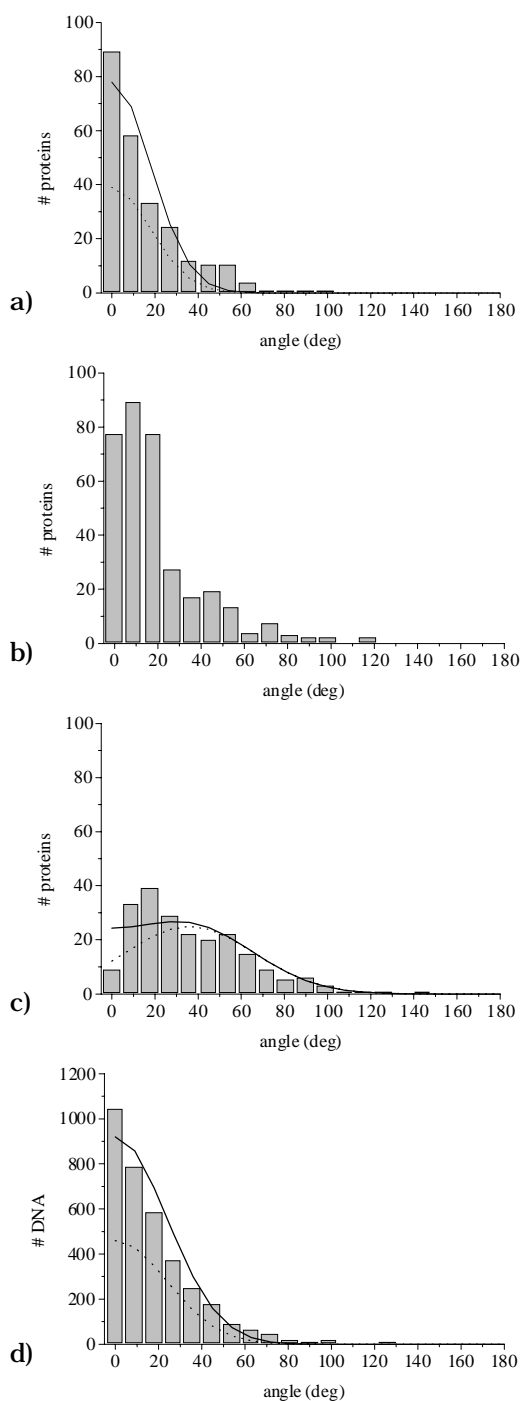
Figure 3.4 Bending angle distributions of photolyase-DNA complexes and naked DNA. Solid line represents fit using equation 3.8. Dotted line represents gaussian distribution of equation 3.6, using the fitted average angle and standard deviation of equation 3.8. a) non-specific complexes on 800 bp DNA. b) mixture of specific and non-specific complexes on 1150 bp DNA. c) specific complexes on 1150 bp DNA obtained by subtraction figure 3.4b by of the distribution obtained from figure 3.4a, corrected for size and number of complexes. Figure 3.4d plots a reference angle distribution of DNA on random positions on the DNA strand.

of DNA, but in specific complexes DNA appears more flexible than unbound DNA.

Table 3.2 Summary of the bending angle distribution, as fitted with equation 3.8, for specific and non-specific photolyase-DNA complexes and for naked DNA.

	$<\Theta>$ (deg)	σ (deg)	n
Non-specific complex	0	18	321
Specific complex	36	30	328
Reference DNA	0	24	3656

3.5 Discussion

We have visualised photolyase-DNA complexes with AFM in air and ana-lysed the global conformation of these complexes. By comparing damaged with undamaged DNA it was possible to discriminate between distributions of specific and non-specific interactions using DNA fragments of different size. It is shown that DNA in the reported experiments was able to equili-brate on the surface, which points at weak DNA surface interactions. Thus the deposition process itself can be expected to have little influence on the number of interactions and the conformation of photolyase-DNA complexes. Recently, a number of studies on the structure of *E. coli* photolyase and its interaction with DNA have been reported in literature [3,4,10,11]. Because of the large degree of similarity with *A. nidulans* photolyase [12], we relate some of these results with the data in this chapter. In contrast to Sancar et al. [13], who imaged individual *E. coli* photolyase-DNA complexes by elec-tron microscopy, we observed a significant number of non-specific com-plexes. The difference may be explained by the different preparation proto-col. For an optimal measurement the AFM image should represent the equi-librium state of the reaction. The association rate constant k_1 for specific complexes is in the range of 10^6–10^7 M^{-1} s^{-1} [3] thus 10 min. incubation should be enough to reach equilibrium. Before DNA immobilisation on mica, the reaction mixture was diluted 10 times in a low salt deposition buffer. In general, low salt conditions enhance non-specific complexes and dilution in this buffer may have increased the number of non-specific complexes. The dissociation rate of specific complexes, k_2 was estimated to be $2 \cdot 10^{-2}$ to $6 \cdot 10^{-4}$ s^{-1} for *E. coli* photolyase [13], but can range up to 0.48 s^{-1} for *S. griseus* photolyase [14], and it may also vary with different buffer condi-tions. When the lifetime of the complexes is in the range of the time neces-sary for dilution and deposition, dissociation of specific complexes is very

a)

b)

c)
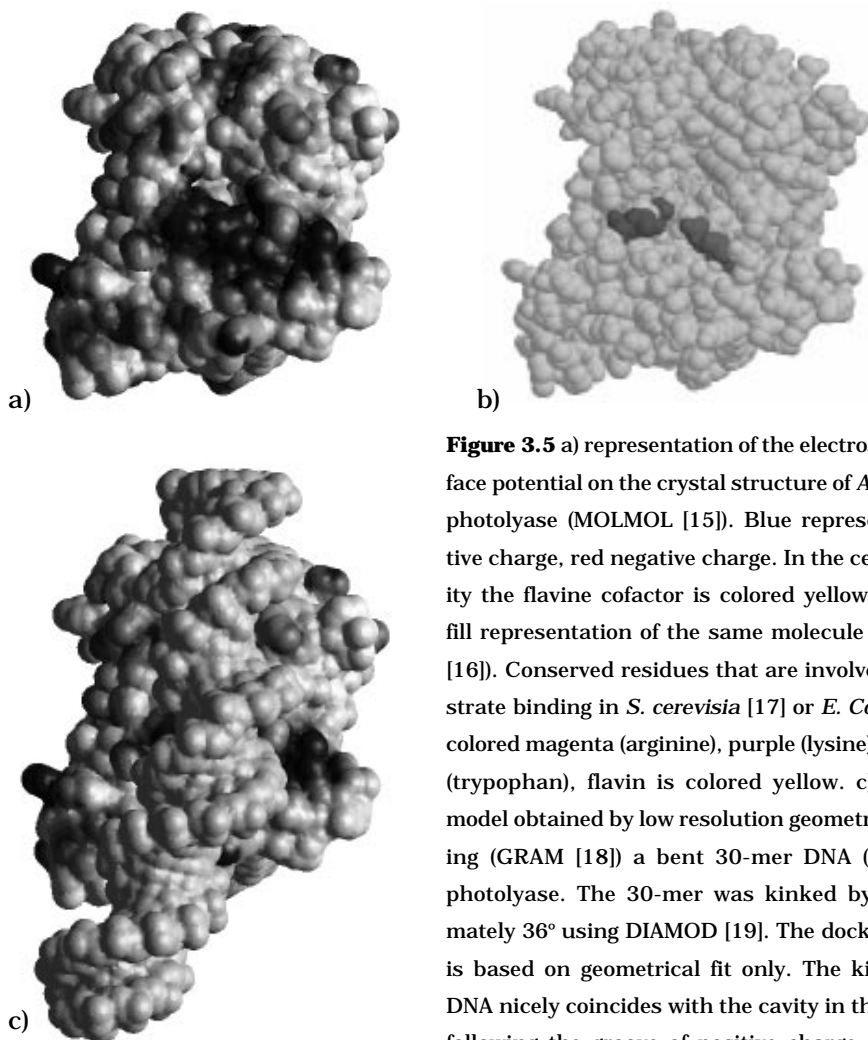
Figure 3.5 a) representation of the electrostatic surface potential on the crystal structure of *A. Nidulans* photolyase (MOLMOL [15]). Blue represents positive charge, red negative charge. In the central cavity the flavine cofactor is colored yellow. b) space fill representation of the same molecule (RASMOL [16]). Conserved residues that are involved in substrate binding in *S. cerevisia* [17] or *E. Coli* [11] are colored magenta (arginine), purple (lysine) and cyan (trypophan), flavin is colored yellow. c) putative model obtained by low resolution geometrical docking (GRAM [18]) a bent 30-mer DNA (green) on photolyase. The 30-mer was kinked by approximately 36° using DIAMOD [19]. The docking model is based on geometrical fit only. The kink in the DNA nicely coincides with the cavity in the protein, following the groove of positive charge, and is in close proximity to the conserverd residues. Docking of a non-bent and a 45° bent DNA fragment did not result in a preferential position near the cavity.

likely and may account for the differences. Indeed for *E. coli* RNA polymerase it has been shown experimentally that the number of specific complexes decreases when rinsing protein-DNA samples thoroughly before drying [20]. The number of specific interactions and therefore the estimated number of damaged sites on UV-irradiated DNA fragments will be underestimated if dissociation during sample preparation is not taken into account. In non-specific complexes photolyase does not bend DNA. This observation is in contrast to Cro protein [21] and other sequence specific DNA binding proteins that have been studied [2], which bend DNA when bound to spe-

cific and non-specific sequences. DNA bound by protein is expected to have less conformational freedom, and hence to be more rigid than naked DNA. The narrower bending angle distribution, and thus increased rigidity of non-specific complexes suggests close contact between DNA and photolyase over several nanometers. It is interesting to compare this result with the reaction mechanism proposed by Park et al. [3] when they presented the crystal structure of photolyase. DNA is suggested to bind to the flat surface of the helical domain with the phosphate backbone of one strand following a trace of positive electrostatic potential that runs across this surface. Consistent with this model, the measured decrease in standard deviation of 6° indicates that the DNA molecule is rigid over a range of about the size of a photolyase molecule. A longer interaction range would require DNA to be wrapped around photolyase, introducing a bend of the DNA, which is not observed.

Usually, the extent of DNA covered by protein is studied using footprinting techniques. Footprinting however, can not be used for non-specific complexes as no unique binding site can be defined. Based on AFM data we suggest that photolyase binds to DNA over several nanometers, without distorting the structure of DNA. From this data, it is tempting to suggest a mechanism of photolyase diffusion over DNA through the groove in the protein, to find damaged sites. AFM measurements in liquid, that will be discussed in chapter 4, indeed show one-dimensional movement along DNA strands [22].

Recently the structure of a duplex DNA dodecamer containing a cyclobutane thymine dimer was determined by NMR [23]. It is shown that a thymine dimer introduces a small bend of 7° in the DNA molecule. Such small distortions in the DNA structure are not likely to be distinguished using AFM. Indeed, in the experiments no obvious changes in conformation, like sharp kinks, were observed on the 1150 bp fragments.

We showed that photolyase bends DNA by 36° when bound to damaged sites. The 36° bending angle of photolyase at damaged sites may include a slight intrinsic bend of the damaged site, but is likely to be mainly protein induced.

In specific complexes four to five phosphates on the damaged strand around the dimer contact photolyase in the groove of positive electrostatic charge, as measured by footprinting [10] and site specific mutation experiments [11]. In the centre of this groove is a hole that has the right dimensions and polarity to include a thymine dimer that has been flipped out of the DNA helix, see figure 3.5a and 3.5b. At the heart of the protein the pyrimidine

dimer can approach the central flavin cofactor close enough to allow electron transfer, necessary for the dimer splitting reaction.

Our observation that DNA is significantly bent by photolyase in specific complexes is consistent with a structure where the damaged bases are flipped out of the DNA helix into a pocket in the protein. So far, two examples of DNA repair enzymes that bind to bases flipped out of the DNA helix have been reported. The damaged nucleotide acted on by human 3-methyl adenine DNA glycosylase is isolated out of the DNA helix, and is bent by 22° at this point [24]. T4 endonuclease V, that cuts a DNA strand next to pyrimidine dimers, also binds to an extra helical base, but in this case a nucleotide from the strand opposite to the damaged strand is flipped out of the helix. Damaged DNA in complex with T4 endonuclease V is bent by 60° [25]. Preliminary docking simulations, using a 36° bent DNA strand, show that the kink in the DNA fragment nicely coincides with the cavity in photolyase, as can be seen in figure 3.5c. These docking simulation are solely based on geometrical fitting. Both non-bent and 45 degree bent DNA fragments did not result in a good fit at a location near the cavity. Global comparison with the electrostatic surface potential of the protein and comparison with the location of residues that are known to play an important role in substrate recognition, shows that also on these grounds a good fit is obtained. However, these simulations are very speculative and we have no evidence that DNA actually follows this path over the protein, or that this would necessarily cause the bend of the trajectory of DNA outside the complex that we measured. Clarification of the exact structure must await high resolution structure determination of the damaged DNA-photolyase cocrystal.

The increased flexibility of DNA that we observe in specific complexes was initially puzzling, as one would expect that bound protein would restrict the conformational freedom of DNA. However, this result could be accounted for by the model with the thymine dimer is flipped out of the helix. It is difficult to predict the precise structural consequences this would have for the DNA, but it obviously necessitates leaving two unpaired bases on the opposite strand. Recently, Rivetti et al. [26] have shown that even a single base gap in a double stranded DNA molecule greatly increases the flexibility, characterised by a decrease in persistence length from 53 to 1.7 nm. Though unpaired bases are not the same as a gap we may expect some increase in flexibility of the DNA. Photolyase is a relatively small protein of approximately 5 nm in diameter, and is unlikely to secure both strands above and below the damaged site. Thus extra flexibility of the DNA due to unpaired bases would be evident, even in the complex.

3.6 Conclusions

By using undamaged and damaged DNA fragments with different length, populations of specific and non specific protein-DNA complexes can easily be discriminated. While other techniques require highly specific substrates for the study of protein-DNA interactions, we present an approach using AFM that is far less demanding for sample preparation. In addition it is possible to compare the structure of proteins bound to specific and non-specific sites in the same sample, thus formed under identical conditions. We have shown that photolyase induces DNA bending only when bound to specific sites, whereas non-specific complexes do not bend DNA. At non-specific interaction sites DNA is shown to be more rigid than unbound DNA, while in specific complexes DNA appears more flexible.

3.7 References

1   Schepartz, A. 1995. Nonspecific DNA bending and the specificity of protein-DNA interactions. *Science* 269: 989-990.

2   Bustamante, C., C. Rivetti. 1996. Visualizing protein-nucleic acid interactions on a large scale with the scanning force microscope. *Annu. Rev. Biophys. Biomol. Struct.* 25: 395-429.

3   Sancar, A. 1994. Structure and function of DNA photolyase. *Biochemistry* 33: 2-9.

4   Park, H.-W., S.-T Kim, A. Sancar, and J. Deisenhofer. 1995. Crystal structure of DNA photolyase from Escherichia coli. *Science* 268:1866-1872.

5   Hansma, H. G., and D. E. Laney. 1996. DNA binding correlates with cationic radius: assay by atomic force microscopy. *Biophys. J.* 70: 1933-1939.

6   Rivetti, C., M. Guthold, C. Bustamante. 1996. Scanning force microscopy of DNA deposited onto mica, equlibrium versus kinetic trapping studied by statistical polymer chain analysis. *J. Mol. Biol.* 264: 919-932.

7   Eker, A.P.M., P. Kooiman, J.K.C. Hessels, and A. Yasui. 1990. DNA photoreactivating enzyme from the cyanobacterium Anacystis nidulans. *J. Biol. Chem.* 265: 8009-815.

8   Van der Werf, K.O., C.A. Putman, B. G. de Grooth, F.B. Segerink, E.H. Schipper, N. F. van Hulst, and J. Greve. 1993. Compact stand-alone atomic force microscope. *Rev. Sci. Instr.* 64: 2892-2897.

9   Van Noort, S.J.T., K.O. van der Werf, B. G. de Grooth, N. F. van Hulst, and J. Greve. 1997. Height anomalies in tapping mode atomic force microscopy in air caused by adhesion. *Ultramicroscopy* 69: 117-127.

10 Husain, I., G. B. Sancar, S.R. Holbrook, and A. Sancar. 1987. Mechanism of damage recognition by Escherichia coli DNA photolyase. *J. Biol. Chem.* 262: 13188-13197.

11 Van de Berg, B.J. and G. B. Sancar. 1998. Evidence for dinucleotide flipping by DNA photolyase. *J. Biol. Chem.* 273: 20276-20284.

12 Tamada, T., K. Kitadokoro, Y. Higuchi, K. Inaka, A. Yasui, P.E. de Ruiter, A.P.M. Eker, and K. Miki. 1997. Crystal structure of DNA photolyase from Anacystus nidulans. *Nature Stuct. Biol.* 4: 887-891.

13 Sancar, G. B., F. W. Smith, R. Reid, G. Payne, M. Levy, and A. Sancar. 1987. Action mechanism of Escherichia coli DNA photolyase, *J. Biol. Chem.* 262: 478-485.

14 Eker, A. P. M., J. K. C. Hessels, and R. H. Dekker. 1986. Photoreactivating enzyme from Streptomyces griseus VI. Action spectrum and kinetics of photoreactivantion. *Photochem. Photobiol.* 44: 197-205.

15 Koradi, R., Billeter, M., and Wüthrich, K. 1996. MOLMOL: a program for display and analysis of macromolecular structures. *J. Mol. Graph.* 14: 51-55.

16 Sayle, R. A., and Milner-White E.J. 1995. RASMOL: biomolecular graphics for all. *Trends Biochem. Sci.* 20:374.

17 Bear, E. E., and Snacar, G. B. 1993. The role of conserved aminoacids in substrate binding and discrimination by photolyase. *J. Biol. Chem.* 268: 16717-16724.

18 Vakser, I.A.1996. Low-resolution docking: prediction of complexes for underdetermined structures. *Biopolymers* 39: 455-464.

19 Dlakic, M., and Harrington, R.E. 1998. DIAMOD: display and modeling of DNA bending. *Bioinformatics* 14: 326-331.

20 Schulz, A., N. Mücke, J. Langowski, and K. Rippe. 1998. Scanning force microscopy of Escherichia coli RNA Polemerase σ^{54} holoenzyme complexes with DNA in buffer and in air. *J. Mol. Biol.* 283: 821-836.

21 Erie, D.A., G.Yang, H.C. Schultz, C. Bustamante. 1994. DNA bending by Cro protein in specific and nonspecific complexes: implications for protein site recognition and specifity. *Science* 266: 1562-1566.

22 Van Noort, S.J.T., K.O. van der Werf, A.P.M. Eker,C. Wyman, B.G. de Grooth, N.F. van Hulst, and J. Greve. 1998. Direct visualisation of dynamic protein-DNA interactions with a dedicated Atomic Force Microscope. *Biophys. J.* 74: 2840-2849.

23 McAteer, K., Y. Jing, J. Kao, J.-S. Taylor, and M. A. Kennedy. 1998. Solution-state structure of a DNA dodecamer duplex containing cis-syn thymine cyclobutane dimer, the major UV product of DNA. *J. Mol. Biol.* 282:1013-1032.

24 Lau, A. Y., O. D. Schärer, L. Samson, G. L. Verdine, and T. Ellenberger. 1998. Crystal structure of a human alkylbase-DNA repair enzyme complexed to DNA: mechanisms for nucleotide flipping and base excision. *Cell* 95:2 49-258.

25 Vassylyev, D. G., T. Kashiwagi, Y. Mikami, M. Ariyoshi, S. Iwai, E. Ohtsuka, and K. Morikawa. 1995. Atomic model of a pyrimidine dimer excision repaire enzyme complexed with a DNA substrate: structural basis for damaged DNA recognition. *Cell* 83:773-782.

21 Rivetti, C., C. Walker, and C. Bustamante 1998. Polymer Chain Statistics and Conformational analysis of DNA molecules with bends or sections of different flexibility. *J. Mol. Biol.* 280:41-59.

Chapter 4

Direct visualization of dynamic protein-DNA

interactions

Abstract

Photolyase DNA interactions and the annealing of restriction fragment ends are directly visualised with the Atomic Force Microscope. To be able to interact with proteins, DNA must be loosely bound to the surface. When $MgCl_2$ is used to immobilise DNA to mica, DNA is attached to the surface at distinct sites. The pieces of DNA in between are free to move over the surface and are available for protein interaction.

After implementation of a number of instrumental improvements, the molecules can be visualised routinely, under physiological conditions and with molecular resolution. Images are acquired reproducibly without visible damage for at least 30 minutes, at a scan rate of 2 x 2 μm^2 per minute and a Root Meam Square (RMS) noise of less than 0.2 nm.

Non-specific photolyase DNA complexes were visualised, showing association, dissociation and movement of photolyase over the DNA. The latter result suggests a sliding mechanism by which photolyase can scan DNA for damaged sites. The experiments illustrate the potential that AFM presents for modern molecular biology.

4.1 Introduction

With the introduction of Atomic Force Microscopy (AFM), imaging of biological samples under physiological conditions with nanometer resolution became possible and the use of AFM to study processes between active individual molecules became a challenging goal [1, 2]. However, because of the many difficulties that arise during such experiments [3] only few examples visualising single molecular interactions have been reported so far.

In one of the first papers describing direct measurement of single molecular activity with AFM, height variations on lysozyme were observed and attributed to enzyme activity [4]. Ligand-receptor interactions between various functional molecules have been measured in force-distance mode [5] and only very recently Kasas et al. [6] have impressively used the imaging possibility of AFM to visualise the process of RNA transcription. The mobility of the DNA molecules, which was necessary for RNA polymerase activity, however, prevented the DNA from being imaged clearly, complicating the interpretation of the measurements.

In order to reproducibly achieve good quality AFM data in physiological conditions, high demands are made on the AFM system, the imaging parameters and the sample preparation. In this paper both AFM parameters which result in reproducible images and the reaction conditions allowing imaging of interactions between single photolyase molecules and DNA are discussed. The stability demands and improvements, which have been implemented in our AFM setup, are described and the temporal resolution was maximised for commercially available cantilevers, without giving in on image quality. In this way time series of images were obtained, showing many different intra- and intermolecular events.

4.2 AFM imaging of DNA

Because of its essential role in biology DNA has been studied extensively with AFM [7]. Studies of protein DNA complexes in air have provided information about binding sites and stoichiometry of the proteins and ligand-induced bending of DNA [8, 9] that is also described in chapter 3. Even the double helix structure has been resolved with AFM when the DNA was imaged under propanol or butanol [10]. However, most importantly, AFM is unique in the possibility to study biochemical processes at a single molecule level, under physiological conditions, as demonstrated in the study of RNA polymerase [6].

As AFM is a surface technique, the reactions have to proceed on a surface. In fact a paradoxical problem has to be overcome. To be able to image DNA

reproducibly and with high resolution it is necessary that the DNA is attached to the surface. Otherwise the DNA molecules would be swept away when the tip taps on the molecules and the image would be severely distorted. However, to be available for interaction with other molecules, DNA must be free from the surface to avoid steric hindrance that might affect the reactions. Thus DNA should be immobilised just firmly enough to allow both imaging with AFM and interaction with proteins.

Because of its flatness mica is the most commonly used substrate for DNA imaging [12]. DNA, with its negatively charged phosphate backbone, is bound to the negatively charged mica surface by addition of bivalent cations, which function as an electrostatic bridge. In addition to this effect ions in the buffer will shield electrostatic charges and thus lower the repulsion between DNA and mica. A compromise between firm and loose immobilisation has been achieved by optimising the concentration and type of mono and bivalent cations [13]. In this paper we will show that DNA immobilised on mica in a buffer containing 1 mM $MgCl_2$ and 1 mM NaCl, is only partially bound to the mica surface at specific binding points; the loose parts move over the surface and are free to interact with proteins.

4.3 Non-specific protein DNA interactions

To show the ability to study protein-DNA interactions with AFM, formation of non-specific complexes of DNA with photolyase was monitored. Photolyase is a well-studied enzyme responsible for the removal of thymine dimers in DNA [14, 15, 16]. The crystal structure was resolved [15,17] and structural features have been related to results from photochemistry. Although the reaction has been extensively described biochemically, AFM can contribute to a better understanding of the dynamic aspects of the reaction such as the process of locating the damaged site.

Proteins that bind to specific sites on DNA can find these sites by two general mechanisms [18]. Facilitated one-dimensional diffusion involves first binding non-specifically to DNA, then moving along the DNA in search of specific sites [19]. Alternatively, proteins can locate specific sites on DNA by simple diffusion from solution. Though these dynamic protein-DNA interactions have not been demonstrated directly, in some cases biochemical evidence favours one mechanism over the other.

For instance T4 endonuclease V, a repair enzyme that incises one strand at the site of pyrimidine dimers, is believed to slide along DNA in search of damaged sites. The mechanism photolyase uses to locate damaged sites is not known yet. In this paper we use AFM to directly visualise the interac-

tion between photolyase and DNA. Though we only studied non-specific interactions, we will show that AFM can be used to directly determine whether proteins are able to slide along DNA.

4.4 Materials and methods

Sample preparation

Freshly cleaved mica discs (Ted Pella, Ca, USA) were used as a substrate for immobilising DNA. Undamaged 500 bp dsDNA (Gensura, Ca, USA), obtained by digesting plasmid DNA with EcoRI, was diluted to a final concentration of 2 ng/ml in a buffer containing 4 mM Hepes, 1 mM NaCl and 1 mM $MgCl_2$, pH 6.5. The buffers were made in MilliQ filtered de-ionised water. Photolyase, obtained from *Anacystis Nidulans*, [20, 17], was added to a final concentration of 0.12 ng/ml in the reaction buffer.

After 10 minutes at room temperature 5 ml of the reaction mixture was deposited on mica. Directly after deposition the AFM was mounted over the sample and after a minute the liquid cell of the AFM was thoroughly rinsed with Hepes buffer, without DNA and photolyase. During sample preparation, mounting of the AFM and measurements, biomolecules remain in buffer and are never dehydrated in order to keep them functional.

The AFM setup

A home built stand-alone AFM [21] was modified for the measurements reported. Triangular Si_3N_4 cantilevers purchased from Park Scientific instruments (Sunnyvale, Ca, USA), with a spring constant of 0.5 N/m were used. For our experiments it was not necessary to use electron beam deposited supertips to get reproducible images, as suggested in literature [6]. Images with a scan area of 2 x 2 μm^2, 512 x 512 pixels, were continuously acquired in tapping mode, at a frequency of 25 – 35 kHz, a free amplitude of 6 nm, a peak-peak amplitude set-point of 5 nm and a frame rate of 1 image per minute.

Time series of images were processed using Interactive Data Language (RSI, Co, USA) in a self-written software package. Standard image processing consisted of line subtraction by fitting of a 2nd-order polynomial to each line in the image. Residual lateral drift in the images was corrected for by cross-correlation of successive images, as described in chapter 5.

Imaging parameters

For stable imaging of the loosely bound DNA with a high resolution it is essential to keep destructive tip-sample interaction forces to a minimum. AFM in liquid has the advantage that capillary forces, which are responsible for large tip adhesion at ambient conditions, are absent. However, it was only after the introduction of tapping mode AFM in liquid [22, 23] that weak biological samples could be imaged reliably without considerable damage, because of the reduction of destructive lateral forces between the tip and the sample.

Though lateral forces are absent in tapping mode, normal forces can have a great impact on the sample stability and image quality. In general the smaller the amplitude, the less energy is available for damaging work during the impact on the sample. Keeping the tapping amplitude small is advantageous for keeping the sample stable for a second reason. In tapping mode in liquid the cantilever is driven by acoustic waves in the liquid [22]. The acoustic vibrations do not only excite the cantilever, they will also shake up loose parts of the sample. In addition to tip-induced damage, sonication will remove loose parts from the surface, which is in conflict with the need to keep DNA bound to the surface. Thus it is favourable to keep vibrations in the liquid cell minimal.

After each impact of the tip on the sample, enough oscillatory energy must remain available in the cantilever to overcome tip sample adhesion [24]. Non-specific adhesion forces can range up to a few hundred piconewtons, which would require a peak-peak amplitude of at least 2 nm when a cantilever with a spring constant of 0.5 N/m is used. Furthermore, for a linear amplitude response to a changes in topography, which is required for the feedback loop, the linear regime of the amplitude versus distance should be large enough to overcome steep height variations when the tip is scanned over the surface at high velocities. In our experiments a free peak-peak oscillation amplitude of 6 nm proved to be the best choice for good quality images.

In addition to a small driving amplitude the damping of the oscillation should be minimal in order to prevent sample damage [25]. We used an amplitude set-point of 5 nm, corresponding to a 15 % reduction of the free oscillation amplitude.

4.5 Improvements in the AFM setup

Increase of deflection sensitivity

For an accurate measurement of the topography it is necessary to be able to detect all topography induced amplitude variations. The sensitivity of the deflection detection scheme, and thus the amplitude detection, is limited for two reasons. First, the RMS noise in the detection electronics of the whole system is generally about 0.5 mV. Second, and more fundamentally, the thermal movement of the cantilever introduces extra deflection, independent of the topography of the surface. By matching electronic noise with thermal noise of the cantilever, a lower limit for deflection sensitivity can be obtained. Thermal noise can be described by the equipartition theorem, demanding $0.5 \, k_b T = 0.5 \, kx^2$ [26]. Where k_b is Boltzmann's constant, T is the absolute temperature, k is the spring constant and x^2 is the mean square deflection of the cantilever. For T = 293 K and k = 0.5 N/m, $\sqrt{x^2}$ becomes 0.09 nm. Thus, to reach the thermal noise limit, the deflection sensitivity should be at least 5.6 mV/nm. In order to qualify for this requirement laser power was increased to about 2 mW, which results in an optical power of 0.2 mW on the quadrant detector, due to reflection losses at the surfaces in the light path. The resulting deflection sensitivity was 9 mV/nm, limited by the range of the detector, making thermal noise of the cantilever the dominant noise source.

Modifications to the AFM design

During long-term experiments, the buffer in an open liquid cell is prone to evaporation. The change in liquid volume can have a dramatic effect on stability of the AFM measurement. As the cantilever is excited by acoustic waves in the liquid cell, a peak in the frequency spectrum points at an acoustic mode in the liquid cell, which is excited very efficiently, depending on the dimensions of the liquid cell [22, 27]. The tapping frequency is generally chosen on a peak in the frequency spectrum of the cantilever deflection. Even a small loss in liquid volume causes a change in the acoustic modes in the cell, resulting in less efficient excitation of the cantilever. These unanticipated changes in tapping amplitude, not originating from the topography of the sample and thus resulting in severe image distortions, motivated us to design a closed liquid cell for our stand-alone microscope.
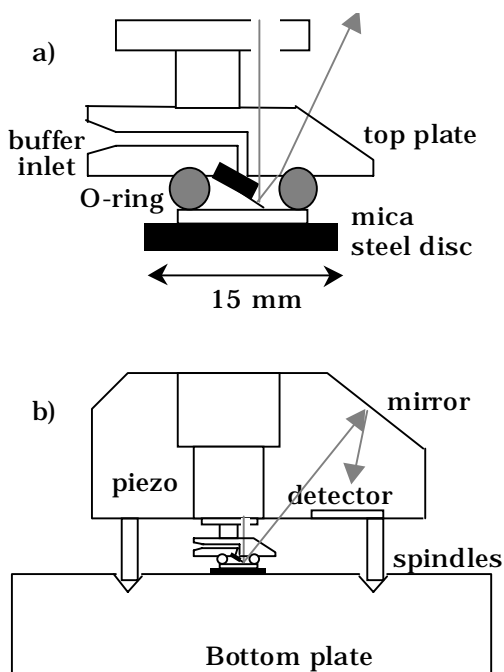
Figure 4.1 shows a schematic drawing of the AFM scanner with the closed liquid cell. In this setup the sample is mounted on a steel disk, which sticks to a magnet. To reduce environmental vibrations, the bottom plate on which

the sample is mounted consists of 30 mm thick aluminium. On the mica sheet a 5 mm inner diameter silicone o-ring is placed, on which the stand-alone AFM is mounted. The o-ring tightly fits in a groove, which is cut in a 5 mm Plexiglas top plate. The cantilever is mounted in a second groove in the top plate, which is screwed on a piezo scanner (Stavely Sensors Inc., CT, USA), with a scan range of 3 x 3 µm². In the top plate, two channels are drilled and sealed with a little rubber cork. Injecting liquid through a tube with an injection needle, which passes through the cork, enables exchange of buffers. To reduce image distortions caused by vibrations of the long tubes, the tubes are rigidly connected to the housing of the AFM. A practical advantage of the stand-alone concept is that residual leakage of the liquid cell does not damage the piezo scanner, as the latter is positioned above the liquid cell. Measurements using this setup resulted in thermal drift of the scanner of typically 0.1 nm/s if the o-ring was properly inserted in the groove; sufficient for most imaging applications.

Optimization of the bandwidth of the feedback loop

In the study of biological processes at the single molecule level good *temporal* resolution is essential. In redesigning the AFM setup, attention was paid to optimise the temporal resolution, under the condition that commercially available cantilevers should be used. For this reason the bandwidth

**Figure 4.1** a) Schematic drawing of the liquid cell, which is attached to the piezo scanner. In this setup the Plexiglas top plate, on which the cantilever is mounted, scans over the mica substrate. b) Schematic drawing of the whole stand-alone AFM. The microscope head is put on three spindles on the bottom plate. The scanner, the laser diode and the detection electronics are built inside the housing.

of the detection scheme was matched with the resonance frequencies of the cantilever and the piezo. The cantilevers used for tapping mode in liquid are generally operated at 10 to 40 kHz, depending on acoustic modes in the liquid cell. We chose to use only the higher frequencies from 25 to 35 kHz. Amplitude was measured, using a true RMS decoder, with a detection bandwidth of 5 kHz, thus averaging over only 5-6 oscillations. In order to compensate for all amplitude variations in the feedback loop, and thus minimising tip-sample interactions, the piezo has to follow these variations with the same frequency. A tube piezo scanner with a resonance frequency of 1.6 kHz was chosen. A smaller piezo tube with a higher resonance frequency would better match the bandwidth of the RMS decoder, but then scan range would be sacrificed. With this configuration maximum spatial frequencies corresponding to 1.6 kHz can be measured, while carefully keeping the tapping amplitude constant.

Maximum scan velocity

In order to make full use of the bandwidth of the feedback loop, the line frequency, at which the surface is scanned, can be increased until the highest frequency of height variations in a line scan matches the feedback bandwidth. In our experiments the sharpness of the features in the AFM images, like proteins and DNA, is limited by the convolution with the tip. Due to this tip-sample convolution the width of dsDNA generally broadens to 20 nm. In our experiments the fastest changes in height will occur when the tip scans perpendicular to a DNA molecule. When an area of 2 x 2 μm^2 is scanned with a line frequency of 20 Hz, the spatial frequency of a 20 nm wide feature, like a DNA molecule scanned perpendicular to the line scan, corresponds to 2 kHz, which is just above the bandwidth of the feedback loop. With these settings all topography induced amplitude changes are carefully compensated by retraction of the piezo. Thus the surface can be scanned at a maximal velocity of 20 $\mu m/s$ while the tip-sample interaction forces are kept minimal. For back traces of the tip the same velocity is used.

For an accurate measurement of the width of tip-convolution limited features in the images four pixels are sampled per 20 nm, resulting in an image size of 512 x 512 pixels for a 2 x 2 μm^2 scan area. The resulting typical maximal frame rate is one image per 50 seconds. To improve the temporal resolution further, the scan area and frame rate can be interchanged, maintaining the same scan velocity. However, if the scan area is reduced too far, drift may cause the object to move out of the field of view. In chapter 5 of this thesis a drift compensation scheme is presented that avoids this problem.
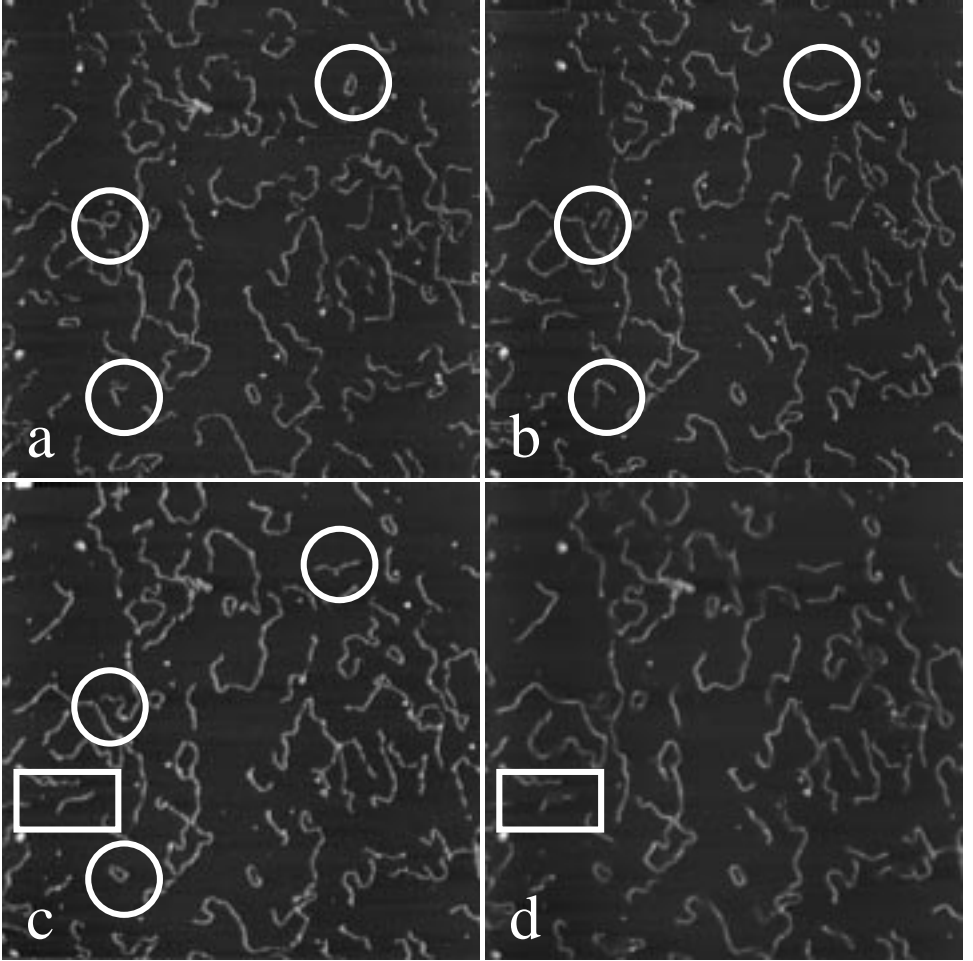
Figure 4.2 a, b and c) Three frames from a 30 minutes sequence of topography images obtained by tapping mode AFM. The scan area was 2 x 2 μm², height range 4 nm. The frames acquired at t = 1, 10 and 25 minutes are displayed. d) time average of 25 frames of this sequence. The height range is equals the height range of the single frames for easy compari-son. Mobile molecules in the time averaged image become fuzzy and less intense, while im-mobile molecules remain sharp and have the same intensity as in a single frame.

4.6 Experiments

DNA movement over the mica surface

Figure 4.2 shows three frames from a typical time series measurement of the photolyase DNA mixture. In this measurement the surface was scanned during 30 minutes at one frame per minute; three frames measured at 1,

10 and 25 minutes are displayed in figures 4.2a - 4.2c. During the 30 minutes of scanning no damage to the sample was visible, while the RMS roughness in the height of the atomically flat mica amounted less than 0.2 nm. The drift during the measurement, as measured by cross-correlation of sequential images, amounted 80 nm in 30 minutes.

For binding of photolyase to DNA, it is important that the DNA strands can come loose from the surface. The stability of the AFM and the drift correction allowed detailed comparison of the images and enables us to show that we really achieved conditions where the DNA is only loosely attached to the surface. In figure 4.2d a time average of 25 topographic images obtained over 25 minutes is shown. The parts of the DNA that are not attached to the surface can move during the experiment; in the resulting average height image the DNA strands at these positions become fuzzy and have a lower intensity. Parts of the DNA that are immobile will keep the same position in the sequential images; these features appear sharp and the intensity will equal the height of the feature in a single frame. The box drawn in the figure 4.2c indicates a DNA strand that is only attached to the surface at its ends. In figure 4.2d the corresponding box clearly shows the two distinct sites where the DNA is fixed and the middle part of the DNA strand that is free to move, disappears in the time-averaged image. This behaviour is observed for many DNA molecules in this image. The fixed DNA parts are generally separated by loose parts of DNA, which range on the average about 80 nm. This may indicate that the mica surface is only partly covered with Mg^{2+}-ions, which points at a stable, specific local interaction of the Mg^{2+}-ions with mica. In our experiments the mobility of DNA on the surface varied a lot when identical reaction buffers were used. Varieties in DNA binding affinity can only be attributed to non-reproducible surface properties of mica.

During the experiment a variety of molecular movements took place. One of the most striking was the opening and closing of 500 bp DNA circles. Some of these events are denoted with a circle in the figures 4.2a-4.2c. In figure 4.3 the 500 bp DNA fragment in the bottom left circle is magnified and followed in time at one frame per minute. These frames clearly show that in spite of the movement of the DNA molecule over the mica surface the scanning tip can image it with a fairly good quality. Halfway through the sequence the two ends stick together and while the DNA molecule still has some freedom to move over the surface the ends are tied together. The DNA fragments were cut with EcoRI resulting in ends with single stranded overhangs of four complementary bases (AATT). Breaking the hydrogen bonds between four base pairs requires a few kT (0.6 kcal/mol) [28], which can be
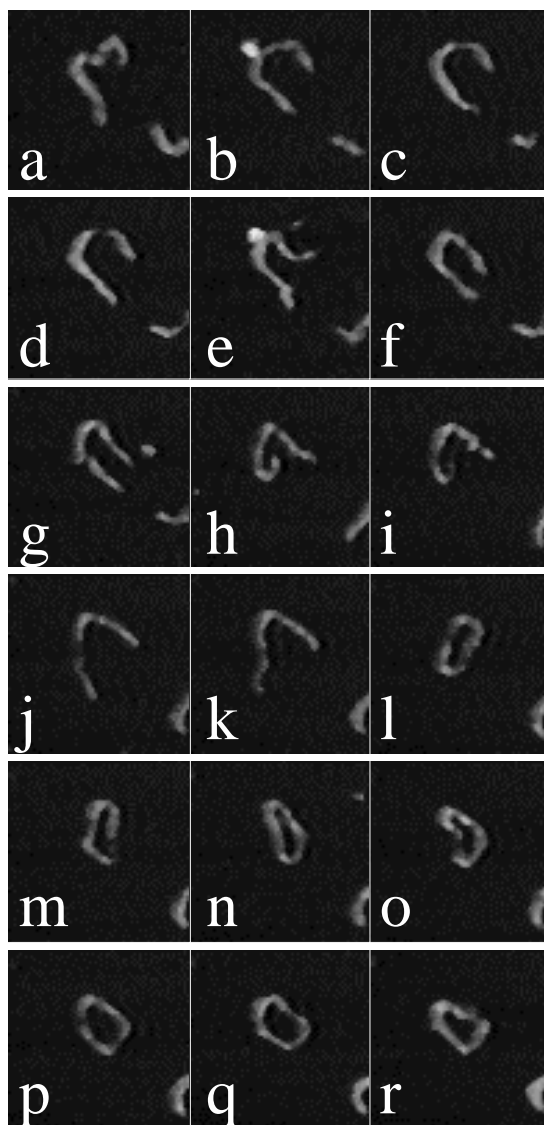
Figure 4.3 Sequence of 18 successive topography images obtained by tapping mode AFM showing one 500 bp DNA molecule, with an interval of 1 minute. The images where cut out of the sequence displayed in figure 4.2. Scan area 250 x 250 nm², height range 4 nm.

provided by thermal energy. Indeed annealing and breaking of these hydrogen bonds occurs several times in the sequence displayed in figure 4.2, as indicated by the circles. The scanning tip does not seem to disrupt hydrogen bonding between the ends, indicating minimal interference of the scanning tip with the loose molecules on the surface.

Imaging of photolyase

In figure 4.4a the white arrows indicate two photolyase molecules. The photolyase molecules appear as globular structures, which measure on

average about 4 nm, slightly smaller than the dimensions obtained by crystallography [17]. In AFM images, the shape of small objects like proteins, is dominated by the convolution of the protein and the tip, resulting in features with a height corresponding to the height of the protein, but a lateral size, that is mainly determined by the tip dimensions. Thus, on the basis of their height, the globular structures can be attributed to photolyase molecules. To confirm this we checked that the concentration of these features on the substrate is directly related to the photolyase concentration in the buffer.

Like DNA, photolyase molecules are only loosely bound to the mica surface. While the molecule indicated by the arrow on the right in figure 4.4a remains at the same position during the whole experiment, pointing at a firm attachment to the surface, the molecule on the left in this figure is only loosely bound to the surface.

In figure 4.4 it can be seen that the tip can move the photolyase while it stays on the surface. During imaging, the tip scans horizontally over the surface from left to right and back. Starting at the bottom the tip is slowly scanned upward until the whole field of view is covered, as depicted schematically with the arrows below figure 4.4g. The sequential images are all acquired in this way, from top to bottom. When the tip taps at the edge of the protein the molecule moves up. In frame 4b the photolyase is moved up, perpendicular to the scan direction, as indicated by the white arrow. In the succeeding line scans, further upward in the image, the same molecule is detected and pushed away again, causing the bright 'tail' under the molecule. In figure 4.4c the protein stays at the position it was left in the previous scan. Then in figure 4.4d either it is moved up again, or it dissolves in the solution and another molecule adsorbs on the surface. In the next panel, figure 4.4e, the molecule is only loosely attached to the surface. At its centre, the middle two scan lines, it is temporarily moved 10 nm to the left, to move back to the right in the next scan line. Only after another 6 frames, 6 minutes later, photolyase is swept up again in figure 4.4g, to a position it stayed during the rest of the experiment. In figure 4.4e in the bottom right corner a new photolyase molecule adsorbs to the surface from the buffer solution. The behaviour of the molecules displayed in figure 4.4 is typical for the photolyase molecules in this sequence; only directional movement upward, perpendicular to the linescan direction is observed. The scanning tip sweeps the photolyase molecules away, and as the tip is slowly moving upward, no downward movement of photolyase molecules is observed. Again a large variety between experiments occurs, pointing at non-reproducible surface properties. As the photolyase covers only a few nm² of

Scan direction
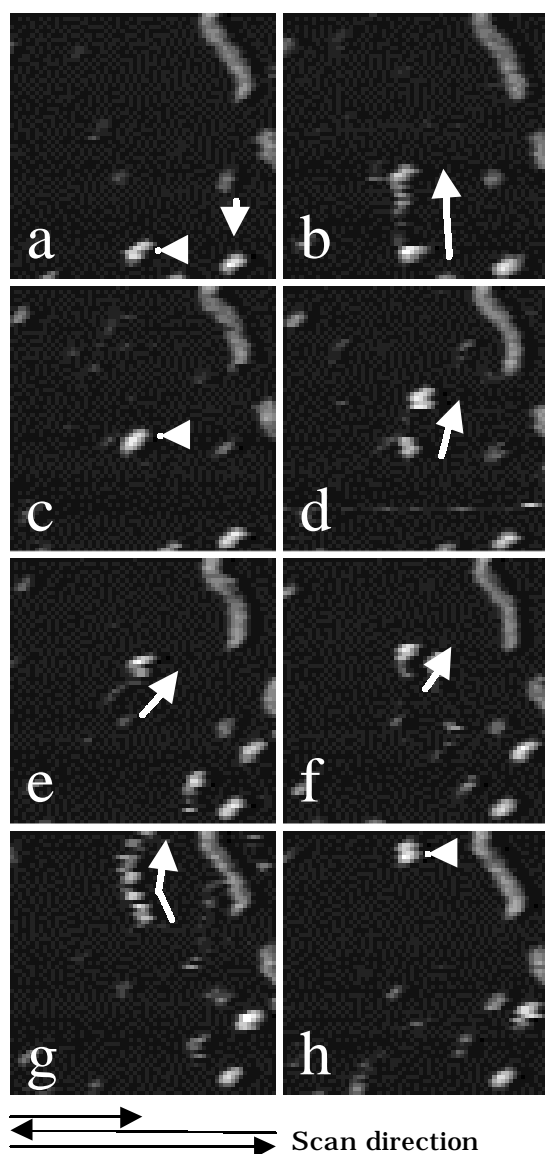
Figure 4.4 Sequence of 8 successive topography images obtained by tapping mode AFM at times t = 1, 2, 3, 4, 5, 6, 11 and 12 min. Two Photolyase molecules are depicted with white arrows in figure 4.4 a. White arrows in figures 4.4b – 4.4h depict the movement of one photolyase molecule. The black arrows below the figure indicate the scan direction of the tip. Scan area 250 x 250 nm², height range 4 nm.

the surface, it is much more dependent of the local variations of the surface, and is thus more mobile than the DNA molecules. Next to the smaller contact area, the non-uniform surface charge of photolyase [15], that is shown in figure 3.5a in the previous chapter, may create large differences in binding affinity to the surface, depending on the orientation of the molecule.
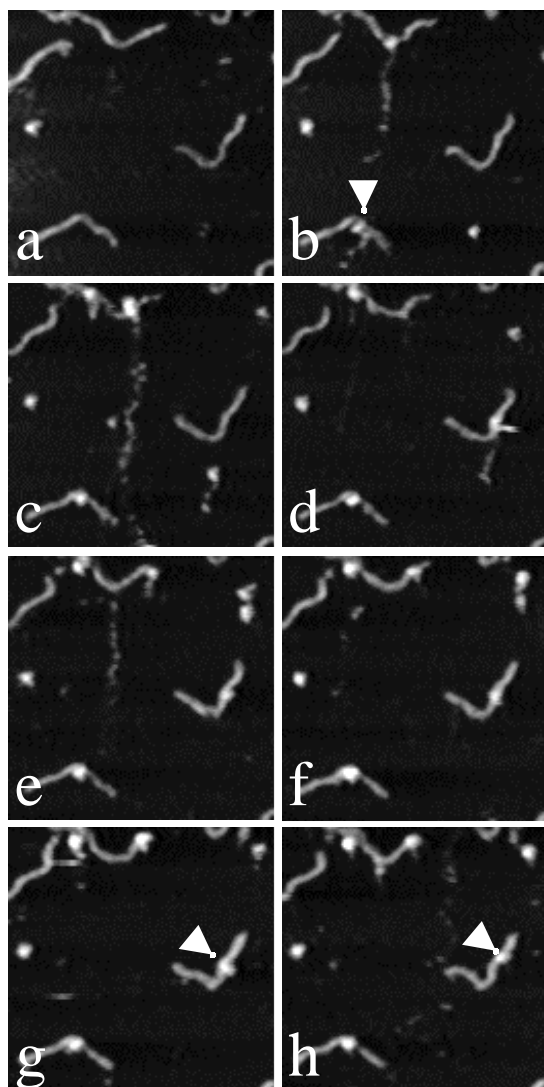
Figure 4.5 Sequence of 8 topography images obtained by tapping mode AFM showing photolyase and DNA molecules. The arrows indicate positions where DNA and photolyase interact non-specifically. Scan area 500 x 500 nm², height range 4 nm at times t = 1, 4, 7, 8, 9, 10, 11 min.

Photolyase DNA interactions

In the sequence displayed in figure 4.5 the tapping tip sweeps up photolyase molecules as described in the previous section, but when a DNA strand comes in the way photolyase sticks to the DNA forming a complex. Most complexes remain stable during the rest of the experiment, like the complex indicated by the arrow in figure 4.5b. On some occasions, photolyase dissociates from the DNA, even when the complex has been stable during a few scans. In figure 4.5g and h photolyase in the indicated complex, stays

on the DNA, but appears to have moved over it. This suggests the possibility for photolyase to use a sliding mechanism to scan the DNA in order to find damaged sites.

In figure 4.6 another example is shown where photolyase apparently slides over the DNA strand in the centre of the image. In four frames taken directly after the formation of the complex, the position of photolyase changes 80 nm. As the movement is downwards, opposite of the scan direction of the tip, it is unlikely that the tip pushed the photolyase molecule over the DNA strand. In the time span between figure 4.6c and figure 4.6d the protein hardly changed position, and in the succeeding frames, which are not shown, the protein remains at the same position. The range over which the photolyase has moved agrees well with the range over which the DNA is loosely bound. In figure 4.6e an average of 25 frames shows that the movement of the photolyase is confined to the range where DNA appears fuzzier than on the boundaries of the movement, indicating that the DNA is only loosely bound in this region. Thus it is likely that the photolyase is stopped by steric hindrance at the position where DNA is firmly attached to the surface.

4.7 Conclusions and discussion

Improvements of the AFM setup

The modifications implemented on our AFM setup enabled us to routinely image DNA and proteins under physiological conditions at high quality. The AFM system was optimised to keep interaction forces down to a minimum. For carefully adjusting the tapping parameters the ability to monitor the deflection signal and to adjust the feedback parameters on-line appeared crucial. Thus the feedback loop could very accurately be kept stable for more than half an hour resulting in no recognizable damage and background RMS noise of less than 0.2 nm. Even loose molecules can be imaged with the tip, though sometimes very mobile photolyase proteins were swept away.

Further reduction of interaction forces would not only require smaller tapping amplitudes, lower damping or weaker spring constants; tip-adhesion would have to be reduced as well. One way to fulfil this requirement is to use electron beam deposited (EBD) supertips. These supertips decrease tip-sample adhesion, as the tip-sample contact area is smaller. Thus smaller tapping amplitudes may be used, which would further decrease interaction forces. In addition to this effect the spatial resolution of the measurements
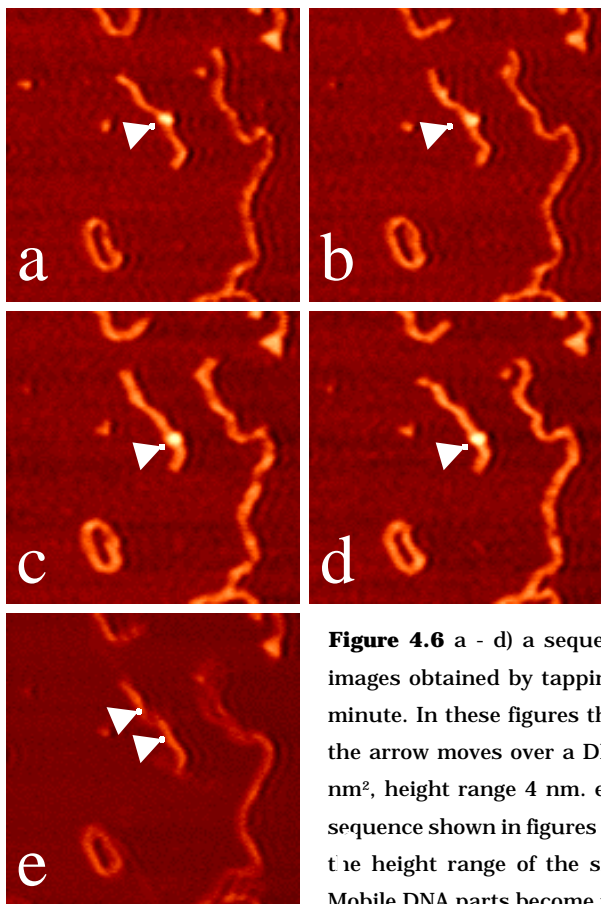
Figure 4.6 a - d) a sequence of four successive topography images obtained by tapping mode AFM with an interval of 1 minute. In these figures the photolyase molecule depicted by the arrow moves over a DNA molecule. Scan area 500 x 500 nm², height range 4 nm. e) Time average of 25 frames of the sequence shown in figures 4.6a - 4.6d. The height range equals the height range of the single frames for easy comparison. Mobile DNA parts become fuzzy and less intense, while immobile parts remain sharp and have the same intensity as in a single frame.

would further improve, though the spatial resolution of the reported measurements is sufficient for easily identifying single proteins and DNA strands. Preliminary experiments with EBD supertips did not result in significantly better results.

Another way to reduce artifacts may be to use direct, magnetic excitation of the cantilever [25]. Direct excitation of the cantilever minimizes acoustic vibrations in the liquid, which may stabilize the loosely bound molecules on the surface better than using acoustic excitation. Promising results have been reported, indicating a more gentle way to scan the surface [29]. Although we have shown that good results can be obtained using acoustic excitation when all parameters are carefully optimised, this new way of excitation may improve the image quality even further.

The scan rate of our system was maximised for commercially available cantilevers to 20 mm/s. For the experiments reported in this study this was sufficient to distinguish between different positions of the DNA on the surface, and even the dynamics of non-specific protein-DNA interactions could be observed. As for most of our analysis only part of the images was used, the scan area could be decreased in order to increase the frame rate, keeping the scan velocity constant. As the frame rate is inversely proportional to the scan area, the scan area could be sacrificed as much as the drift allows, as will be shown in chapter 5. However, due to the variations in behaviour of the individual molecules, a better representation of the processes between these molecules is obtained when more of these molecules are followed simultaneously. This is especially important because the surface properties of the mica vary between experiments, which make quantitative comparison between different experiments difficult.

To increase the scan rate without sacrificing the field of view a number of improvements need to be made. First cantilevers with a higher resonance frequency must be made [30]. In order to keep sample damage limited it is necessary to keep the spring constant as small as possible. Furthermore a piezo with higher resonance frequency should be used, to compensate all amplitude variations accurately with the feedback loop.

Immobilisation of DNA

In this paper we have shown that DNA is very inhomogeneously bound to the mica substrate in a buffer containing 1 mM NaCl and 1 mM $MgCl_2$. The data presented here are all from experiments in which DNA was bound loosely to the surface. In some experiments, not presented in this paper, the DNA does not move at all during 30 minutes of image acquisition. The natural diversity of the mica may explain the large variation in the binding of DNA.

It is very likely that the presence of the surface slowed down the movements of the molecules. Guthold et al. [31] measured a two-dimensional diffusion constant of 2,5 nm^2/s for 1000 bp DNA fragments over a mica surface under similar imaging conditions, though the ability of the DNA to diffuse over the surface depended strongly on the DNA-mica adsorption and the resulting friction. The data presented in our study show very inhomogeneous, localised absorption of DNA to mica. Thus the model of free two-dimensional diffusion of DNA over the surface, which implies a homogeneously distributed potential well for DNA adsorption on the surface, does not apply for our measurements.

In the case of loosely bound DNA time averaging of a series of images reveals sites on the mica where the DNA is tightly bound, and other parts

that are loose from the surface. This nicely exposes the very local interaction responsible for immobilising DNA. Hansma and Laney [12] showed that K$^+$-ions at the mica surface are exchanged with Mg^{2+} from the buffer. This interpretation suggests that only part of the K$^+$-ions are replaced when the buffer contains 1 mM NaCl and 1 mM MgCl$_2$.

DNA photolyase interactions

We used AFM to visualise dynamic interactions between photolyase and DNA. As the DNA was undamaged we do not address actual damage recognition with these experiments, but we studied the previous step of locating these sites. On loose pieces of DNA we did observe photolyase moving over the DNA, suggesting that photolyase uses one-dimensional diffusion to scan the DNA for damaged sites. Points of firm DNA attachment appeared to stop photolyase movement. Thus, the presence of the surface will have a great influence on the observed rate and extent of sliding.

In the experiments where no movement of DNA was observed (not shown) photolyase did not move over the DNA. This did not prevent photolyase from association and dissociation with undamaged DNA fragments. Photolyase has only a low affinity ($K_d = 10^{-4}$ M) for undamaged double stranded DNA [15]. Any one-dimensional diffusion on the DNA has to compete with dissociation of the complex. Furthermore, as no energy source is available for the proposed sliding of the photolyase on the DNA, friction or steric hindrance would be expected to prevent the protein from sliding over the DNA.

Competition with dissociation of the complex reduces the effective range over which the photolyase might slide. Indeed the average range other proteins, like T4 endonuclease V, scan over DNA is dependent of the ionic strength of the buffer, which strongly affects the binding affinity of this protein [19]. In this study relatively low ion concentrations were used in order to favour possible sliding of photolyase over DNA.

Like the movement of photolyase over the surface, the scanning tip may induce movement of photolyase over DNA. However, as sliding of photolyase over DNA was observed in all directions independent of the direction of the scanning tip, it seems unlikely that effects of the scanning tip dominate the movement of photolyase along the DNA. Another observation, which points at a one-dimensional diffusion of photolyase over DNA is that the mobility is limited to loose parts of the DNA. As no energy is available for the motion, DNA can not actively be pulled off of the surface by the protein. Future studies will have to establish whether photolyase indeed slides along the DNA. In this paper we have shown that, when all measurement param-

eters are carefully optimised, AFM measurements under physiological conditions provide a tool to investigate the dynamics of molecular interaction mechanisms between DNA and proteins on a single molecule scale.

4.8 References

1   Hansma, H. G. 1995. Atomic force microscopy of biomolecules. *J. Vac. Sci. Technol. B.* 14: 1390-1395.

2   Lal, R., and S. A. John, 1994. Biological applications of atomic force microscopy. *Am. J. Physiol.* 266: 1-21.

3   Thomson, N. H., S. Kasas, B. Smith, H.G. Hansma, and P.K. Hansma. 1996. Reversible binding of DNA to mica for AFM imaging. *Langmuir* 12: 5905-5908.

4   Radmacher, M., M. Fritz, H.G. Hansma, and P.K. Hansma. 1994. Direct observation of enzyme activity with the atomic force microscope. *Science* 265: 1577-1579.

5   Florin, E.-L., V.T. Moy, and H.E. Gaub. 1994. Intermolecular forces and energies between ligands and receptors. *Science* 266: 257-259.

6   Kasas, S., N. H. Thomson, B. L. Smith, H. G. Hansma, X. Zhu, M. Guthold, C. Bustamante, E.T. Kool, M. Kashev, and P. K. Hansma. 1997. Escherichia coli RNA Polymerase activity observed using atomic force microscopy. *Biochemistry* 36: 461-468.

7   Hansma, H. G., I. Revenko, K. Kim, and D.E. Laney. 1996. Atomic force microscopy of long and short double-stranded, single-stranded and triple-stranded nucleic acids. *Nucleic Acids Research* 24(4): 713-720.

8   Erie, D.A., G. Yang, H.C. Schultz, and C. Bustamante. 1994. DNA bending by Cro protein in specific and nonspecific complexes: implications for protein site recognition and specifity. *Science* 266: 1562-1566.

9   Wyman, C., E. Grottkopp, C. Bustamante, and H.C.M. Nelson. 1995. Determination of heat-shock transcription factor 2 stoichiometry at looped DNA complexes using scanning force microscopy. *EMBO J.* 14: 117-123.

10 Hansma, H. G., J. Vesenka, C. Siegerist, G. Kelderman, H. Morrett, R. S. Sinsheimer, C. Bustamante, and P. K. Hansma. 1992. Reproducible imaging and dissection of plasmid DNA under liquid with the AFM. *Science* 256: 1180-1184.

11 Wyman, C., I. Rombel, A. K. North, C. Bustamante, and S. Kustu. 1997. Unusual oligomerisation required for activity of NtrC, a bacterial enhancer-binding protein. *Science* 275: 1658-1661.

12 Hansma, H. G., and D. E. Laney. 1996. DNA binding correlates with cationic radius: assay by atomic force microscopy. *Biophys. J.* 70: 1933-1939.

13 Guthold, M., X. Zhu, C. Rivetti, G. Yang, N.H. Thomson, S. Kasas, H.G. Hansma, B. Smith, P.K. Hansma, and C. Bustamante. 1997. One-dimensional diffusion and transcription by E. coli RNA polymerase observed with the scanning force microscope. *J. Biol. Chem.* "submitted for publication"

14 Sancar, A., 1994. Structure and function of DNA photolyase. *Biochemistry* 33: 2-9.

15 Park, H.-W., S.-T Kim, A. Sancar, and J. Deisenhofer. 1995. Crystal structure of DNA photolyase from Escherichia coli. *Science* 268: 1866-1872.

16 Hearst, J. E. 1995. The structure of photolyase: using photon energy for DNA repair. *Science* 268: 1858-1868.

17 Tamada, T., K. Kitadoro, Y. Higuchi, K. Inaka, A. Yasui, P.E. de Ruiter, A.P.M. Eker, and K. Miki. 1997. Crystal structure of DNA photolyase from Anacystus nidulans. *Nature Stuct. Biol.* 4: 887-891.

18 Berg, O., R.B. Winter, and P.H. von Hippel. 1981. Diffusion-driven mechanism of protein translocation on nucleic acids. 1. Models and Theory. *Biochemistry* 20: 6929-6948.

19 Dowd, D. R. and R. S. Lloyd. 1990. Biological significance of facilitated diffusion in protein-DNA interactions. *J. Biol. Chem.* 265: 3424-3431.

20 Eker, A.P.M., P. Kooiman, J.K.C. Hessels, and A. Yasui. 1990. DNA photoreactivating enzyme from the cyanobacterium Anacystis nidulans. *J. Biol. Chem.* 265: 8009-815.

21 Van der Werf, K.O., C.A. Putman, B. G. de Grooth, F.B. Segerink, E.H. Schipper, N. F. van Hulst, and J. Greve. 1993. Compact stand-alone atomic force microscope. *Rev. Sci. Instr.* 64: 2892-2897.

22 Putman, C.A., K.O. van der Werf, B. G. de Grooth, N. F. van Hulst, and J. Greve. 1994. Tapping mode atomic force microscopy in liquid. *Appl. Phys. Lett.* 64: 2454-2456.

23 Hansma, P.K., J.P. Cleveland, M. Radmacher, D.A. Walters, and P. Hillner. 1994. Tapping mode atomic force microscopy in liquids. *Appl. Phys. Lett.* 64: 1738-1740.

24 Van Noort, S.J.T., K.O. van der Werf, B. G. de Grooth, N. F. van Hulst, and J. Greve. 1997. Height anomalies in tapping mode atomic force microscopy in air caused by adhesion. *Ultramicroscopy* 69: 117-127.

25 Han, W., and S.M. Lindsay. 1996. A magnetically driven oscillating probe microscope for operations in liquids. *Appl. Phys. Lett.* 69: 4111-4113.

26 Butt, H.-J., and M. Jaschke. 1995. Calculation of thermal noise in atomic force microscopy. *Nanotechnology* 6: 1-7.

27 Schäfer, T.E., J.P. Cleveland, F. Ohnesorge, D.A. Walters, P.K. Hansma. 1996. Studies of vibrating atomic cantilevers in liquid. *J. Appl. Phys.* 80: 3622-3627.

28 Saenger, W. 1986. Principles of nucleic acid structure. Springer-Verlag, New York, NY.

29 Han, W., and S.M. Lindsay. 1997. Kinked DNA. *Nature* 386: 563.

30 Walters, D.A., J.P. Cleveland, N.H. Thomson, and P.K. Hansma. 1996. Short cantilevers for atomic force microscopy. *Rev. Sci. Instr.* 67: 3583-3590.

31 Guthold, M., M. Bezanilla, D. A. Erie, B. Jenkins, H.G. Hansma, and C. Bustamante. 1994. Following the assembly of RNA polymerase-DNA complexes in aqueous solutions with the scanning force microscope. *Proc. Natl. Acad. Sci USA* 91: 12927-12931.

Chapter 5

High speed visualization of biomolecules by image tracking

Abstract

An image tracking procedure for Atomic Force Microscopy is proposed and tested which allows repeated imaging of the same area without suffering from lateral drift. The drift correction procedure is based on on-line cross-correlation of succeeding images. Using the image tracking procedure allows zooming in on a small scan area over a long period and thus increases the frame rate inversely proportional with the scan area. Application of the procedure is demonstrated for diffusion of 5.4 kb DNA plasmids. With a scan area of 500 * 500 nm² a single plasmid can be imaged for more than 30 min at 4 s per frame, with a drift less than 10 nm. The high temporal resolution allows detailed analysis of the diffusion of DNA molecules. A diffusion coefficient of 30 nm²/s is found for most DNA molecules, though many molecules are temporally pinned to the mica surface, restricting diffusion.

5.1 Introduction

The possibility to operate an Atomic Force Microscope (AFM) in physiological buffers, allows visualization of individual biological molecules in their natural environment [1,2]. It is this feature that makes the AFM an unique tool to study both the dynamics of single molecules and the interactions between individual molecules [3,4], which is demonstrated in the previous chapter. Visualization of molecular processes requires a time resolution at least comparable with the time constant of the process. The acquisition time of a single AFM image of soft biological material however, is in the order of one minute, which is much slower than most biological processes. To increase the frame rate, the scan velocity can be increased, but this generally results in higher interaction forces that may cause damage to the sample. Another way to increase the frame rate is to reduce the scan area [5]. If the scan velocity is kept constant, zooming in allows an increase of the frame rate inversely proportional with the scan area.

In order to get sufficient accuracy of the stochastic movement of individual molecules, it may be necessary to follow the molecules of interest over a long period. Thermal drift of the piezo scanner is then a major problem because it causes the scanner to move away from the original field of view. Performing such an AFM experiment therefore requires a correction of the lateral drift during data acquisition. Such a drift correction procedure should then be flexible, that is applicable independent of the shape of the sample, reliable and not time consuming. In this study we present a general approach for drift compensation based on on-line cross-correlation of succeeding images. This allows an optimization of the frame rate by zooming in, while avoiding the problem that drift causes molecules to disappear out of the scanned field of view.

In this paper we will apply the image tracking procedure to zoom in on a individual DNA plasmids. Though for AFM imaging molecules are usually immobilized on a surface, lateral diffusion of biomolecules only loosely attached to the surface and the assembly of protein DNA complexes have been imaged by AFM [6]. A complicating factor in visualizing the movement of such loosely attached molecules is the interaction of the scanning tip with the molecules [7,8]. Using a high time resolution, in combination with an accurate drift correction, it should be possible to analyse diffusion-related processes of individual molecules in more detail. In this analysis, it should be possible to distinguish the influences of the scanning tip from molecular movement by diffusion.

5.2 Theory

Maximum scan velocity

Tapping mode AFM is most often used for imaging biological samples because of the absence of friction forces [9]. Keeping the oscillation amplitude constant in a feedback loop controls the tip-sample interaction. The maximal scan velocity of the tip and thus the maximal frame rate, is limited by the bandwidth of the feedback loop, that is schematically drawn in figure 5.1.

To achieve maximal scan rate all components of the feedback loop need to be optimised. The first element in the setup is the force sensor, the cantilever itself. The cantilever behaves as a second order damped harmonic oscillator and is driven at its resonance frequency. The stiffer the cantilever, the higher its resonance frequency and thus the higher the allowed scan velocity. However, stiff cantilevers put high demands on the force detection. The fundamental lower limit to the force that is applied by an AFM cantilever, is the force that is generated due to the thermal movement of the cantilever itself [10]. For minimal damage to occur, the cantilever deflection measurement should be sensitive enough for thermal noise to be the dominant noise source. For this reason Si cantilevers, with a spring constant in the order of several tens of N/m can be discarded. Using these cantilevers the amplitude of thermal fluctuations is smaller than the noise in the beam deflection scheme that is limited by shot noise of the laser
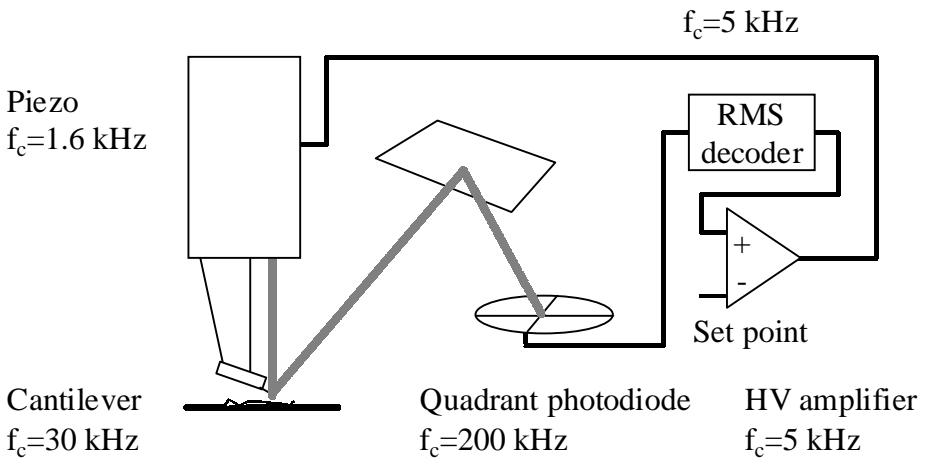
Figure 5.1 Schematic drawing of the AFM setup. For each component the bandwidth is given. In this case the piezo tube is the rate limiting factor for tapping mode AFM.

diode. Though the amplitude is very small, the thermal fluctuations in terms of forces can be quite large, i.e. ~10 nN, because of the high spring constant. Such high forces may cause severe damage to the sample.

In this study we use Si_3N_4 cantilevers purchased from Park Scientific (Sunnyvale, Ca, USA), with a spring constant of 0.5 N/m. The resonance frequency drops from 110 kHz in air to 38 kHz immersed in buffer and the quality factor Q reduces to ~2. The sensitivity of the beam deflection in the setup is just sufficient to measure thermal movement of this cantilever. Thus a compromise is found between a small spring constant and maximal resonance frequency.

For amplitude detection a true RMS decoder with a bandwidth of 5 kHz is used. This means that for a tapping frequency of 30 kHz, only 6 tip-sample contacts are used to measure the tapping amplitude. Finally, the amplified difference between the amplitude and the amplitude set point is applied to the piezo. In the setup the bandwidth of the feedback loop is limited by the resonance frequency of the piezo which amounts 1.6 kHz, followed by the bandwidth of the RMS decoder. Using this setup, maximum bandwidth is combined with optimal force sensitivity.

The bandwidth of the feedback loop should match the spatial frequencies that occur while scanning the tip over the surface. The apparent width w of molecular features on the surface is determined by convolution of the tip with radius R and the sample with radius r and can be approximated by:

$$w \approx \sqrt{rR} \qquad\qquad\qquad (5.1)$$

For a tip radius of 50 nm, a molecule with a radius of 2 nm results in an image feature of 10 nm. The spatial frequencies of the features in the image should match the bandwidth of the feedback loop f_c, resulting in a maximum scan velocity v

$$v = 2\ w\ f_c \qquad\qquad\qquad (5.2)$$

For 10 nm features and a bandwidth of 1.6 kHz the maximal scan velocity amounts 32 μm/s. Following all topographical features with the feedback loop for N pixels of size p, the time per frame t is

$$t = N^2\ p\ /\ w\ f_c \qquad\qquad\qquad (5.3)$$

A scan range of 2 μm and 512^2 pixels, thus a pixel size of 4 nm, can be scanned in 65 s. Reducing the scan range to 500 nm, measuring 128^2 pixels, results in an acquisition time of only 4 s. In conclusion, considerable decrease of the frame time can be achieved by zooming in, i.e. decreasing the number of pixels, and keeping the resolution p the same.

The reduced frame time minimizes artifacts caused by drift, which is schematically shown in figure 5.2. Drift during imaging results in a skewed shape distortion and stretching of the scanned area. Also, as the image range decreases, sequential frames have a relatively larger area in common. The latter effect is counterintuitive as generally one uses a larger scan area to prevent features of interest to drift out of the field of view.
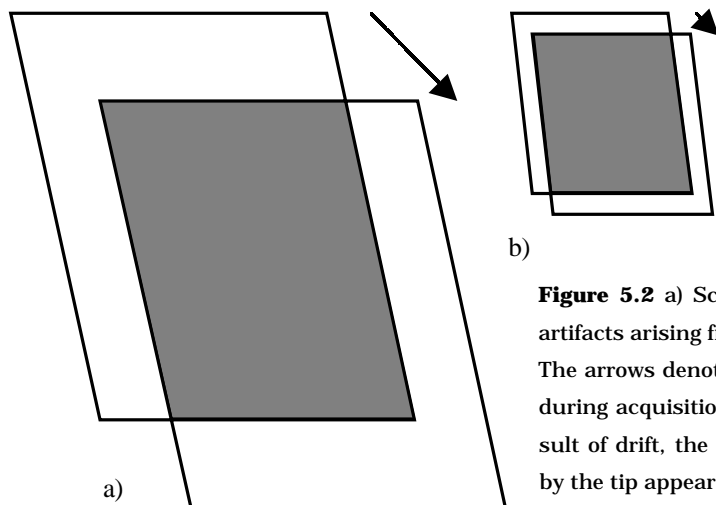
Figure 5.2 a) Schematic drawing of the artifacts arising from drift of the scanner. The arrows denote the accumulated drift during acquisition of one frame. As a result of drift, the surface that is scanned by the tip appears stretched and skewed, compared to the movement of the tip. Furthermore, in a succeeding scan only part of the scanned area, the shaded region, coincides with the area scanned in the previous scan. b) When the scan area is reduced, the time per frame decreases proportional with the scan area, and as a result the artifacts caused by drift are also reduced.

Cross-correlation image tracking

Though zooming in can considerably increase the number of frames that are measured of a single molecule, in practice the duration of an AFM experiment is still limited. During imaging thermal drift may accumulate to displacements greater than the scan range, and may cause the molecules to move out of the field of view of the scanner. Thomson et al. [11] presented a way of solving this problem: by continuously determining the position of a protein under investigation relative to the tip position and repositioning the tip accordingly, proteins could be tracked for more than 1 hour. The position of a molecule was measured by crosswise scanning over the molecule. Using this method all image information is lost, which yet is

essential for the determination of the conformation of a molecule or the relative displacement of interacting molecules.

For drift compensation we propose a very general method based on cross-correlation of succeeding images. The cross-correlation between frames i_1 and i_2 is defined as:

$$\text{Corr}(i_1, i_2) \equiv \int\limits_{-\infty}^{\infty} \int\limits_{-\infty}^{\infty} i_1(x - s_x, y - s_y) i_2(x - s_x, y - s_y) \, ds_x \, ds_y \qquad (5.4)$$

where s_x and s_y denote the shift of the image in x and y direction. In our implementation we make use of the *discrete correlation theorem* [12]:

$$\text{Corr}(i_1, i_2) \Leftrightarrow I_1 I_2^* \qquad (5.5)$$

Where I_1 and I_2 represent the Fast Fourier Transform (FFT) of the images i_1 and i_2 and the asterisk denotes the complex conjugation. Thus the product of FFT(i_1) and the complex conjugate of FFT(i_2) is inversely transformed, resulting in the cross-correlation of the images. Drift between two frames is measured from the position at which the maximum in the cross-correlation occurs. In the succeeding scan a negative offset that compensates for the measured drift, is applied to the scanner. In this way drift is compensated on-line. The method is limited to non-periodic features, as in periodic structures multiple peaks will appear in the correlation image. If enough common features appear in succeeding frames, the image tracking procedure provides a stable method to compensate for lateral drift of the scanner.

Surface diffusion of DNA molecules

In this paper we use diffusion theory, commonly used for single particle tracking [13], to quantify diffusion of a single DNA molecule. Hereto, a sequence of n_f digitized frames is obtained that show the detailed position and conformation of DNA molecules. For diffusion analysis the position of the centre of mass of a single DNA plasmid is followed in time. For all N_{DNA} pixels, that represent one DNA molecule the center of mass, c_m is calculated as:

$$c_{m,x} = \frac{1}{N_{DNA}} \sum_{i}^{N_{DNA}} x_i$$
$$c_{m,y} = \frac{1}{N_{DNA}} \sum_{i}^{N_{DNA}} y_i \qquad (5.6)$$

To follow the movement of the plasmid, the Mean Square Displacement (MSD) of the centre of mass is calculated. The MSD can be expressed in terms of n times the acquisition time of a single frame, t as:

$$MSD_x(nt) = \sum_{i=0}^{n_f-n} \frac{[c_{m,x}(i+n) - c_{m,x}(i)]^2}{n_f - n + 1}$$

$$MSD_y(nt) = \sum_{i=0}^{n_f-n} \frac{[c_{m,y}(i+n) - c_{m,y}(i)]^2}{n_f - n + 1}$$

(5.7)

In the case of simple diffusion the MSD should be proportional with time:

$$MSD = 4D\, n\, t \tag{5.8}$$

using a diffusion coefficient D.

A plot of the MSD versus time should be linear if the movement of the molecule is characterized by diffusion only. Due to the stochastic movement of the molecule however, the trajectory of the centre of mass of a single molecule will show statistical variations around such a linear behaviour. Only by averaging sufficient data points the MSD can be measured accurately. The standard deviation σ_{MSD} of the MSD can be expressed in terms of the number of data points and the time resolution of the measurement as [13]:

$$\sigma_{MSD}^2 = \frac{2n^2 + 1}{3n[n_f - n + 1]} (4Dnt)^2 \tag{5.9}$$

An accurate determination of the diffusion characteristics therefore benefits from a high frame rate and a long time range over which the molecule is followed.

5.3 Materials

AFM setup

For the experiments a home built stand-alone AFM was used, as described elsewhere [14]. The data acquisition and image-tracking procedure was implemented in a LABView (National Instruments, Tx, USA) programming environment using an AT-MIO-16E data acquisition board (National Instruments, Tx USA). For scanning, software generated scan arrays are applied to the piezo tube. After acquisition of the second frame the cross-

correlation with the previous frame is calculated, and the scan arrays are adjusted to compensate for the measured drift, before automatic acquisition of the next frame. On a Pentium II 350 MHz PC the cross-correlation algorithm typically takes less than 1% of the frame time, thus the frame acquisition rate is not significantly reduced by the procedure.

Sample preparation

5 µl of a solution containing 1 ng/µl 5.4 kb plasmid (pcDNA3), 5 mM $MgCl_2$ and 10 mM Hepes pH 7 and 20 mM KCl was pipetted onto a freshly cleaved mica disk. After approximately 30 s the AFM was mounted onto the sample, and 200 µl 5 mM $MgCl_2$, 10 mM Hepes pH 7 and 20 mM KCl buffer was added to the liquid cell. In this way dehydration of the DNA was avoided. Immediately after mounting the AFM it was possible to start the experiment; it was not necessary to wait for thermal equilibrium of the scanner.

Data analysis

Off-line data processing and analysis was implemented in IDL (RSI, Co, USA). Image processing consisted of line subtraction, by fitting a second order polynome to each line, and subtraction of this fit. For off-line cross-correlation, the drift was measured between two frames, and the second frame was shifted accordingly to correct for drift. For determination of the centre of mass of DNA plasmids all pixels with a height of 0.5 nm or higher were used, except obvious pollution particles, that were manually discarded.

5.4 Results

Cross-correlation of AFM images

Two typical unprocessed topography images of a 5.4 kbp DNA plasmid are shown in figure 5.3a and 5.3b. The apparent width of the DNA strand is 20 nm allowing a frame time of approximately 4 s with a scan range of 500 nm. The DNA molecules are loosely attached to the surface and though parts of the molecules remain at the same position, other parts have moved between acquisition of figure 5.3a and 5.3b. In spite of the very weak attachment to the surface, DNA molecules are not swept away by the scanning tip. The cross-correlation image of figure 5.3a and 5.3b is plotted in figure 5.3c. A maximum is observed at a displacement of 30 nm in the x direction and 70 nm in the y direction.

Image artifacts like tilt of the surface or drift of the scanner perpendicular to the surface sometimes dominate the topography image over real topo-
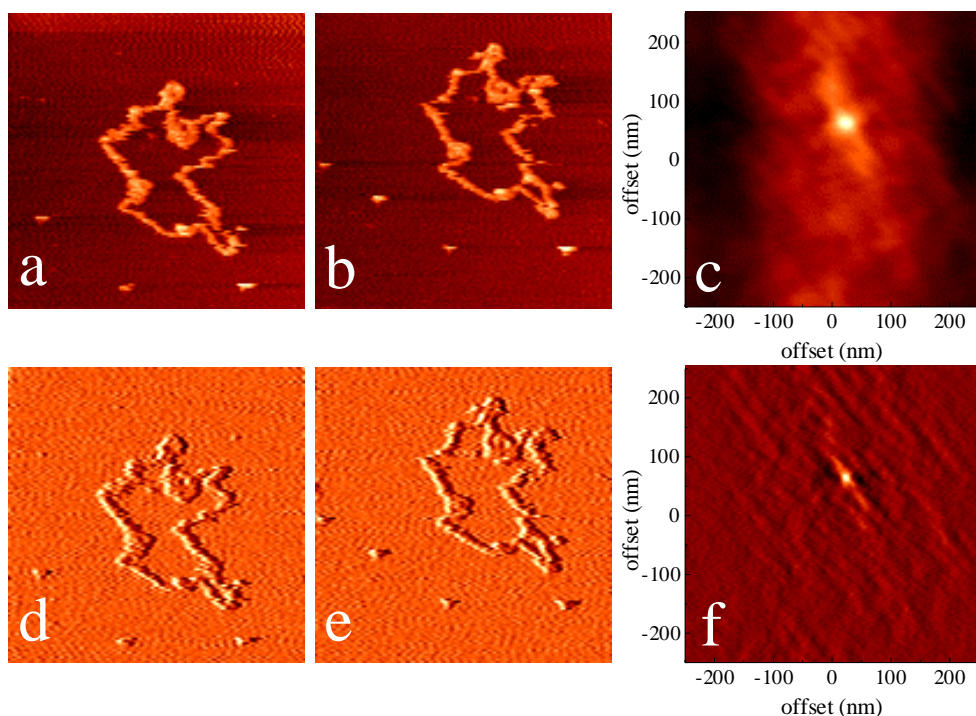
Figure 5.3 a and b) two succeeding frames of topography images of a 5.4 kbp DNA plasmid, scan area 500 * 500 nm², height range = 5 nm. c) The corresponding cross-correlation image d and e) The simultaneously acquired error-mode images and f) their cross-correlation. At a x, y displacement of 30, 70 nm a maximum in the cross correlation image occurs that corresponds to the drift between imaging the two frames.

graphical features. An elegant way to avoid low frequency artifacts is by using the error-mode image for image tracking. The error-mode, in the case of tapping mode AFM the amplitude signal, produces differentiated topography images, especially sensitive for edges [15]. The error-mode images corresponding to figure 5.3a and 5.3b are plotted in figure 5.3d and 5.3e. The amplitude signal can be regarded as the band pass filtered topography image, with a lower cut off frequency determined by the bandwidth of the feedback loop, and an upper cut off frequency determined by the bandwidth of the RMS amplitude detector. Thus only features that occur with a frequency between 1.6 and 5.0 kHz contribute to the error-mode image. The edges of topographical features, like the molecules under investigation, are included in this bandwidth, but tilt and vertical drift of the scanner generally have a much lower frequency and do not contribute to the error-mode image. The cross-correlation of figures 5.3d and 5.3e is shown in figure 5.3f and shows a sharper, more distinct peak than that of the

unprocessed topography image. Using the error-mode for cross-correlation image tracking proved to be much more reliable than using topography images.

Drift compensation by image tracking

The cross-correlation algorithm was implemented in the data acquisition software, and before acquisition of the next frame the measured drift between two previous frames is fed back to the piezo scanner in order to compensate for it. During the acquisition of a sequence of frames the voltage necessary for the drift compensation is recorded. In figure 5.4a the accumulation of drift of a typical experiment is plotted as a function of time. The scan range was 500 nm measuring 128^2 pixels, at a frame time of 4 s. During the measurement the average drift amounted 0.1 nm/s in the x direction and 0.2 nm/s in the y direction. At the end of the experiment the total drift accumulated to more than 200 and 400 nm in the x and y direction. Without image tracking after 40 min only 12% of the area scanned in the first frame would still be in the field of view of the last frame.

To check the accuracy and reliability of the on-line image-tracking algorithm we measured the residual drift of the images by a similar off-line cross-correlation algorithm. However, instead of the previously acquired frame we used the first frame of the sequence as a reference, in order to prevent accumulation of errors in the drift measurement. This procedure was applied to the topography images, that were corrected for tilt and vertical drift by line subtraction of a second order polynome. The resulting

a)   b)
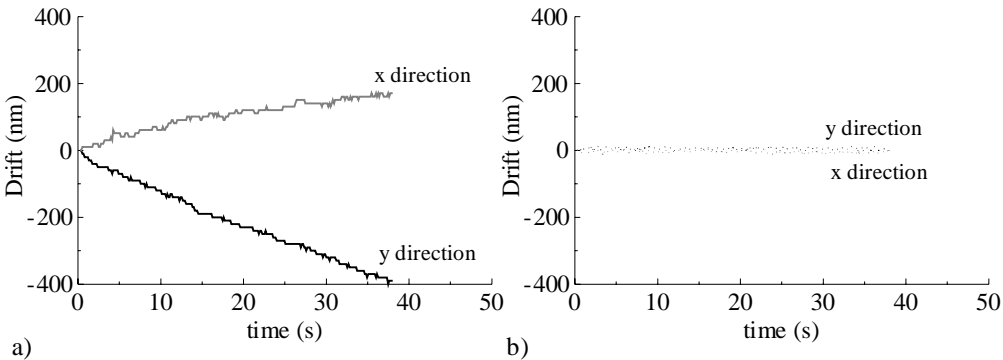
Figure 5.4 a) lateral drift as measured by on-line image tracking as a function of time. Drift amounted 0.2 nm/s in the x direction and 0.3 nm/s in the y direction. b) residual error calculated off-line. The error was obtained by using the cross-correlation algorithm, but now each frame was compared with the first frame of the sequence, in stead of the previous one. The error in the drift compensation is less than 10 nm.
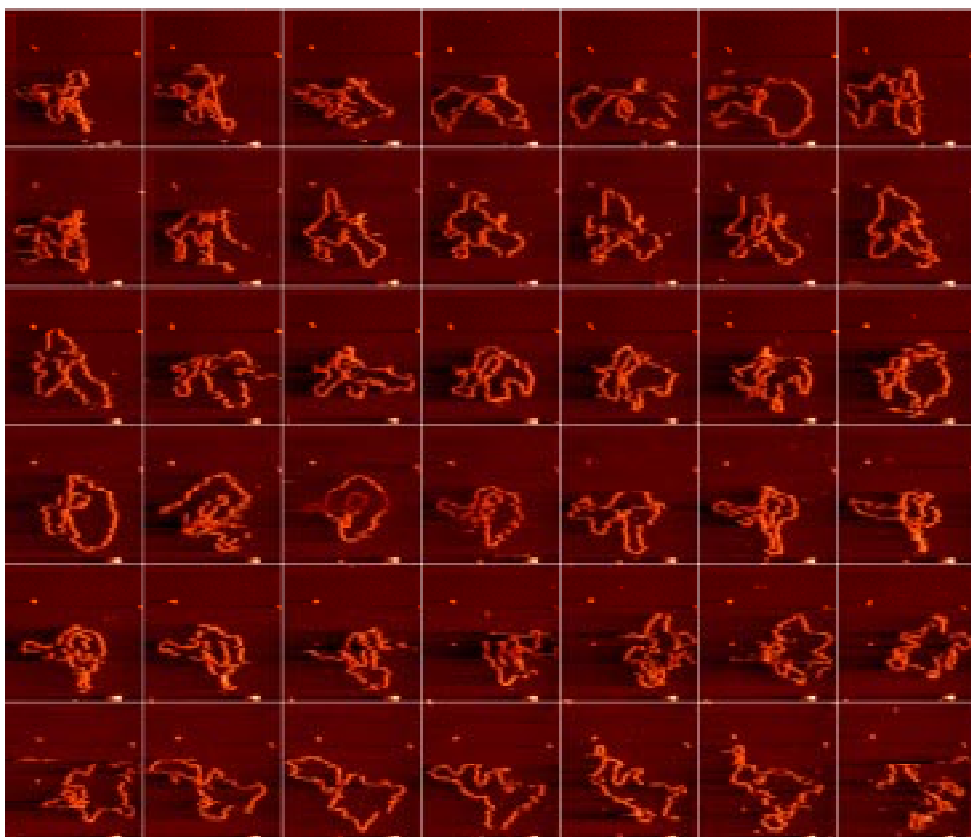
Figure 5.5 Sequence of topography images of a single 5.4 kb DNA plasmid on mica followed in time. Scan area 500 * 500 nm², corresponding to 128² pixels, height range = 5 nm, frame rate 0.25 Hz. Pollution particles form convenient position markers, and show negligible drift during the sequence.

drift is plotted in figure 5.4b. The error in the image tracking procedure amounted only 6 ± 3 nm, and never exceeded 10 nm. Small errors in the drift compensation do not accumulate, as during 40 min the residual drift does not show a systematic increase. Thus on-line image tracking provides a reliable and accurate way to correct for drift.

Diffusion of DNA plasmids

We used the image-tracking algorithm to keep track of a 5.4 kb DNA plasmid. In figure 5.5 part of a sequence of images measured at a frame rate of 4 s per frame is shown. To be able to follow this molecule, image tracking was necessary, as drift exceeded several hundreds of nanometers during

the experiment. Since at least some parts of the molecule do not move between succeeding frames, cross-correlation of the images still results in an accurate drift measurement. Pollution particles that are also present in the image remain at the same location during the sequence of images, confirming accurate drift compensation.

The DNA mobility of this plasmid is not the representative for all molecules. We observed a large variation in the mobility of DNA molecules that is also expressed in the quality with which the topography image can be measured. In figure 5.6c and 5.6e two typical frames of other, similar DNA plasmids in the same buffer are plotted. In the case of figure 5.6e the mobility of the plasmid is so high that the topography image shows apparently uncorrelated features that can not be reconstructed to the shape of the DNA plasmid. To get a clear image of the plasmid an even much better time resolution would be necessary. When the topography signal recorded scanning a single line is compared with the topography signal that is recorded on the linescan back, which has a delay of only 15 ms, a very faint correlation is measured. The time resolution is in this case at least one order of magnitude too small for an accurate measurement of the conformation of the molecule. However the cross-correlation procedure still works, which was confirmed by qualitative evaluation of the peak in the cross-correlation image. In all cross-correlation images a distinct peak occurred, that is necessary for reliable measurement of the drift.

Diffusion analysis of DNA plasmids

Though the conformation of a DNA plasmid can sometimes not be reconstructed from the topography image, its centre of mass can still be calculated fairly accurately, though averaged over the frame time. In figure 5.6b, 5.6d and 5.6f the MSD trajectory of the molecules in figure 5.6a, 5.6c and 5.6e is plotted for the scan direction and perpendicular to the scan direction. The standard deviation of the MSD measurement as calculated by equation 5.9 is plotted as error bars in figures 5.6b, 5.6d and 5.6f. Although the slope of the MSD plot and thus the diffusion coefficient should be direction independent, in figure 5.6b and 5.6d a significant difference is observed between the diffusion coefficient in the fast scan direction (horizontal) and the slow scan direction (vertical).

In the case of the plasmids shown in figure 5.6a and 5.6c this observed difference in slope, and thus the difference in diffusion coefficient, exceeds the expected statistical variation of the MSD. The difference however, can not be attributed to the scanning tip. This is evident as in figure 5.6d diffusion in the fast scan direction has a higher diffusion coefficient whereas in
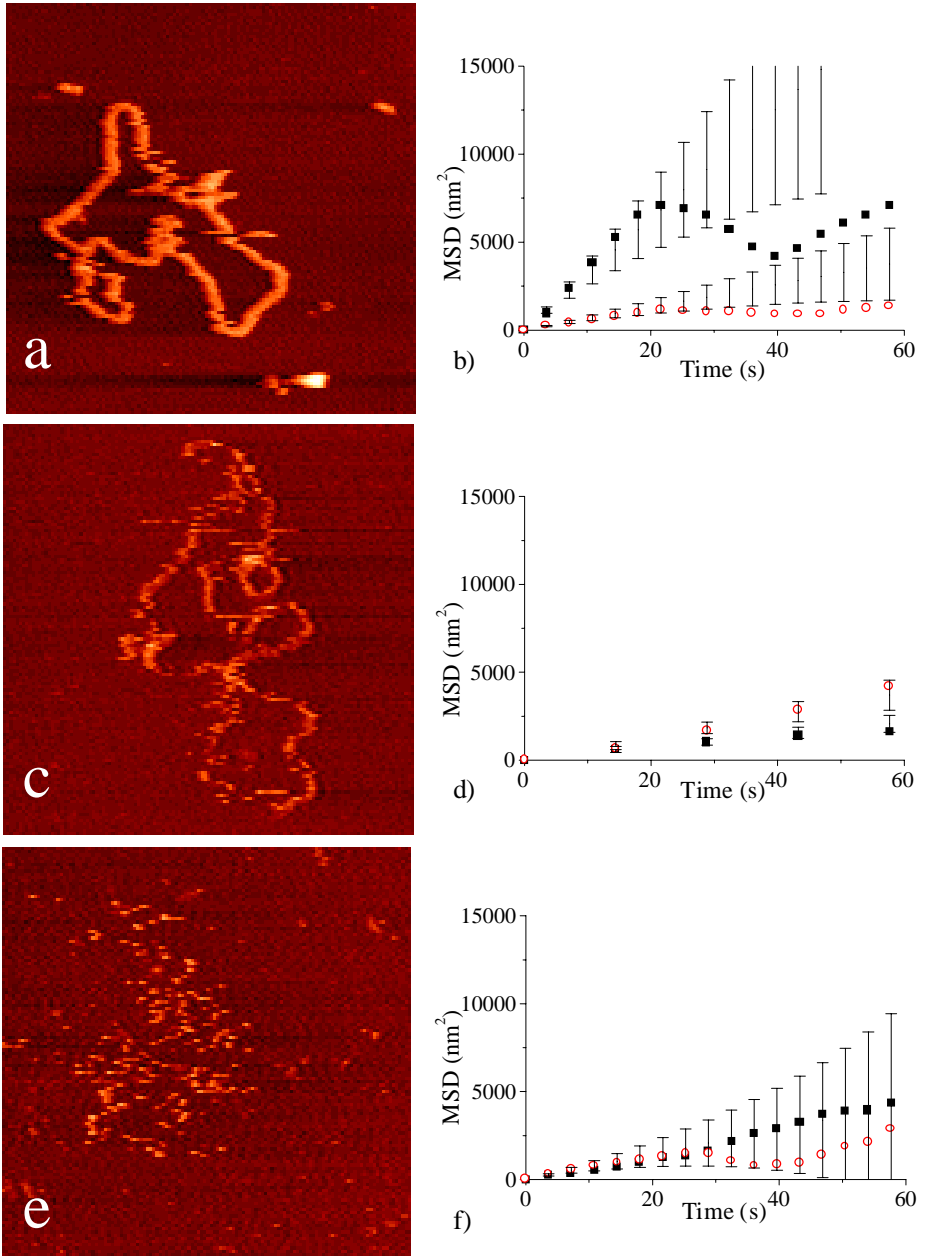
Figure 5.6 a, c and e) one frame out of a sequence of topography images of a 5.4 kb DNA plasmid is shown. Scan area 500 * 500 nm², height range 5 nm, n_f = 54, 67 and 23 for figures 5.6a, 5.6c and 5.6e. The corresponding MSD as a function of time is plotted in figure 5.6b, 5.6d and 5.6f. Solid squares are MSD values measured in the fast scan direction, open circles in the slow scan direction. Error bars correspond to $\sigma_{MSD}{}^2$ following equation 5.9. Diffusion coefficients were fitted from the first 3 points, resulting for figure 5.6b, 5.6d and 5.6f in diffusion coefficients of b) 158, 33 nm²/s d) 18, 27 nm²/s f) 31 and 28 nm²/s, in the fast and slow scan direction.

figure 5.6b diffusion in the fast scan direction has a lower diffusion coefficient. If the scanning tip would influence the movement of the DNA, the observed diffusion coefficient should also vary with the scan velocity. Except for the diffusion observed in the slow scan direction in figure 5.6a, all the measured diffusion coefficients have the same magnitude of approximately 30 nm²/s. Figure 5.6c however, was imaged at a frame rate 4 times less than the frame rate in figure 5.6a and 5.6e, which apparently does not influence the measured diffusion coefficient. The MSD trajectory shown in figure 5.6b is typical for a molecule that is locally pinned to the surface. Though the regions of DNA that are pinned to the surface do not remain fixed during the entire series of frames, which can be seen in figure 5.5, temporary fixation of the plasmid does have a major influence on the dynamics of the molecule as can be seen in both the MSD trajectory and the topography image.

The plasmid that is shown in figure 5.6e shows unrestricted diffusion. The MSD increases linear in time, and the slope of the MSD is equal for both scan directions. Deviations from a linear fit fall well within the expected standard deviation of the MSD versus time plot. As a result of unrestricted diffusion the movement of the DNA plasmid is too fast for imaging by AFM. Using the image tracking procedure thermal drift of the scanner did not limit the duration of the imaging experiment. The experiments were stopped when the molecule itself diffused out of the scan area.

5.5 Discussion and conclusion

The scan velocity of tapping mode AFM is limited by the hardware of the setup. Custom-made cantilevers, with a high resonance frequency, may help to increase the scan velocity [16], but these cantilevers are not easily available and they would require additional modifications of the existing AFM hardware as well.

Zooming in allows an increase of the frame rate, without extra damaging of the sample. Thus, images of 500 * 500 nm² of a single DNA molecule can be measured at only 4 s/frame for more than 200 frames without visible damage. To prevent that drift causes the molecules to move out of the scanned area, we have described a simple and reliable method to correct for thermal drift. An image-tracking algorithm allows zooming in on a small area over a long period. Because the error-mode image contains only features with spatial frequencies that correspond to the molecules of interest, for on-line applications use of the error-mode image as input for the algorithm yields a more reliable result than using the topography image. The procedure can

be applied independent of the sample shape, provided that succeeding frames have enough, non-periodical, features in common. Using the image-tracking algorithm we measured in the setup a drift of typically 0.2 nm/s, comparable with values reported in literature [11]. Off-line application of the cross-correlation procedure may be used additionally, to correct for residual drift. By using the image-tracking procedure the positions of fixed pollution particles, which form convenient position markers, on mica remain stable for at least 80 min, despite of a significant drift of the scanner.

The high frame rates and the large number of frames allow single particle tracking analysis, which is commonly used in studies on single molecules. DNA plasmids on a mica surface show a linear dependence of the MSD on time. Different values are sometimes obtained for directions parallel and perpendicular to the scan direction. This directional dependence can be caused by a disturbance of the free diffusion by the tip, but this effect seems not to be related with scan velocity. Local pinning of the DNA plasmids on mica can also account for the observed behaviour. Temporary immobilization of parts of the plasmids restricts diffusion and will decrease the MSD at long time intervals. This explains why the deviation from a linear dependence of the MSD on time is greater than expected from the measurement inaccuracy.

The mechanism of the interaction between DNA and mica in $MgCl_2$ buffer has been the subject of discussion in several papers [17,18]. Differences in the composition of mica are presumably responsible for the poor reproducibility of these experiments. Guthold et al. [6] report free two-dimensional diffusion of DNA fragments on Mg treated mica. In Chapter 4 we have shown that immobilization of DNA on mica can be located at distinct points on the mica surface [4] . In the present study we observed a large variation in the mobility of DNA plasmids and despite the reproducibility of the measured diffusion coefficient of the centre of mass of the plasmid, the appearance of the DNA molecule varied a lot.

The measured diffusion coefficients of the centre of mass in this paper are one order of magnitude higher than observed in a study by Guthold et al. [6]. Different batches of mica and different buffer solutions may account for this, but the poor reproducibility of the mobility of DNA makes it hard to evaluate these effects. The high mobility of the DNA may facilitate studies of protein DNA interactions as less hindrance by the surface can be expected when DNA is only loosely bound to the surface [19].

A frame rate one order of magnitude higher than generally achieved with an AFM, allowed visualization and detailed analysis of the diffusion of these relatively mobile molecules. Application of the image tracking procedure

will simplify future experiments visualizing single molecules with an AFM at a high temporal resolution, and will increase the accuracy of relative displacement determination of these molecules.

5.6 References

1   Han, W., and S.M. Lindsay. 1997. Kinked DNA. *Nature* 386: 563.

2   Hansma, H. G. 1995. Atomic force microscopy of biomolecules. *J. Vac. Sci. Technol. B.* 14: 1390-1395.

3   Guthold, M., M. Bezanilla, D. A. Erie, B. Jenkins, H.G. Hansma, and C. Bustamante. 1994. Following the assembly of RNA polymerase-DNA complexes in aqueous solutions with the scanning force microscope. *Proc. Natl. Acad. Sci USA* 91: 12927-12931.

4   Van Noort, S.J.T., K.O.van der Werf, A.P.M. Eker,C. Wyman, B.G. de Grooth, N.F. van Hulst, and J. Greve. 1998. Direct visualisation of dynamic protein-DNA interactions with a dedicated Atomic Force Microscope. *Biophys. J.* 74: 2840-2849.

5   Lal, R., and S.A. John. 1994. Biological applications of atomic force microscopy. *Am J. Physiol.* 266 (Cell Physiol. 35): C1-C21.

6   Guthold, M., X. Zhu, C. Rivetti, G. Yang, N.H. Thomson, S. Kasas, H.G. Hansma, B. Smith, P.K. Hansma, and C. Bustamante. 1997. One-dimensional diffusion and transcription by E. coli RNA polymerase observed with the scanning force microscope. *J. Biol. Chem.* "submitted for publication.

7   Hansma, H. G., and D. E. Laney. 1995. Applications for Atomic Force Microscopy of DNA. *Biophys. J.* 68: 1672-1677.

8   Hansma, H. G., and D. E. Laney. 1994. Motion and Enzymatic Degradation of DNA in the Atomic Force Microscope. *Biophys. J.* 67: 245-2459.

9   Putman, C.A., K.O. van der Werf, B. G. de Grooth, N. F. van Hulst, and J. Greve. 1994. Tapping mode atomic force microscopy in liquid. *Appl. Phys. Lett.* 64: 2454-2456.

10 Gittes, F. and C. F. Schmidt. 1998. Thermal noise limitations on micromechanical experiements. *Eur. Biophys. J.* 27: 75-81.

11 Thomson, N. H., M. Fritz, M. Radmacher, J. P. Cleveland, C. F. Schmidt, and P. K. Hansma. 1996. Protein tracking an detection of protein motion using Atomic Force Microscopy. *Biophys. J.* 70: 2421-2431.

12 Press, W. H., B. P. Flannery, S. A. Teukolsky, and W. T. Vetterling. 1986. Numerical recipies. Cambridge Press, New York.

13 Qian, H., M. P. Sheetz, and E. L. Elson. 1991. Single particle tracking, analysis of diffusion and flow in two-dimensional systems. *Biophys. J.* 60: 610-921.

14 Van der Werf, K.O., C.A. Putman, B. G. de Grooth, F.B. Segerink, E.H. Schipper, N. F. van Hulst, and J. Greve. 1993. Compact stand-alone atomic force microscope. *Rev. Sci. Instr.* 64: 2892-2897.

15 Putman, C. A., K.O. Van der Werf, B. G. de Grooth, N. F. van Hulst, J. Greve, an P. K. Hansma. 1992. A new imaging mode in Atomic Force Microscopy dase on error signal. *SPIE Scanning Probe Microsc.* 1693: 198-204.

16 Walters, D.A., J.P. Cleveland, N.H. Thomson, and P.K. Hansma. 1996. Short cantilevers for atomic force microscopy. *Rev. Sci. Instr.* 67: 3583-3590.

17 Hansma, H. G., and D. E. Laney. 1996. DNA binding correlates with cationic radius: assay by atomic force microscopy. *Biophys. J.* 70: 1933-1939.

18 Rivetti, C., M. Guthold, and C. Bustamante. 1996. Scanning Force Microscopy of DNA deposited onto mica: equilibration versus kinetic trapping studied ba statistical polymer chain analysis. *J. Mol. Biol.* 264: 919-932.

19 Keller, D. 1998. Making movies of molecular motions. *Biophys. J.* 74: 2743-2744.

Chapter 6

Mapping electrostatic forces using higher

harmonics tapping mode in liquid

Abstract

A simple model of a damped, harmonic oscillator is used to describe the motion of an Atomic Force Microscope cantilever tapping in fluid. Using experimentally obtained parameters, excellent agreement is found between theory and experimental results. From the model we estimate that the force applied on the sample can range up to 100 nN, depending on the surface charge density. Detailed analysis of the cantilever deflection reveals subtle differences in the oscillatory motion, as a result of differences in the tip-sample interaction, which can conveniently be visualized by spectral analysis. The amplitudes of the higher harmonic frequencies are shown to be sensitive for electrostatic interactions. Mapping of higher harmonic amplitudes is applied to qualitatively map the surface charge density of DNA molecules on poly-L-lysine coated mica.

6.1 Introduction

Electrostatic forces play an important role in the interaction between biological molecules. Many techniques, like electrophoresis, titration, electrokinetic and redox measurements are available for measuring the average surface charge density. Variations in the local charge density on the surface of single molecules may have a profound impact on the structure and function of the molecule, but this distribution of surface charges is experimentally more difficult to obtain.

The Atomic Force Microscope (AFM) has been used to map the surface charge density under physiological conditions with a high spatial resolution by measuring tip-sample interaction forces [1,2]. The most common way to probe tip-sample interactions is by acquisition of force versus distance curves while raster-scanning the tip across the surface. Force-distance curves obtained in this way are well understood and it has been demonstrated that from such curves adhesion forces, hydration forces and electrostatic forces can be extracted, together with topography information [3]. Only recently simultaneous mapping of both topography and adhesion force with molecular resolution has been reported [4]. Though analysis of force-distance curves directly provides force information, experimentally the procedure is quite demanding both on time and computer memory.

Other schemes have been demonstrated to provide surface charge density related contrast. Surface charge densities on several biological samples in solution have been extracted by analysis of changes in apparent height with applied force using constant force mode AFM [2,5]. However, due to the high frictional forces not all samples can be imaged successfully in constant force mode. Tapping mode AFM has proved to be the most reliable way to obtain high-resolution topography images of biological molecules in liquids [6,7]. In tapping mode the cantilever is oscillated and brought to the surface. Like in force-distance mode, in tapping mode the tip is moved to and from the surface, thus in principle similar information can be obtained. Recently Czajkowsky et al. [8] have shown experimentally that the phase shift of the oscillating cantilever can be related to the surface charge, though the mechanism that causes the phase contrast remained unclear.

In spite of the apparently similar way of operation, remarkable differences in the movement of the cantilever between tapping mode AFM in air and in liquid have been reported [7]. In contrast to tapping mode AFM in air [9] however, only few papers deal with the tip-sample interaction of a tapping tip in liquid [10,11]. In this paper we present a simple theoretical model to describe the dynamics of a cantilever tapping in liquid. We use data, obtained from force-distance mapping, to explain the response of the tapping

tip on substrates with different surface charge densities. Using this, we show that simultaneous mapping of higher harmonics of the cantilever deflection can be used to visualize differences in surface charge density of biological molecules with tapping mode AFM. From the calculations it is also possible to evaluate the forces that are applied by the tip on the sample in tapping mode AFM in liquid.

6.2 Theory

As a model for a tapping cantilever we use a driven, damped harmonic oscillator, with a spring constant k, an effective mass m and a damping γ The motion of the system is described by:

$$m \frac{\partial^2 z}{\partial t} + \gamma \frac{\partial z}{\partial t} + kz(t) = F(z, t) \tag{6.1}$$

where z is the position of the tip and t represents time. F(z,t) is the sum of the remaining forces that act on the cantilever and can be split into the driving force that oscillates the cantilever and tip-sample interaction forces. When the cantilever is immersed in liquid, both the effective mass and the damping increase, the spring constant does not change. From the thermal noise spectrum of the cantilever the spring constant can be calculated using the equipartition theorem [12]. The effective mass equals k / w_0^2, where ω_0 is the resonance frequency and the damping can be obtained from the Q factor, as $\gamma = m \omega_0 / Q$.

The forces that act on the cantilever can be split into time dependent and distance dependent forces. Far away from the surface the latter can be neglected and, on top of thermal movement, the cantilever is oscillated using a driving force $F_{drive}(t)$ generated by a dither piezo. Tapping mode AFM is simulated by applying $F_{drive} = F_0 \sin(\omega t)$ to the cantilever, force-distance experiments can be simulated by applying a sawtooth-shape in stead of a sinusoidal signal to the dither piezo.

When the tip approaches the surface the forces between the tip and the sample can be described by DLVO (Derjaguin-Landau-Verwey-Overbeek) theory, as the sum of Born repulsion, Van der Waals forces and electrostatic double layer forces [13]. Van der Waals attraction and Born repulsion between a sphere and a flat surface can be described using the Derjaguin approximation [1] as:

$$F_{VdW}(d) = \frac{HR}{3} \left(\frac{1}{d^2} - \frac{r_0^6}{d^8} \right) \tag{6.2}$$

where H is the Hamaker constant, R the radius of a sphere representing the tip, d the distance between the tip and a planar surface, and r_0 the smallest separation between the tip and the sample that follows the Pauli exclusion force. Butt has shown that the attractive Van der Waals force of an AFM tip interacting with a surface can be better approximated as $0.9/d^{1.4}$ in stead of $1/d^2$, accounting for the conical shape of the tip [3,13]. The electrostatic force between a sphere with radius R and charge density σ_R and a flat surface with charge density σ_s can be described as:

$$F_{el}(d) = \frac{4\pi\lambda\sigma_R\sigma_s}{\varepsilon}\, e^{-\frac{d}{\lambda}}$$
$$= F_{el,max}\, e^{-\frac{d}{\lambda}} \tag{6.3}$$

where ε is the dielectric constant of the medium. The Debye length λ is characterized by the salt concentration c as $\lambda = 0.304$ nm $/ \sqrt{c}$, for monovalent salt. The surface charge density is directly proportional with the electrostatic force as all other factors are only tip dependent.

Thus by solving equation 6.1, using $F_{drive}(t)$, $F_{vdW}(z-d_0)$ and $F_{el}(z-d_0)$, where d_0 is the rest position of the tip, the complete trajectory of a tip interacting with a surface can be calculated.

6.3 Materials and methods

Numerical simulations

The second order differential equation 6.1 was split into two coupled first order differential equations. A fourth-order Runge-Kutta method [14] was used to advance a solution to this system using constant time steps of 10^{-7} s. For boundary conditions we used z(0) = 0 and dz(0)/dt = 0. Tapping mode simulations showed that after 2 oscillation cycles a stationary solution was reached. The software was implemented in IDL (RSI, Co, USA).

AFM setup

Experiments were performed using a home built stand-alone AFM [15]. For both force-distance and tapping mode AFM, triangular cantilevers (Park, Ca, USA) with a spring constant, k = 0.5 N/m were used, allowing direct comparison between both types of experiments. For data acquisition we used a PCI 16E-1 data acquisition board (National Instruments, Tx, USA) with a maximum data acquisition rate of 2 MHz for two channels. Force-distance mode was implemented as described elsewhere [16]. Like in force-

distance mode, in tapping mode not only the topography signal, but also the deflection signal was measured. The MHz sampled deflection signal, acquired during scanning, allows detailed analysis of tip-sample contact. Because topography was measured simultaneously with these deflection curves, differences in response can directly be attributed to molecular features on the surface that appear in the topography image.

Sample preparation

Mica disks (Ted Pella, Ca, USA) were treated with a 0.01 % poly-L-lysine (PPL) solution for 30 s , rinsed with MilliQ water and blown dry with nitrogen gas. PLL adheres to the negatively charged mica surface, forming a substrate for DNA immobilization [17]. A 5 μl drop of 1 μg /ml DNA, either 700 bp PCR fragments or 5.4 kb pcDNA3 plasmids, was pipetted onto the PLL treated mica disk and after 30 s. 200 μl 75 mM KCl, 25 mM Hepes pH 7.0 was added. Without rinsing the sample, the AFM was mounted on top of the sample, and imaging was started directly after mounting.

6.4 Results and discussion

Thermal noise measurements

As described in the theory section, the parameters that characterize the oscillator can be obtained from the thermal noise spectrum of the free cantilever shown in figure 6.1. From the thermal noise spectrum a spring constant of 0.5 N/m, a resonance frequency of 38 kHz and a quality factor of 2 is obtained. Using these values the experimentally obtained cantilever response differs from the response curve of a simple damped harmonic oscillator, that is also plotted in figure 6.1 (dotted line). At low frequencies laser and electronics noise dominate the signal. This noise should not affect our interpretation of the data because it is not related to cantilever movement. At frequencies above the resonance frequency, the experimentally obtained
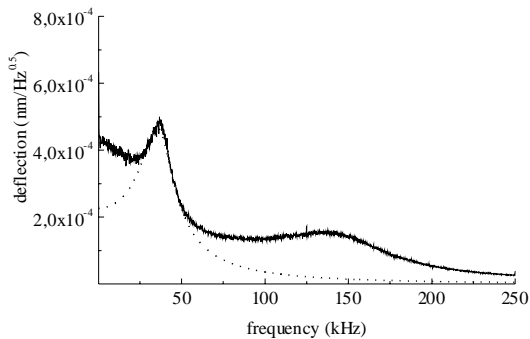

Figure 6.1 Thermal noise spectrum of the cantilever just above the surface (solid line). The dotted line denotes the response curve of a damped harmonic oscillator using ω_0= 38 kHz, k = 0.5 N/ m and Q = 2.

curve shows a higher amplitude than is expected of a simple damped harmonic oscillator. This signal exceeds the system noise and can be attributed to a higher order bending mode of the cantilever, which has a resonance frequency at 145 kHz. In order to take this movement of the cantilever into account a more complex model should be used for the cantilever, describing its distributed mass [18]. In this study we will limit our interpretation of the cantilever movement to frequencies close to resonance of the first order mode. However one should realize that in tapping mode AFM also higher bending modes may be exited, albeit with an amplitude that is generally an order of magnitude smaller that of the first bending mode.

Force-distance mode measurements

For determination of the parameters describing the electrostatic and the Van der Waals forces between the tip and the sample we measured force-distance mode images of the DNA sample using the same cantilever and tip as used for tapping mode AFM in liquid. Figure 6.2a shows a topography image that is obtained simultaneously with the force-distance measurements, at a maximum force of 750 pN. Because of the poor time resolution in force-distance mode, in combination with the weak attachment of DNA to PLL treated mica, DNA can move during the experiment, resulting in a sometimes-disrupted appearance of DNA strands, that is also discussed in chapter 5. DNA molecules have a width of 3 ± 1 nm and a height of 2.0 ± 0.1 nm. From the apparent width of the DNA molecules we estimate the effec-
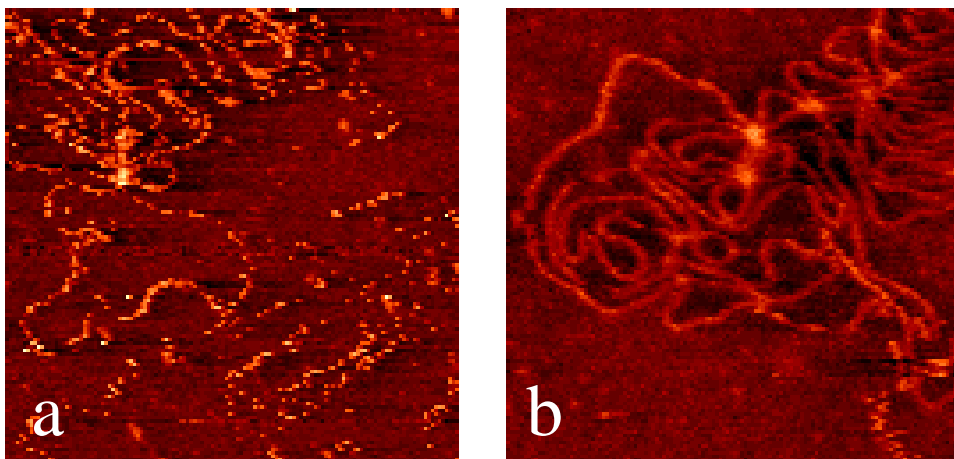
Figure 6.2 Topography images of plasmid DNA. a) Force-distance mode, b) Tapping mode. Scan area 250 * 250 nm², height range 4 nm. Both apparent height and width of the DNA differ between force-distance mode and tapping mode.
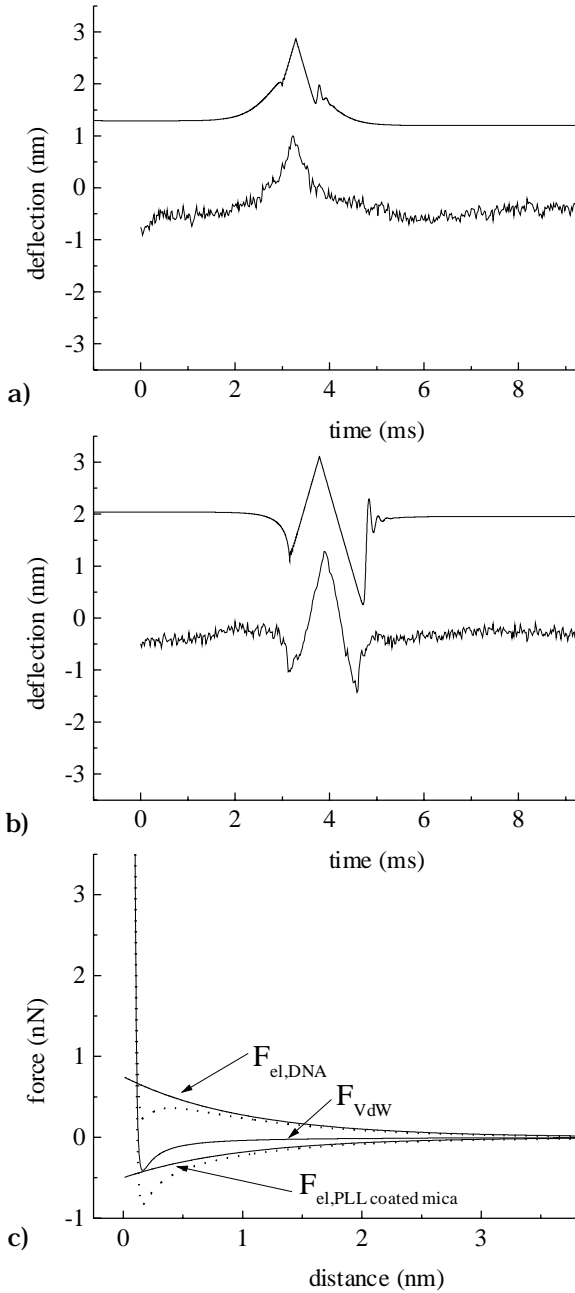
Figure 6.3 a) Deflection traces on DNA, the bottom line shows a measured trace, the top line shows a calculated trace, using $F_{el,max}$ = 750 pN. b) Deflection traces on PLL coated mica, the bottom line shows a measured trace, the top line the calculated trace using $F_{el,max}$ = -500 pN. In both figure 6.3a and 6.3b the deflection traces are given an arbitrary offset for better visualization. c) Tip-sample forces as a function of the distance for both the repulsive and the attractive interactions (dotted lines). Solid lines represent the electrostatic and Van der Waals components separately. Parameters used: k=0.5 N/m, Q=2, ω_o=38 kHz, R=5 nm, H = 2.61 10^{-21} J, r_0= 0.1 nm, ramp frequency 500 Hz, ramp amplitude 12 nm, Maximum force 750 pN.

tive tip radius to be 5 nm. Using a constant force of 750 pN the apparent height corresponds to the height that can be expected for B-DNA. For comparison a tapping mode image of the same sample, using the same tip is shown in figure 6.2b. Both the width of the DNA, 5 ± 1 nm, and the height,

1.4 ± 0.1 nm, are different when tapping mode is compared to force-distance mode.

Because in figure 6.2a force-distance curves were measured for every pixel, the height of the image can be used to select force-distance curves that were acquired on DNA and on PLL coated mica. In figure 6.3a in the bottom trace a force curve measured on DNA is plotted as a function of time. As the tip approaches the DNA molecule, the cantilever gradually bends up until a maximal force of 750 pN is reached. When the cantilever retracts a slightly different response is measured. Filling in the experimentally obtained cantilever parameters and a Debye length of 1 nm, corresponding to a salt concentration of 100 mM, equation 6.1 was numerically solved for different values of $F_{el,max}$. The best agreement between experimental and theoretical curves was found for an electrostatic force at the surface of 750 pN on DNA. The resulting force trace is plotted in figure 6.3a in the top line. A snap into contact can be seen when the Van der Waals force becomes dominant over electrostatic interactions, which is also present in the experimental curve. The hysteresis in the force trace also closely resembles the experimental data.

The bottom curve in figure 6.3b shows a force trace that was measured on PLL coated mica. Whereas DNA shows a repulsive force while the tip approaches the sample, on PLL the tip is first attracted to the surface, and then repelled from the surface. The best agreement was found between the experimental and theoretical curves using an electrostatic force of –500 pN, which is plotted in the top trace in figure 6.3b. Again details of the theoretically obtained force curve, like hysteresis, are also present in the measured curve. The good resemblance between experimental and theoretical curves supports the validity of our model of the cantilever interacting with a charged surface. The tip-sample interaction forces that cause the different interaction between DNA and PLL coated mica are plotted in figure 6.3c. For the interaction between the tip and DNA, the sum of the electrostatic force and the Van der Waals force is repulsive over the whole trajectory. As both forces are attractive in the case of PLL coated mica a distinct minimum in the interaction force of –800 pN is found.

Tapping mode measurements

It should be possible to deduce the information that can be obtained from force-distance mode experiments from the deflection trace, while tapping on a surface, as the tip follows the same trajectory. To be able to study the response of the cantilever in great detail we measured the deflection of the cantilever during scanning, with a much higher bandwidth than the topog-
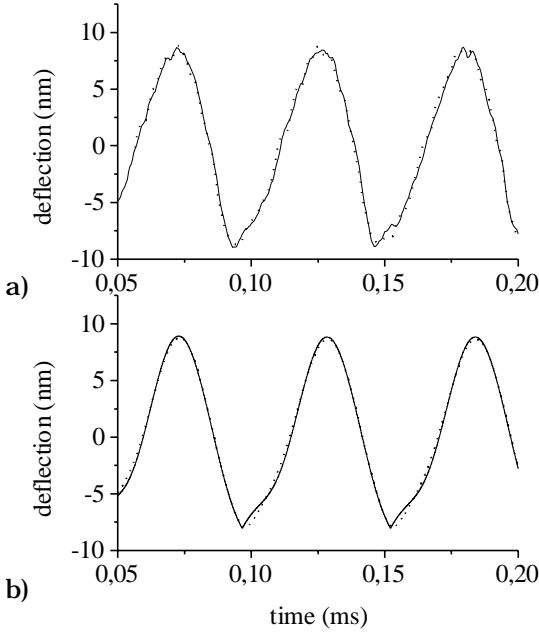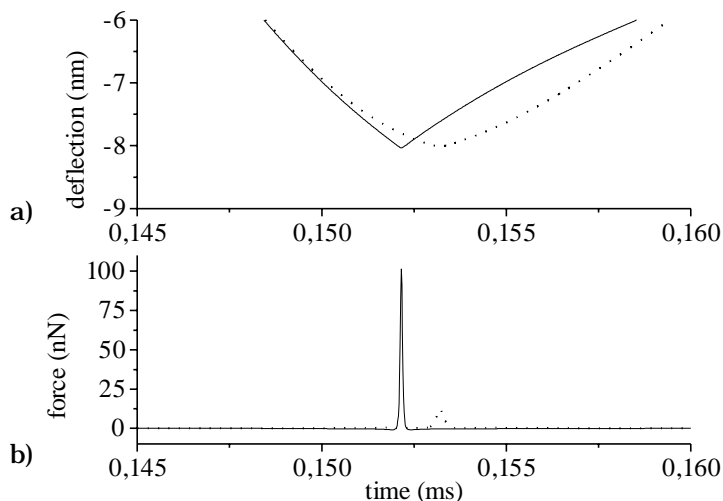
Figure 6.4 a) Measured deflection versus time traces of the cantilever tapping on PLL coated mica (solid lines), and on DNA (dotted lines). b) Corresponding calculated traces. Parameters: a = 8.5 nm, d_0 = 8.3 nm, ω = 18 kHz, all other parameters are the same as used for figure 6.3.

raphy. Signal acquired while tapping on DNA can be separated from signal acquired while tapping on PLL based on height differences that are visible in the simultaneously acquired topography image. In figure 6.4a two typical deflection traces are plotted that were measured on both types of surfaces. The global shape of the deflection curve is similar for both situations. A roughly sinusoidal signal that is clipped at the bottom, as was already demonstrated by Putman et al. [7]. Because of the very high viscous damping of the cantilever and the resulting low Q factor, the cantilever directly bends up in response to the high force gradient that the tip experiences as it approaches the surface. In the upward stroke the cantilever deflection regains its sinusoidal shape again. The fast response of the cantilever is very much in contrast to a cantilever tapping in air, with a high Q factor that effectively slows down the response of the cantilever.

At the bottom of the deflection curves, a small difference can be observed between the traces while tapping on DNA and on PLL coated mica. Where on DNA the deflection curve is slightly rounded off, on PLL coated mica a sharp kink in the deflection curve is observed.

Using the parameters obtained from the thermal noise spectrum and the force-distance curves, we solved equation 6.1 for a sinusoidal driving signal with the frequency and amplitude that corresponds to the experimental parameters used for figure 6.4a. The results nicely matched the experimentally obtained deflection curves as can be seen in figure 6.4b. Both the non-

Figure 6.5 a) Zoom-in on the calculated deflection traces of the cantilever tapping on PLL mica (solid lines), and on DNA (dotted lines). b) Corresponding forces that are applied to the surface. For parameters see figure 6.4.

sinusoidal movement of the cantilever and the behaviour of the signal when the tip is close to the surface are clearly visible in the simulations.

From the numerical solution a good estimation can be made of the forces involved in tapping mode AFM in liquid. In figure 6.5a a zoom-in of the calculated deflection curve close to the surface is plotted. The first striking feature is the delay of the tip-impact on DNA. In the case of a repulsive interaction between the tip and the sample the tip is deflected upward before it impacts on the surface, resulting in a phase lag of the cantilever oscillation. During the upward stroke in the oscillation this phase lag is inverted, which can be seen in figure 6.4b. However, the net phase shift that results from the difference in interaction may be sufficient to be used as a contrast parameter related to the surface potential, which has recently been confirmed experimentally [8].

Another subtle difference, that can only be seen by further magnification of figure 6.5a, between the two curves is the maximal deflection of the cantilever. Where on the positively charged surface the tip reaches down to 0.068 nm above the surface, on the negatively charged surface the minimal tip-sample distance is 0.088 nm. Though this difference is beyond the resolution of the AFM and can thus not be observed as a height difference by itself, the difference has a big effect on the applied force as the tip experiences a very large force gradient when it approaches the surface. In figure

6.5b the force applied by the tip on the sample is plotted as a function of time. Like in force-distance mode, at relatively large distances the force is dominated by the electrostatic interaction, that can only be seen in figure 6.5b as a slight deviation from 0. However, the magnitude of the electrostatic force is negligible compared to the Born repulsion that can range up to 100 nN in the case of a tip tapping on a positively charged surface. During the short interaction time of order 10^{-6} s the cantilever appears very stiff, resulting in a surprisingly large force applied to the surface. The symmetry of the force versus time curves shows that no energy is dissipated during the impact. Thus despite the large peak forces that can occur in tapping mode AFM in liquid, tapping is still relatively gentle because of the elastic response of the cantilever and the sample.

Spectral analysis

Distortions of the sinusoidal deflection signal can conveniently and accurately be analysed by evaluation of the higher harmonics of the driving frequency. In figure 6.6 the Fourier spectra calculated from the deflection traces shown in figure 6.4 are plotted for both the experimentally obtained data and the simulations. Attractive interactions, like between PLL coated mica and the Si_3Ni_4 tip, result in increased amplitudes of the higher harmonics. For the second and third harmonic the experimental amplitude increase of ~0.1 nm qualitatively agrees with the calculated results. For the fourth and fifth harmonics, the theoretically calculated spectra do not match the experimental data. At these high frequencies probably higher order bending modes of the cantilever are dominant, and these have not been included in our model.
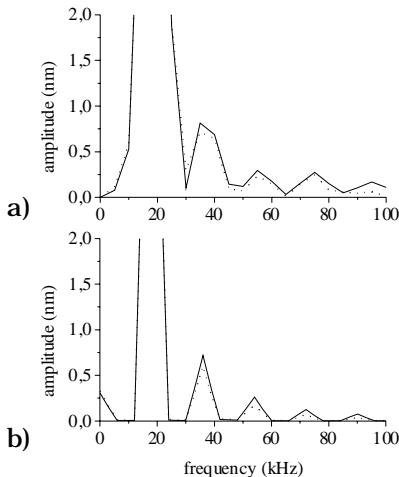
Figure 6.6 a) Measured deflection spectra of the cantilever tapping on PLL mica (solid lines), and on DNA (dotted lines). b) Corresponding calculated traces. For parameters see figure 6.4.

Using the simulations we can calculate the sensitivity of the amplitude of the higher harmonics for the surface potential. In figure 6.7 the amplitudes of the second and third harmonics are plotted as a function of the electro-
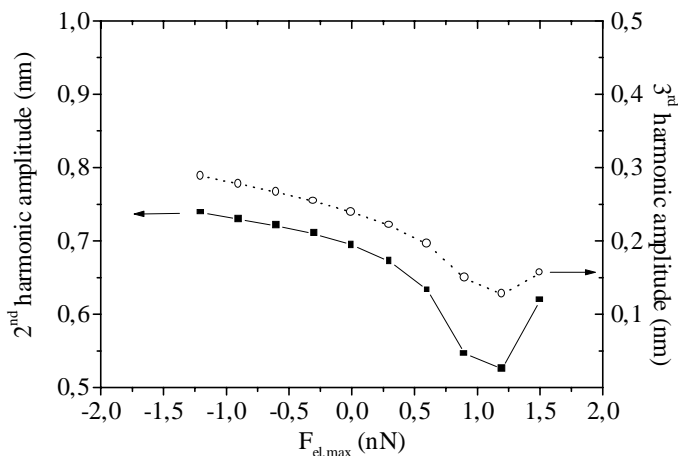

Figure 6.7 Calculated response of the second (solid lines), and third (dotted lines) harmonic amplitudes as a function of the surface charge density. For parameters see figure 6.4.

static force. The amplitudes of both signals decrease with increasing electrostatic force with an average slope of approximately -0.05 nm/nN. However, the dependence is not linear and when the attractive electrostatic force between the tip and the sample exceeds ~1.2 nN the amplitudes of both signals increase again.

In order to measure amplitude differences of the higher harmonics this difference should exceed the noise, which is dominated by thermal fluctuations of the cantilever. For a 5 kHz bandwidth, as used in our experiments, the noise level amounts 0.03 nm, so differences in the electrostatic force of 0.6 nN should be distinguishable in both the second and the third harmonic signal.

Higher harmonics mapping

A tapping mode topography image of a few 700 bp DNA molecules on a PLL treated mica surface is shown in figure 6.8a. DNA molecules have an apparent height of 1.4 ± 0.2 nm and a width of 5.0 ± 1.0 nm. For each pixel the deflection signal was Fourier transformed, resulting in a frequency response of the cantilever while tapping on the surface. From these spectra we generated images of the amplitudes observed at the driving frequency and at its higher harmonics, which are shown in figures 6.8b-6.8d. At this
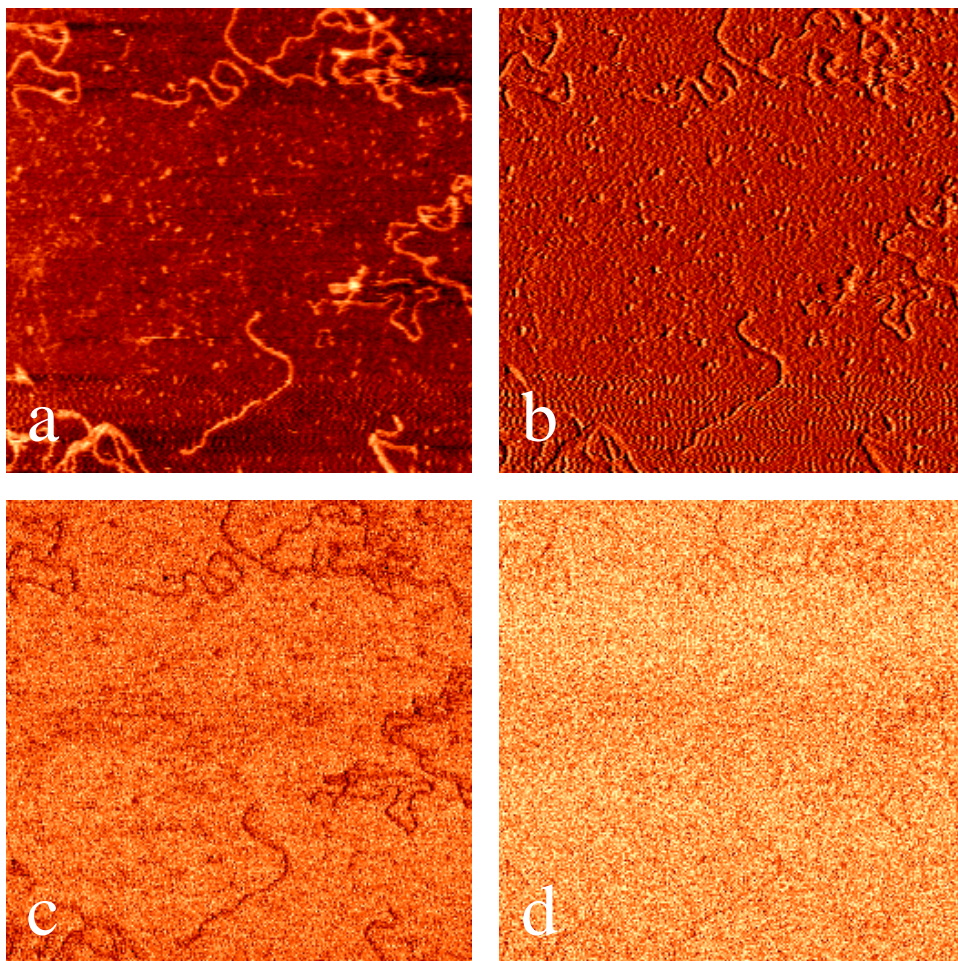
Figure 6.8 a) Topography image of 700 bp DNA, scan area 250 * 250 nm², height range 4 nm. b) driving frequency, amplitude range 3.5 - 4.5 nm. c) second harmonic, amplitude range 0.5 - 0.75 nm. d) third harmonic, amplitude range 0- 0.25 nm.

point it should be noted that higher harmonics are easily accessible experimentally, using lock-in techniques. With a lock-in amplifier similar results can be obtained on-line, without the need to sample deflection traces with a very high bandwidth.

Figure 6.8b shows the amplitude at the driving frequency. The contrast in this figure resembles the error mode image. This should be expected, since this frequency is the main component that contributes to the RMS amplitude that is used for feedback. When using the second harmonic amplitude for imaging (figure 6.8c), DNA molecules appear as dark regions, with a width of 5.0 nm ± 1.0 nm, comparable to the resolution obtained in the
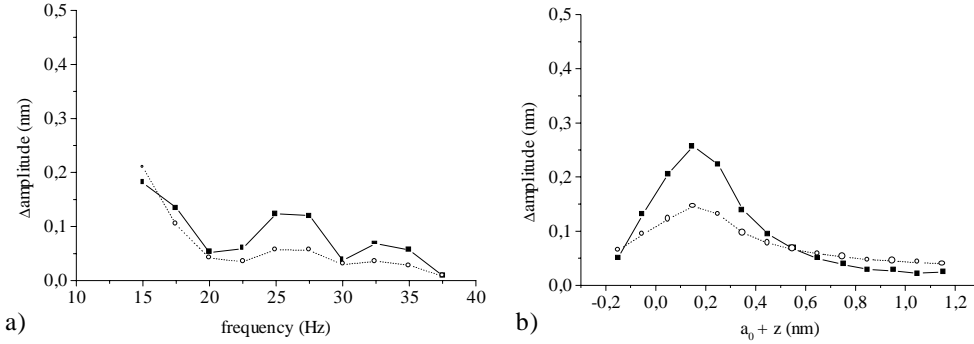
Figure 6.9 Calculated difference in response that can be expected between PLL mica and DNA of the second (solid lines), and third (dotted lines) harmonic as a function of the frequency (a) and the amplitude setpoint (b). For parameters see figure 6.4.

topography image. On DNA molecules the second harmonic amplitude is 0.6 nm where on the PLL surface the second harmonic amplitude is 0.7 nm. In the image of the third harmonic amplitude (figure 6.8d) only a very faint contrast can be seen, even though the average amplitude of 0.2 nm exceeds the noise level of 0.03 nm at 5 kHz bandwidth.

Experimental parameters

The results shown in the previous paragraph are very dependent on the imaging parameters used. In general the signal measured on DNA molecules have decreased higher harmonics contributions when compared to PLL treated mica. To find the optimal settings for surface charge related contrast in higher harmonics mapping, we calculated the effects of the chosen driving frequency and the amplitude set-point on the obtained contrast.

The response of the higher harmonic amplitudes is plotted as a function of the driving frequency in figure 6.9b. In general the lower the frequency, the higher the contrast in the higher harmonics, though at ± 22 kHz and at ± 30 kHz a dip appears in the difference in second and third harmonic amplitude response. However, in spite of the irregularity of the frequency response, that makes it hard to quantify the electrostatic potential of the surface, qualitatively the amplitude difference of both the second and the third harmonic show an increased amplitude for attractive tip-sample interactions at all frequencies.

The amplitude of the higher harmonics increase when the amplitude setpoint of the feedback is reduced (data not shown) as the motion of the cantilever is more severely distorted. The amplitude difference that can be

expected between DNA and PLL coated mica however, does not increase with increased damping of the oscillation. The amplitude difference of the second and third harmonic is plotted as a function of the distance from the surface, in figure 6.9a. Maximal contrast is obtained when the cantilever oscillation is reduced by 0.2 nm. Using this set-point, the tip remains in the electrostatic regime in the case of repulsive interaction, showing only subtle rounding-off of the deflection curve. In the case of attraction by the surface the tip enters the force regime dominated by Van der Waals forces, resulting in a sharp kink in the deflection. Using this amplitude set-point the contrast between the higher harmonics measured on molecules and substrate is maximal. This is also the regime in which the interaction forces are minimal. The topography image appears severely blurred because in the repulsive regime the tip remains quit far from the surface. Indeed imaging DNA molecules Argaman et al. [19] reported a very sharp phase contrast, that may be attributed to electrostatic interactions, whereas topography images appeared blurred. When the amplitude set-point is reduced more than 0.6 nm the third harmonic contrast exceeds the second harmonic contrast, though the amplitude difference is less than 0.05 nm. Thus, based on the simulation, for optimal surface charge related contrast in higher harmonics mapping, tapping mode AFM should be operated at low frequencies and low amplitude reduction.

6.5 Conclusions

Using a model of a damped harmonic oscillator both force-distance mode and tapping mode AFM was described quantitatively. The parameters that are necessary for the model can be obtained experimentally. Using DVLO theory for the tip-sample interaction excellent agreement was found between experiment and model. From the simulations we estimate that the tip-sample interaction force in tapping mode AFM can range up to 100 nN, depending on the sign and the magnitude of the electrostatic interaction. Detailed analysis of the cantilever deflection shows subtle differences in the cantilever movement that can be attributed to differences in surface charge density. Evaluation of the higher harmonics of the cantilever reveals this difference in cantilever response, both theoretically and experimentally. We have shown that at least qualitatively, the amplitude of the higher harmonic frequencies can be applied for mapping of the surface charge density with nanometer resolution, using the gentleness of tapping mode. Preliminary measurements on cell surfaces also show changes in higher harmonics amplitudes, suggesting that (visco-) elasticity of the sur-

face can be mapped using this parameter. Measuring higher harmonic amplitudes can easily be implemented in existing setups, providing a new means of contrast that is independent of topography.

6.6 References

1   Rotsch, Ch., and M. Radmacher. 1997. Mapping electrostatic forces with the atomic force microscope. *Langmuir* 13: 2825-2832.

2   Heinz, F. H., and J. H. Hoh. 1999. Relative surface charge density mapping with the atomic force microscope. *Biophys. J.* 76:528-538.

3   Butt, H-J. 1991. Electrostatic interaction in atomic force microscopy. *Biophys. J.* 60: 777-785.

4   Willemsen, O.H., M. M. E. Snel, B. G. de Grooth, J. Greve, P. Hinterdorfer, H. J. Gruber, H. Schindler, Y. van Kooyk, and C. G. Figdor. 1998. Simultaneous height and adhesion imaging of antibody-antigen interactions by atomic force microscopy. *Biophys. J.* 75: 2220-2228.

5   Müller, D. J., and A. Engel. 1997. The height of biomolecules measured with atomic force microscopy depends on electrostatic interactions. *Biophys. J.* 73:1633-1644.

6   Hansma, P.K., J.P. Cleveland, M. Radmacher, D.A. Walters, and P. Hillner. 1994. Tapping mode atomic force microscopy in liquids. *Appl. Phys. Lett.* 64: 1738-1740.

7   Putman, C.A., K.O. van der Werf, B. G. de Grooth, N. F. van Hulst, and J. Greve. 1994. Tapping mode atomic force microscopy in liquid. *Appl. Phys. Lett.* 64: 2454-2456.

8   Czajkowsky, D. M., M. J. Allen, V. Ellings, and Z. Shao. 1998. Direct visualization of surface charge in aqueous solutions. *Ultramicroscopy* 74:1-5.

9   Tamayo, J., and R. García. 1996. Deformation, contact time, and phase contrast in tapping mode scanning force microscopy. *Langmuir* 12: 4443-4435.

10 Liu, Y. Z., X. D. Cui, and S.M. Lindsay. () Model of dynamic force microscopy in fluid. submitted for publication.

11 Burnham, N.A., A. J. Kulik, and G. Gremaud. 1995. Nanosubharmonics: the dynamics of small non-linear contacts. *Phys. Rev. Lett.,* 74-25: 5092-5095.

12 Butt, H.-J., and M. Jaschke. 1995. Calculation of thermal noise in atomic force microscopy. *Nanotechnology* 6: 1-7.

13 Willemsen, O.H., M. M. E. Snel, L. Kuipers, C. G. Figdor, J. Greve, and B. G. de Grooth. 1999. A physical approach to reduce nonspecific adhesion in molecular recognition atomic force microscopy. *Biophys. J.* 76 :716-724.

14 Press, W. H., B. P. Flannery, S. A. Teukolsky, and W. T. Vetterling. 1986. Numerical recipies. Cambridge Press, New York.

15 Van der Werf, K.O., C.A. Putman, B. G. de Grooth, F.B. Segerink, E.H. Schipper, N. F. van Hulst, and J. Greve. 1993. Compact stand-alone atomic force microscope. *Rev. Sci. Instr.* 64: 2892-2897.

16 Van der Werf, K.O., C.A. Putman, B. G. de Grooth, and J. Greve. 1994. Adhesion force imaging in air and liquid by adhesion mode atomic force microscopy. *Appl. Phys. Lett.* 65: 1195-1197.

17 Williams, R. C. 1977. Use of polylysine for adsorption of nuclei acids and enzymes to electron microscope specimen films. *Proc. Natl. Acad. Sci. USA* 74: 2311-2315.

18 Schäffer, T. E., J. P. Cleveland, F. Ohnesorge, D. A. Walters, and P. K. Hansma. 1996. Studies of vibrating atomic force microscope cantilevers in liquid. Studies of vibrating atomic force microscope cantilevers in liquid. *J. Appl. Phys.* 80: 3622-3627.

19 Argaman M., Golan R., Thomson N. H., and Hansma H. G. 1997. Phase imaging of moving DNA molecules and DNA molecules replicated in the atomic force microscope. *Nucleic Acids Res* 25: 4379-84.

Summary

In this thesis a dedicated Atomic Force Microscopy (AFM) setup is used for imaging biochemical reactions with molecular resolution. The basis for the high resolution of AFM is the combination of a small probe, close proximity to the sample and a short-range interaction between the probe and the sample. The tip-sample interaction forces that are used in AFM allow imaging in various environments, including physiological buffers. However, although a decade has passed since DNA was first imaged using an AFM, most studies are still performed in air, and by doing so the sample is dehydrated and fixed. Visualization of protein-DNA interactions in physiological buffer would exploit the advantages of AFM that make it a unique tool for studying these reactions, namely its molecular resolution of functional complexes in combination with only limited sample preparation. It is shown in this thesis that high-resolution topography maps of these biomolecules can be measured with AFM reproducibly, over a long period of time, and with a fairly good temporal resolution. A careful optimization of the imaging parameters is required for this.

In chapter 2, first the contrast mechanism of tapping mode AFM in air is studied. In spite of the high normal resolution that is generally attributed to AFM, height anomalies ranging up to 10 nm can be measured due to tip-sample adhesion. Depending on the damping of the oscillation, the apparent height of sticking surfaces is reduced compared to less sticking surfaces. It is shown that these height artifacts result from a modulation of oscillatory movement of the cantilever. Damping and excitation of the cantilever by the driver continuously compete. As a consequence a severe modulation of the cantilever oscillation occurs, depending on the phase mismatch between the driver and the cantilever. Phase images of tapping mode AFM show a contrast that correlates with adhesion. Examples of a partially removed gold layer on mica, a Langmuir-Blodgett film and DNA are shown.

Structural changes in DNA in complex with photolyase, a small DNA repair enzyme are studied in chapter 3. Fixed specific and non-specific photolyase-DNA complexes are visualized in air. As a substrate for photolyase a

1150 bp DNA restriction fragment is UV-irradiated to produce damaged sites at random positions. Comparison with an 800 bp undamaged DNA fragment makes it possible to separate populations of specific and non-specific photolyase complexes on the 1150 bp fragment, relieving the need for highly specific substrates. Non-specific complexes show no significant bending but an increased rigidity compared to naked DNA, whereas specific complexes show DNA bending by 36º and higher flexibility.

Using tapping mode in liquid, non-specific photolyase-DNA interactions, that mimic the search of photolyase for damaged sites, are studied in chapter 4. After implementation of a number of instrumental improvements, the molecules can be visualised routinely, under physiological conditions and with molecular resolution. Images are acquired reproducibly without visible damage for at least 30 minutes, at a scan rate of 2 x 2 μm^2 per minute and a RMS noise of less than 0.2 nm. Non-specific photolyase-DNA complexes are visualised, showing association, dissociation and movement of photolyase over the DNA. The latter result suggests a sliding mechanism by which photolyase can scan DNA for damaged sites. It is shown that DNA must be only loosely bound to the surface to be able to interact with proteins. When $MgCl_2$ is used to immobilise DNA to mica, DNA is pinned to the surface at distinct sites. The pieces of DNA in between are free to move over the surface and are available for protein interaction. With AFM it is shown that even the annealing of restriction fragment ends can be directly visualised, though the energy required for disrupting these interactions is of the order of thermal energy.

In chapter 5 the temporal resolution that can be achieved with AFM is discussed in detail. An image tracking procedure for AFM is proposed and tested which allows repeated imaging of the same surface area without suffering from lateral drift. The drift correction procedure is based on on-line cross-correlation of succeeding images. Use of the image tracking procedure allows zooming in on a small scan area over a long period and thus reduces the frame rate inversely proportional with the scan area. Application of this procedure is demonstrated for diffusion of 5.4 kb DNA plasmids. With a scan area of 500 * 500 nm^2 a single plasmid can be imaged for more than 30 min at 4 s per frame, with a drift less than 10 nm. The high temporal resolution allows detailed analysis of the diffusion of DNA molecules. A diffusion coefficient of 30 nm^2/s is found for most DNA molecules, though many molecules are temporarily pinned to the mica surface, restricting diffusion.

Finally in chapter 6, the tip-sample interaction in tapping mode is studied. A simple model of a damped, harmonic oscillator is proposed to describe

the motion of a cantilever tapping in fluid. Using experimentally obtained parameters, excellent agreement is found between the theoretical and experimental results. From the model it is estimated that the force applied on the sample can range up to 100 nN, depending on the electrostatic potential of the surface. Detailed inspection of the cantilever deflection shows subtle differences in the oscillatory motion as a result of differences in the tip-sample interaction, which can conveniently be revealed by spectral analysis. The amplitude of the higher harmonic frequencies is shown to be sensitive for electrostatic interactions, and this is used to qualitatively map the electrostatic surface potential of DNA molecules on poly-L-lysine coated mica with a spatial resolution of 5 nm.

In conclusion, in this thesis it is shown that by carefully optimising the imaging parameters that control the forces and scan velocity, DNA and proteins can be visualized in physiological buffer routinely, reproducibly, without damage, over a long time window, and with a fairly good temporal resolution. With the present developments full advantage can be taken of the unique possibilities of atomic force microscopy in a wide range of biological applications.

Samenvatting

In dit proefschrift wordt de ontwikkeling van Atomic Force Microscopie (AFM) beschreven voor het afbeelden van biochemische reacties met moleculaire resolutie. De basis voor deze hoge resolutie ligt in de combinatie van een scherpe tip, een korte afstand van deze tip tot het oppervlak en een grote afstand afhankelijkheid van de krachtsinteractie tussen de tip en het oppervlak. Omdat contrast wordt verkregen op basis van een krachts-interactie tussen de tip en het oppervlak kan AFM gebruikt worden in diverse omgevingen, inclusief fysiologische buffers, waardoor biologische processen in hun natuurlijke omgeving kunnen worden gevisualiseerd. Hoewel de eerste AFM afbeeldingen van een DNA molecuul al tien jaar geleden gepresenteerd zijn, worden de meeste studies nog steeds in lucht uitgevoerd in plaats van in hun natuurlijke omgeving, fysiologische buffer. Door deze preparatie stap worden moleculen gefixeerd en gedehydrateerd, waardoor zij hun functionaliteit verliezen. In de visualisatie van individuele moleculen in fysiologische buffer komen de voordelen van AFM boven andere afbeeldingtechnieken, namelijk de hoge resolutie en de beperkte preparatie, pas echt goed naar voren. In dit proefschrift wordt beschreven hoe hoge resolutie topografie afbeeldingen van moleculaire processen kunnen worden verkregen. Er wordt aangetoond dat individuele moleculen met behulp van AFM reproduceerbaar en met een redelijk hoge snelheid in beeld kunnen worden gebracht gedurende een lange periode, zonder deze moleculen te beschadigen.

Het contrast mechanisme van tapping mode AFM in lucht wordt bestudeerd in hoofdstuk 2. In tapping mode wordt de cantilever in oscillatie gebracht, en wordt de oscillatie amplitude constant gehouden. Ondanks de hoge resolutie die met behulp van (tapping mode) AFM bereikt kan worden, zijn hoogte artefacten tot 10 nm gerapporteerd. Deze hoogte artefacten blijken te worden veroorzaakt door verschillen in tip-oppervlak adhesie. Afhankelijk van de amplitude en demping van de oscillatie van de cantilever, waaraan de tip bevestigd is, wordt op een plakkend oppervlak een kleinere hoogte gemeten vergeleken met een niet plakkend oppervlak. Deze hoogte artefacten

kunnen worden toegeschreven aan een modulatie van de oscillatie beweging van de cantilever. Doordat excitatie en demping van de cantilever oscillatie continue variëren kan, afhankelijk van het fase verschil tussen de cantilever en de excitator, de beweging van de cantilever aanzienlijk worden verstoord. Fase afbeeldingen die simultaan met de topografie gemeten kunnen worden in tapping mode AFM vertonen een contrast dat correleert met adhesie contrast. Aan de hand van voorbeelden van een goud-mica oppervlak, een Langmuir-Blodget film en DNA moleculen wordt dit mechanisme beschreven.

In hoofdstuk 3 wordt AFM gebruikt om structuurveranderingen in DNA te bestuderen als gevolg van complex vorming van DNA en photolyase, een klein DNA reparatie enzym. Gefixeerde photolyase-DNA complexen worden afgebeeld in lucht. Als substraat voor photolyase wordt een 1150 bp DNA fragment gebruikt dat met behulp van UV-straling is beschadigd op willekeurige plaatsen. Door vergelijking van photolyase-DNA complexen op dit DNA fragment met een 800 bp onbeschadigd fragment kunnen populaties van specifieke complexen van niet-specifieke complexen worden onderscheden. Niet-specifieke complexen vertonen geen buiging en minder bewegingsvrijheid van DNA ten opzichte van naakt DNA. Op beschadigingen, waar photolyase een specifiek complex aangaat, is DNA flexibeler en wordt een buigingshoek van 36° gemeten.

Met behulp van tapping mode AFM in buffer worden in hoofdstuk 4 niet-specifieke interacties tussen DNA en photolyase gevisualiseerd, die representatief kunnen zijn voor het proces waarmee photolyase DNA beschadigingen zoekt. Na implementatie van een aantal instrumentele verbeteringen kunnen moleculen routinematig worden afgebeeld in fysiologische buffer, met moleculaire resolutie. In de beelden wordt gedurende een half uur geen door de scannende tip veroorzaakte schade gezien, terwijl de scansnelheid $2 * 2\ \mu m^2$ per minuut bedraagt, en een RMS ruis gemeten wordt van minder dan 0.2 nm. In de 'moleculaire film' die op deze wijze verkregen wordt, zijn processen als associatie, dissociatie en beweging van photolyase over DNA te zien. Het laatste proces laat de mogelijkheid zien dat photolyase over het DNA molecuul scant op zoek naar beschadigingen. Om interacties met eiwitten mogelijk te maken is het noodzakelijk dat DNA slechts in beperkte mate aan het substraat gehecht is. Experimenteel wordt aangetoond dat DNA delen die niet aan het oppervlak gehecht zijn beschikbaar zijn voor eiwitten. De metingen met behulp van AFM zijn zo gevoelig dat zelfs basenparing van restrictie fragmenten direct in beeld gebracht kan worden. De energie noodzakelijk voor het verbreken van deze bindingen is van dezelfde orde van grootte als de thermische energie, en de

mogelijkheid om dit proces af te beelden bevestigt een zeer geringe interactie tussen de tip en de moleculen.

In hoofdstuk 5 wordt de tijdsresolutie van de AFM geoptimaliseerd. Een drift correctiemethode wordt beschreven die het mogelijk maakt om herhaaldelijk hetzelfde oppervlak af te beelden, zodanig dat thermische drift van het instrument slechts in beperkte mate van invloed is op de positie van de tip ten opzichte van het oppervlak. De procedure is gebaseerd op een on-line kruiscorrelatie van opeenvolgende beelden. Door gebruik te maken van deze procedure kan ingezoomd worden op een aanzienlijk kleiner oppervlak gedurende een lange periode, waardoor de meettijd afneemt omgekeerd evenredig met het scanoppervlak. De procedure wordt toegepast voor het meten van diffusie van individuele 5.4 kb DNA plasmiden. Door het scanoppervlak te reduceren tot $500 * 500$ nm^2 kan een enkel molecuul gevolgd worden gedurende meer dan 30 min met een beeldfrequentie van een beeld per 4 s, en een laterale drift van minder dan 10 nm. Door de goede tijdsresolutie is het mogelijk het diffusie proces in detail te bestuderen. Gemiddeld wordt een diffusie coëfficiënt gemeten van 30 nm^2/s, maar bij sommige moleculen wordt diffusie beperkt doordat deze moleculen tijdelijk sterk aan het oppervlak gehecht zijn.

Tenslotte wordt in hoofdstuk 6 de interactie van de tip met het oppervlak bestudeerd. Een eenvoudig model van een gedempte harmonische oscilla- tor wordt gebruikt voor de beschrijving van de beweging van een cantilever in vloeistof. Een goede overeenkomst wordt verkregen tussen experimentele en theoretische resultaten op basis van experimenteel verkregen param- eters. Uit het model volgt dat de kracht die door de tip op het oppervlak wordt uitgeoefend kan oplopen tot 100 nN, afhankelijk van de elektrostatische potentiaal van het oppervlak. Verschillen in tip-oppervlak interactie resulteren in subtiele veranderingen van de cantilever deflectie in tapping mode, die duidelijk naar voren komen in een spectrale analyse. De amplitude van hogere harmonische frequenties blijkt gevoelig voor elektrostatische interacties en kan gebruikt worden om de elektrostatische oppervlakte potentiaal kwalitatief in kaart te brengen. Als voorbeeld worden hogere harmonische afbeeldingen getoond van DNA moleculen op een poly- L-lysine gecoat mica oppervlak. Met deze nieuwe methode kunnen verschillen in de elektrostatische oppervlakte potentiaal worden gevisualiseerd met een spatiele resolutie van 5 nm.

Samenvattend wordt in dit proefschrift beschreven dat door nauwkeurige optimalisatie van de AFM afbeeldingparameters als de krachtsinteractie en de scansnelheid, DNA en eiwitten routinematig kunnen worden afgebeeld

in fysiologische buffer, reproduceerbaar, zonder door de tip veroorzaakte schade, gedurende een lange tijd en met een behoorlijke tijdsresolutie. Door gebruik te maken van deze ontwikkelingen komen de unieke capaciteiten van AFM goed tot z'n recht. Een groot aantal biologische toepassingen van deze vorm van microscopie ligt nu in het verschiet.

Nawoord

Het proefschrift dat nu voor u ligt is niet alleen het resultaat van mijn werkzaamheden de afgelopen 4 jaar aan de vakgroep Biofysische Technieken, maar ook dat van een aantal collega's binnen en buiten de vakgroep. Het is juist deze samenwerking die wetenschap uitdagend maakt, en waar de sappigste vruchten van te plukken zijn, ook al zijn er momenten geweest dat dit niet zo soepel en vlot verliep als ik dat gewild zou hebben. Hoewel ik altijd heb gezegd dat een baan als OIO eigenlijk niet zo veel verschilt van een 'echte' baan, vormt deze mogelijkheid om mensen expliciet te bedanken hierop misschien wel een uitzondering en wil ik hiervan graag gebruik maken. Allereerst wil ik Kees ontzettend bedanken, niet alleen voor de technische ondersteuning, maar ook voor zijn creativiteit, originaliteit en prettige omgang op allerlei andere vlakken. Kees, deze samenwerking had ik nooit willen missen! Verder heb ik continue kunnen sparren met een collega die ongeveer gelijktijdig aan een inhoudelijk verwant project begon. Oscar bedankt, ik denk dat juist in het buitenland onze verbondenheid pas goed tot z'n recht kwam. Ook wil ik Jan in het bijzonder noemen. Hoewel schier onbereikbaar, was je wel altijd 100% aanwezig voor onze besprekingen, en daarmee heb je enorm veel respect bij mij afgedwongen.

Het besmettelijke enthousiasme waarmee Kobus, Maria, Niek en Bart te werk gaan is niet zo vanzelfsprekend als jullie het soms doen lijken, maar wordt zeker wel gewaardeerd. Technische ondersteuning kwam niet alleen van Kees, maar ook van Frans en Jeroen (elektronica), Ine, Kirsten en Yvonne (biochemie) en Sylvia (pennen, koekjes), bedankt! De metingen aan photolyase waren niet mogelijk geweest zonder Claire en Andre van de vakgroep celbiologie en -genetica, Erasmus Universiteit in Rotterdam. Net als vele anderen (Esther !!) waren zij zeer kritisch over de manuscripten, wat de kwaliteit zeker ten goede is gekomen.

Tenslotte ga ik veel mensen onder een noemer bedanken, zij die onze vakgroep tot een ontzettend gezellige, unieke werkplek maakten: TOP10 en BFT.

Curriculum vitae

John van Noort werd geboren op 15 augustus 1971 te Lisse. In 1989 legde hij het eindexamen VWO af aan het Fioretti College in Lisse, om vervolgens te beginnen met de studie Moleculaire Wetenschappen aan de Landbouw Universiteit Wageningen. Deze studie rondde hij af 'cum laude', met afstudeervakken aan de vakgroepen Moleculaire Fysica, Physics and Biophysics (Massey University, Palmerston North, Nieuw Zeeland), Fysische en Koloïdchemie en Agrotechniek en -fysica. In 1995 begon hij als onderzoeker in opleiding bij de vakgroep Biofysische Technieken aan de Universiteit Twente, in dienst van de stichting Fundamenteel Onderzoek der Materie (FOM). Het onderzoek aldaar leidde tot dit proefschrift.